

Citadels Final Report

GMLC 2.2.1: Citadels

April 2023

Kevin P. Schneider (PNNL)

Jim Glass (EPB)

Cecilia A. Klauber (LLNL)

Ben Ollis (ORNL)

Matthew J. Reno (SNL)

Anamika Dubey (WSU)

Michael Burck (OES)

Jing Xie (PNNL)

Todd Wall (PNNL)

Laurentiu D. Marinovici (PNNL)

Thanh L. Vu (PNNL)

Wei Du (PNNL)

David Nordy (EPB)

Aaron Wiley (EPB)

Tim Mannon (EPB)

Derek Holman (EPB)

Nathan K. Smith (LLNL)

Wil Dawson (LLNL)

Neil Shepard (ORNL)

Maximiliano F. Maglia (ORNL)

Javier Hernandez-Alvidrez (SNL)

Nicholas S. Gurule (SNL)

Anjan Bose (WSU)

Joshua Hambrick (OES)

Citadels Final Report

GMLC 2.2.1: Citadels

Kevin P. Schneider (PNNL)	David Nordy (EPB)
Jim Glass (EPB)	Aaron Wiley (EPB)
Cecilia A. Klauber (LLNL)	Tim Mannon (EPB)
Ben Ollis (ORNL)	Derek Holman (EPB)
Matthew J. Reno (SNL)	Nathan K. Smith (LLNL)
Anamika Dubey (WSU)	Wil Dawson (LLNL)
Michael Burck (OES)	Neil Shepard (ORNL)
Jing Xie (PNNL)	Maximiliano F. Maglia (ORNL)
Todd Wall (PNNL)	Javier Hernandez-Alvidrez (SNL)
Laurentiu D. Marinovici (PNNL)	Nicholas S. Gurule (SNL)
Thanh L. Vu (PNNL)	Anjan Bose (WSU)
Wei Du (PNNL)	Joshua Hambrick (OES)

April 2023

DISCLAIMER

This report was prepared as an account of work sponsored by an agency of the United States Government. Neither the United States Government nor any agency thereof, nor Battelle Memorial Institute, nor any of their employees, makes **any warranty, express or implied, or assumes any legal liability or responsibility for the accuracy, completeness, or usefulness of any information, apparatus, product, or process disclosed, or represents that its use would not infringe privately owned rights.** Reference herein to any specific commercial product, process, or service by trade name, trademark, manufacturer, or otherwise does not necessarily constitute or imply its endorsement, recommendation, or favoring by the United States Government or any agency thereof, or Battelle Memorial Institute. The views and opinions of authors expressed herein do not necessarily state or reflect those of the United States Government or any agency thereof.

PACIFIC NORTHWEST NATIONAL LABORATORY
operated by
BATTELLE
for the
UNITED STATES DEPARTMENT OF ENERGY
under Contract DE-AC05-76RL01830

Printed in the United States of America

Available to DOE and DOE contractors from the
Office of Scientific and Technical Information,
P.O. Box 62, Oak Ridge, TN 37831-0062;
ph: (865) 576-8401
fax: (865) 576-5728
email: reports@adonis.osti.gov

Available to the public from the National Technical Information Service
5301 Shawnee Rd., Alexandria, VA 22312
ph: (800) 553-NTIS (6847)
email: orders@ntis.gov <<https://www.ntis.gov/about>>
Online ordering: <http://www.ntis.gov>

Summary

This is the final project report for the Grid Modernization Laboratory Consortium (GMLC) Citadels project. The primary goal of this GMLC project was to increase the operational flexibility of power systems by engaging microgrids distributedly using consensus algorithms. The primary goal, which was successfully achieved, was divided into three areas:

- Implement peer-to-peer control between microgrid controllers using the Open Field Message Bus (OpenFMB) approach;
- Develop and implement consensus algorithms on commercially available hardware that allows a group of microgrids to distributedly implement operational controls; and
- Develop the architectures and controls to enable groups of microgrids to coordinate their operations to support the bulk power system during abnormal events, and end-use loads in the event the bulk power systems fail.

This project addressed the increasingly common challenge of coordinating large numbers of distributed energy resources (DERs) to support the operations of the electric power system. While systems such as distributed energy resource management systems (DERMS) can centrally dispatch DERs, there are practical limits to the number of DERs that can be integrated: the central approach limits operational flexibility in a mixed ownership environment and the DERMS represents a single point of failure. While microgrids have been shown to be an effective way to aggregate the operation of multiple DERs, independently or in coordination with resiliency functions, centralized coordination still limits their full capability. These challenges can be seen in utilities such as the Electric Power Board of Chattanooga (EPB) where microgrids are being deployed to coordinate the operation of DERs and for resiliency purposes. The specific challenge for EPB is to develop methods and approaches to coordinate the operation of numerous mixed-ownership microgrids to support normal and abnormal system-level operations.

The approach developed, deployed, evaluated, and validated in the Citadels project utilized Open Field Message Bus (OpenFMB) to implement a layered control system that increased operational flexibility by facilitating a level of control at the system “edge”. At the edge, consensus algorithms were developed to allow groups of microgrid controllers to communicate, exchange information, determine operational goals, and execute operational actions to achieve global objectives. The work conducted as part of this project, in collaboration with other industry and DOE efforts, has advanced the state-of-the-art for distributed control on the industrial control systems utilized by electric distribution utilities. Specific outcomes of the project included:

- The Citadels project built on past DOE investments to show that OpenFMB can be used for a wide range of distributed control systems that require peer-to-peer communications at the application layer.
- The Citadels project provided a proof of concept that microgrid controllers, using commercial off-the-shelf (COTS) components, can distributedly make operational decisions using consensus algorithms without the need for a central agent. Additionally, the use of consensus algorithms overcomes the issues encountered with mixed ownership where there can be multiple local objectives.
- The field demonstration successfully showed that groups of microgrids can support bulk power system operations, with the microgrid controllers operating without the need for central control. Additionally, the field demonstration validated the technical building blocks for microgrid self-assembly when the bulk power system is not available.

Acknowledgments

Contributions to this project were achieved through the Grid Modernization Laboratory Consortium (GMLC), a strategic partnership between the U. S. Department of Energy and the National Laboratories. The GMLC was established as part of the U.S. Department of Energy Grid Modernization Initiative (GMI) to accelerate the modernization of the U.S. electricity infrastructure. The views expressed in the report do not necessarily represent the views of the U.S. Department of Energy or the United States Government.

The final field demonstration included operations involving a 1.25 MW/ 2.5 MWh Tesla battery that was partially funded by the DOE Office of Electricity Energy Storage Program.

This work was supported in part by the U.S. Department of Energy under contract DE-AC05-76RL01830.

Acronyms and Abbreviations

AMQP	Advanced Message Queuing Protocol
ANSI	American National Standards Institute
BEMS	Building Energy Management System
BESS	Battery Energy Storage System
CA	Collaborative Autonomy
CB	Circuit Breaker
CHIL	Control Hardware-In-the-Loop
CONOPS	Concept of Operations
CSEISMIC	Complete System level Efficient and Interoperable Solution for Microgrid Integrated Controls
D-OPF	Distributed Optimal Power Flow
DDS	Data Distribution Service
DER	Distributed Energy Resource
DMS	Distribution Management System
DNP3	Distributed Network Protocol 3
DOE	Department of Energy
DT	Digital Twin
EENS	Expected Energy Not Served
EERE	Energy Efficiency & Renewable Energy
EMI	Electromagnetic Interference
ENApp	Equivalent Network Approximation
EPI	Expected Probability of Interruption
FMB	Field Message Bus
GFL	Grid-Following
GFM	Grid-Forming
GMI	Grid Modernization Initiative
GMLC	Grid Modernization Laboratory Consortium
GOOSE	Generic Object Oriented Substation Event
GPON	Gigabit Passive Optical Network
GUI	Graphical User Interface
HELICS	Hierarchical Engine for Large-scale Infrastructure Co-Simulation
HIL	Hardware-In-the-Loop
IAP	Integrated Assessment Plan
ICCP	Inter-Control Center Communications Protocol
IEC	International Electrotechnical Commission
IED	Intelligent Electronic Device
IEEE	Institute of Electrical and Electronics Engineers
IoT	Internet of Things
IT	Information Technology

ITC	Inertia Time Constant
LLNL	Lawrence Livermore National Laboratory
MG	Microgrid
MQTT	Message Queuing Telemetry Transport
NATS	Neural Automatic Transport System
OE	Office of Electricity
OES	Open Energy Solutions
OpenFMB	Open Field Message Bus
ORNL	Oak Ridge National Laboratory
OS	Operating System
PCC	Point of Common Coupling
pf	Power Factor
PHIL	Power Hardware-In-the-Loop
PLC	Power Line Carrier
PLL	Phase Lock Loop
PNNL	Pacific Northwest National Laboratory
PV	Photovoltaic
ROCOF	Rate of Change of Frequency
RTAC	Real-Time Automation Controller
SETO	Solar Energy Technologies Office
SNL	Sandia National Laboratory
SCADA	Supervisory Control and Data Acquisition
SCCR	Short Circuit Capacity Ratio
SEL	Schweitzer Engineering Laboratory
SNL	Sandia National Laboratories
TES	Transactive Energy System
VA	Volt Ampere
var	Volt Ampere Reactive
VGM	Virtual Generator Mode
W	Watt

Table of Contents

Contents

Summary	v
Acknowledgments	vi
Acronyms and Abbreviations	vii
Table of Contents	ix
Figures	xii
Tables	xiv
1.0 Introduction	1
2.0 Overview of OpenFMB	3
3.0 Overview of EPB Distribution Infrastructure	6
3.1 Overview of EPB System	6
3.2 Local Control Systems	7
3.3 System Operators and Other Involved Personnel	7
4.0 Control Architecture	8
5.0 Consensus Algorithms	12
5.1 Voltage Support Algorithm	12
5.1.1 Robustness	14
5.1.2 Field Implementation	14
5.2 Self-Assembly Algorithms	17
5.2.1 Simple Consensus	18
5.2.2 More Complex Capabilities	19
5.3 Extensibility to Other Systems and Mixed Mode Operations	19
6.0 OpenFMB Harness	20
7.0 Operational Use-Cases	21
8.0 Modeling and Emulation	22
8.1 PNNL Distribution Modeling	22
8.1.1 Unbalanced Dynamic Simulations: GridLAB-D	22
8.1.2 Model Conversion Tools and Scripts	22
8.1.3 Model Conversion Accuracy	23
8.2 LLNL Collaborative Autonomy Modeling	24
8.3 SNL Inverter Modeling and Testing	26
8.4 WSU Co-Simulation	31
8.4.1 Power-Communication-Control Co-simulation Development	31
8.4.2 Distributed Coordination in IEEE Test System	32
8.4.3 Co-Simulation Model Development for EPB System and Validation	35
8.5 ORNL COMMANDER Testbed Emulation	40

9.0	Field Demonstration	42
9.1	Field Demonstration Summary	42
9.2	Description of Field Demonstration Events	43
9.2.1	Event 1: Verify Pub/Sub Data Exchange between All Architecture Components	43
9.2.2	Event 2: Verify that Each Authorized Controller Can Execute Commands on Field Devices and Topology Changes are Tracked by Subscribed Controllers and Consensus Algorithms	44
9.2.3	Event 3: Verify that Change in Topology, as Indicated by Reclosers, is Observed and Changes Tracked	45
9.2.4	Event 4: Coordinate Protection Settings Between Grid Edge Controllers, SCADA, and Breakers/Reclosers.....	46
9.2.5	Event 5: Verify Grid Edge Controllers Can Distinguish between Line Clearances and Hot Line Work Permits	48
9.2.6	Event 6: Add and Drop Authorized Controller and Verify How the Consensus is Affected (Add/Drop a Laboratory Microgrid Controller)	49
9.2.7	Event 7: Microgrid Controllers Able to Determine the Mode of Operation and Coordinate with Other Controllers.....	51
9.2.8	Event 8: Consensus that Results in Voltage/Reactive Power Change (at EPB Microgrid)	53
9.2.9	Event 9: Black Start of a Microgrid (at EPB Microgrid).....	55
9.2.10	Event 10: Failure of One or More Sensors (Laboratory Microgrid).....	56
9.2.11	Event 11: Loss of Communication to a Microgrid (Laboratory Microgrid).....	58
9.2.12	Event 12: Byzantine Actor (Laboratory Microgrid).....	59
10.0	Lessons Learned and Concluding Comments	62
10.1	Lessons Learned	62
10.1.1	Modeling and Simulation	62
10.1.2	Hardware and Software Containerization	62
10.1.3	Consensus Algorithms	62
10.1.4	Sustainability of Deployment.....	62
10.1.5	Distribution and Bulk Power Systems.....	63
10.1.6	Field Demonstration	63
10.2	Concluding Comments and Specific Outcomes	64
10.3	Potential Follow-on Research Areas	65
11.0	References.....	66
Appendix A:	Complete List of Project Publications	68
A.1	Published/Accepted Conference Papers	68
A.2	Published/Accepted Journal Papers	68
A.3	Published Technical Reports	69
A.4	Manuscripts in Preparation or under Review	69
Appendix B:	LLNL Emulation Methodology.....	70

Appendix C: Selected Tests of GridLAB-D Model	72
C.1 Test-01: Operations of Interconnected MG2 and MG3	72
C.2 Test-02: Islanding Operation of MG3	76

Figures

Figure 2.1: Comparison between traditional field devices and OpenFMB nodes.	3
Figure 2.2: OpenFMB adapters.	4
Figure 2.3: Layered architecture of OpenFMB control system.	5
Figure 3.1: Aerial view of EPB microgrid, with one-line notional overlay.	6
Figure 4.1: Conceptual control architecture for Citadels.	8
Figure 4.2: Typical transition of the four MG operation modes.	10
Figure 4.3: Citadels layered control architecture.	11
Figure 5.1: NATS interactions enable CA-agent capabilities.	16
Figure 5.2: NATS interactions which enable voltage support capability.	17
Figure 5.3: Six-step microgrid self-assembly process.	18
Figure 6.1: Structural view of the OpenFMB Harness being deployed on the Duke Energy circuits.	20
Figure 8.1: One-line diagram of model in GridLAB-D.	24
Figure 8.2: Meter voltage from GridLAB-D, without (left) and with (right) the voltage support algorithm.	25
Figure 8.3: Experimental setup for the GFL inverter.	26
Figure 8.4: Voltage traces at PCC for each value of L.	27
Figure 8.5: Current traces for each value of L.	27
Figure 8.6: Control block diagram of PCS100 (courtesy of ABB PCS100 user’s manual) [23]. ...	28
Figure 8.7: Frequency dynamics for different values of H.	29
Figure 8.8: GFL inverter frequency response (100 Hz/s ramp to 61 Hz).	29
Figure 8.9: GFM inverter islanded frequency response (2% droop, 1000 ms inertia time constant).	30
Figure 8.10: GFM inverter and genset responses.	30
Figure 8.11: Cyber-physical co-simulation platform.	31
Figure 8.12: IEEE 123-bus test system divided into four areas.	33
Figure 8.13: Communication stress test.	34
Figure 8.14: EPB systems test case simulation.	38
Figure 8.15: Voltage control using collaborative autonomy on EPB test systems.	40
Figure 8.16: One-line diagram of COMMANDER testbed.	41
Figure B.1: CA container status monitoring during Event 11.	71
Figure B.2: Log file excerpt identifying Byzantine actor during Event 12.	71
Figure C.1: One-line diagram of interconnected MG2 and MG3 (Test-01).	72
Figure C.2: Deviation between the “from” and “to” nodes of the “sync_check” object (Test-01). ...	74
Figure C.3: Measurements of the “from” and “to” nodes of the “sync_check” object (Test-01). ...	74

Figure C.4: Voltage magnitude of Phase A of selected nodes (Test-01).	74
Figure C.5: Frequency of DGs (Test-01).	75
Figure C.6: Active power outputs of DGs (Test-01).	75
Figure C.7: Reactive power outputs of DGs (Test-01).	75
Figure C.8: Active power outputs of inverters (Test-01).	76
Figure C.9: Reactive power outputs of inverters (Test-01).	76
Figure C.10: One-line diagram of islanded MG3 (Test-02).	77
Figure C.11: Voltage magnitude of Phase A of selected nodes (Test-02).	77
Figure C.12: Frequency of DGs (Test-02).	77
Figure C.13: Active power outputs of DGs (Test-02).	78
Figure C.14: Reactive power outputs of DGs (Test-02).	78
Figure C.15: Active power outputs of inverters (Test-02).	78
Figure C.16: Reactive power outputs of inverters (Test-02).	79

Tables

Table 7-1: List of Use-Cases and Scenarios	21
Table 8-1: Numbers of Components of Two Selected Feeders in CYME	23
Table 8-2: Inductor Values and Corresponding SCCR	26
Table 8-3: Loss Minimization and DER Maximization Results Using Different Methods.....	34
Table 8-4: Validation of EPB Co-Simulation	36
Table 9-1: Field Demonstration Events	42
Table 9-2: Field Demonstration Event 1 Results.....	44
Table 9-3: Field Demonstration Event 2 Results.....	45
Table 9-4: Field Demonstration Event 3 Results.....	46
Table 9-5: Field Demonstration Event 4 Results.....	47
Table 9-6: Field Demonstration Event 5 Results.....	49
Table 9-7: Field Demonstration Event 6 Results.....	50
Table 9-8: Field Demonstration Event 7 Results.....	52
Table 9-9: Field Demonstration Event 8 Results.....	54
Table 9-10: Field Demonstration Event 9 Results	56
Table 9-11: Field Demonstration Event 10 Results	57
Table 9-12: Field Demonstration Event 11 Results	59
Table 9-13: Field Demonstration Event 12 Results	60

1.0 Introduction

As part of the Department of Energy Grid Modernization Laboratory Consortium (GMLC), Pacific Northwest National Laboratory (PNNL) was tasked with leading the project titled “GMLC 2.2.1: Citadels”. This GMLC-funded effort was a joint collaboration between the Office of Electricity (OE) and the Office of Energy Efficiency & Renewable Energy (EERE) Solar Energy Technologies Office (SETO). The objective of this GMLC project was to engage DERs through flexible operating strategies, specifically, using peer-to-peer communications between microgrid controls to enable distributed decision-making through consensus algorithms. The distributed decision-making process then allows groups of microgrids to utilize their DERs to support the bulk power system during normal and abnormal events and to support critical end-use loads when the bulk power system fails.

While the utility distribution management system (DMS) maintains a supervisory capability, individual microgrid controllers exchange information peer-to-peer using Open Field Message Bus (OpenFMB), a reference architecture for security and interoperability. Information exchanged between the microgrid controllers is then used by consensus algorithms to determine the actions each of the controllers should take. Using this standards-based approach, it is possible for large numbers of microgrid controllers, and their associated DERs, to securely support both normal and abnormal power system operations. Additionally, the use of consensus algorithms allows for a mixed ownership model where not all of the microgrid controllers are utility owned.

The primary goal of this GMLC project, as outlined in the project proposal, was to increase the operational flexibility of power systems by engaging microgrids distributedly, coordinated using consensus algorithms. The primary goal, which was successfully achieved, was divided into three areas:

- Implement peer-to-peer control between microgrid controllers using the Open Field Message Bus (OpenFMB) approach.
- Develop and implement consensus algorithms on commercially available hardware that allows a group of microgrids to distributedly implement operational controls.
- Develop the architectures and controls to enable groups of microgrids to coordinate their operations to support the bulk power system during abnormal events, and end-use loads in the event the bulk power systems fail.

The operational use-case at Electric Power Board of Chattanooga (EPB) was to examine and develop operating strategies to coordinate the growing number of microgrids. Within the EPB service territory, microgrids are being deployed by EPB for reliability and resilience reasons. Microgrids are also being deployed by non-utility entities for a range of economic and reliability reasons. While the current number of microgrids in the EPB service territory is relatively small, it is expected to increase significantly over the next 5-10 years as DERs continue to be deployed. It is possible to coordinate microgrids with traditional solutions, such as distributed energy management systems (DERMS). However, the desire to gain operational flexibility beyond a simple dispatch requires other options to be considered, in particular when multiple owners are involved.

To this end, the Citadels project examined the distributed coordination of microgrids using consensus algorithms supported by the publish and subscribe capabilities of OpenFMB. The use of OpenFMB to exchange information between microgrid controllers ensured a standards-based approach that facilitates a design that can be implemented with different hardware, software, and operational objectives, supporting interoperability, scalability, and maintainability. The use of consensus algorithms allows for the participation of utility and non-utility microgrids since it preserves privacy and allows users to decide their

level of participation. To ensure a broad ability to implement the concepts developed in the project, to the greatest extent possible work was done with open-source software, implemented in containerized applications, and executed on commercially off-the-shelf (COTS) equipment.

The developed capabilities provided an example of how distributed control of microgrids can be implemented, but the work can be readily modified for other operational goals in different regions. For example, in the field demonstration, it was shown that a group of microgrid controllers can identify low voltage conditions, and exchange information about their current reactive power capabilities. As a group they can determine how much reactive power should be injected to restore voltage, and then execute a change in inverter setpoints to inject the necessary amount of reactive power. While this capability was demonstrated, the specific algorithms, objectives, and set points could be easily changed to reflect different operating conditions and/or utility practices. As a result, the work from this project is applicable to utilities around the nation.

To support the project goals, PNNL engaged numerous partners which include the Electric Power Board of Chattanooga, Lawrence Livermore National Laboratory (LLNL), Oak Ridge National Laboratory (ORNL), Sandia National Laboratories (SNL), Commonwealth Edison (ComEd), Open Energy Solutions (OES), and Washington State University (WSU).

This project was executed over a three-year period, from 10/1/2019 to 1/31/2022. The initial work focused on developing a generalized architecture for the coordination of networked microgrids and exploring various ways consensus algorithms have been used in other domains. This was followed by the construction of electromechanical, dynamic simulation models of the associated portions of the EPB system, and communications systems, based on their planning models and other available information. In parallel with the development of simulation models, containerized applications for OpenFMB translators, microgrids controllers, and consensus algorithms were developed. These containerized applications were then tested in various hardware-in-the-loop (HIL) platforms. The HIL platform testing validated standards compliance and interoperability between the various software containers needed to implement the layered control structures. The project developed a Concept of Operations (CONOPS) document that detailed the use-cases and procedures for operating networked microgrids when coordinated with consensus algorithms, both for supporting the bulk power system during abnormal conditions and supporting end-use loads when the bulk power system fails. Based on the use-cases in the CONOPS, an event-based Integrated Assessment Plan (IAP), which outlined the procedure for executing a field demonstration, was developed. A final field demonstration was held at EPB on September 27th and 28th of 2022, which was executed in accordance with the IAB.

This report outlines the work that was conducted as part of Citadels, from the initial modeling and simulation through the final field demonstration and is organized as follows. An overview of OpenFMB is presented in Section 2.0 and is intended to provide a general background. Section 3.0 presents the EPB electrical distribution infrastructure that was used as part of this project. The control architecture that the project developed is presented in Section 4.0 and is intended to give a high-level overview of the operational structure to be developed. Section 5.0 presents the consensus algorithms that were developed, and Section 6.0 presents the OpenFMB Harness, which is the physical instantiation of the OpenFMB reference architecture. Section 7.0 presents the operational use-cases that were developed as part of the CONOPS, and Section 8.0 contains information on the simulation and analysis work that was conducted based on the use-cases. Section 9.0 details the results of the final field validation and Section 10.0 presents the high-level lessons learned and concluding comments. This includes specific technical lessons learned from the project as well as identifying the impacts the project work will continue to have after the completion of the project. Project publications are listed in Appendix A. Models are not available in open-source sites, since the distribution system model from EPB is under the NDA. Algorithms and code can be uploaded to GitHub for open-source access, while they are not there when this report is finalized.

2.0 Overview of OpenFMB

OpenFMB is a framework and reference architecture for grid edge interoperability and was ratified as a standard by North American Energy Standards Board (NAESB) in 2016. It enables the coordination of grid edge devices through interoperability and distributed controls [1]. The framework reduces the need for a centralized intelligence or control and allows management of distribution systems at the circuit level. Additionally, OpenFMB can be deployed on environmentally hardened hardware, i.e., intelligent electronic devices (IEDs), that electric distribution utilities commonly use. For this reason, OpenFMB was selected for this project.

The grid of the future will require treating data differently, leveraging metadata and performing analysis locally to process the large amounts of new data available from new technologies. Traditional headend systems, illustrated on the left below, have relied on relatively few sources of field information. New asset classes on the grid (AMI, smart inverters, PMUs, etc.) have added large amounts of data that can quickly and accurately describe the state of the power system. Traditional headend systems were not designed to process this increased volume of information as quickly as is needed to react to current operational scenarios and fully realize the benefits of these new grid edge assets.

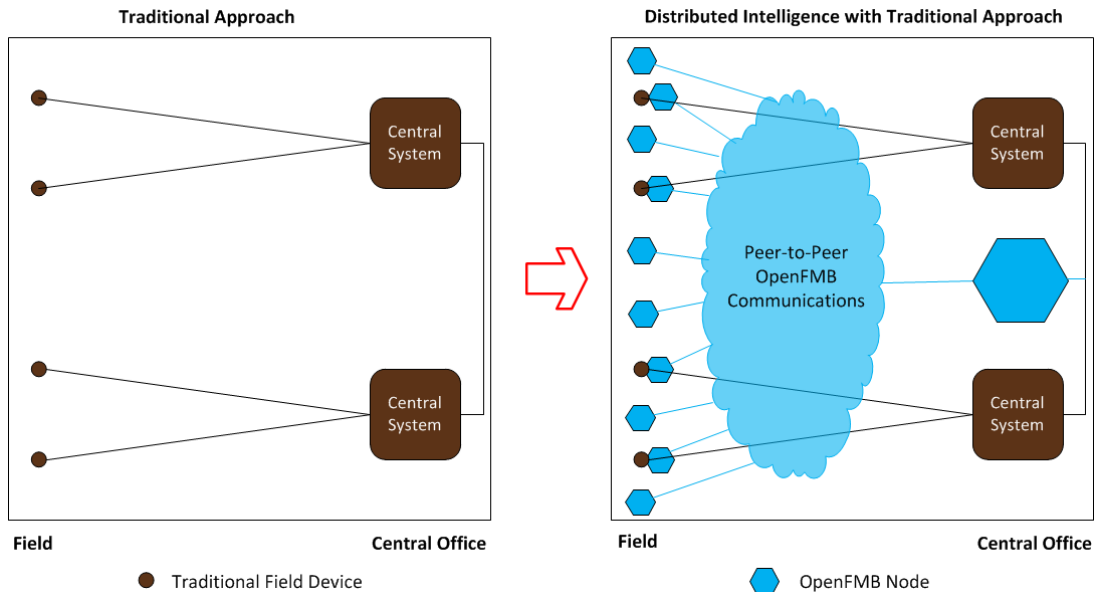


Figure 2.1: Comparison between traditional field devices and OpenFMB nodes.

Information no longer needs to go to the central system to enable decision making. Federated local data can be made securely available between assets at the grid edge to complement and enhance operations. OpenFMB nodes, shown as blue hexagons on the right of the figure above, host applications that analyze information to develop a higher resolution of situational awareness, and provide the ability to affect local control in coordination with other operational decision making.

The OpenFMB framework offers additional benefits, such as:

- Optimize investment for existing and future assets (i.e., freedom to maintain existing infrastructure while choosing technology and devices from diverse vendors).
- Enhanced Security around Communications at Grid Edge.
- Provide Device Readings & Statuses while Enabling Analysis & Control at Grid Edge.

- Increase Opportunities & Capabilities of DERs and Microgrids.
- Faster Return on Program/Infrastructure Investments (e.g., decreased schedule and cost through standards-based integration).

These are the reasons why OpenFMB was selected for this project. The OpenFMB adapters provided to the Citadels project by Open Energy Solutions (OES) are the manifestation of the NAESB standard via (1) protocol translation to OpenFMB data model, (2) data transport with publish/subscribe capabilities, and (3) various technical features for support and operation of the solution. The adapters provide interoperability and integration between applications and devices at any point on the grid, but in this instance, the focus was inter- and intra-communication with the microgrids associated with the field demonstration.

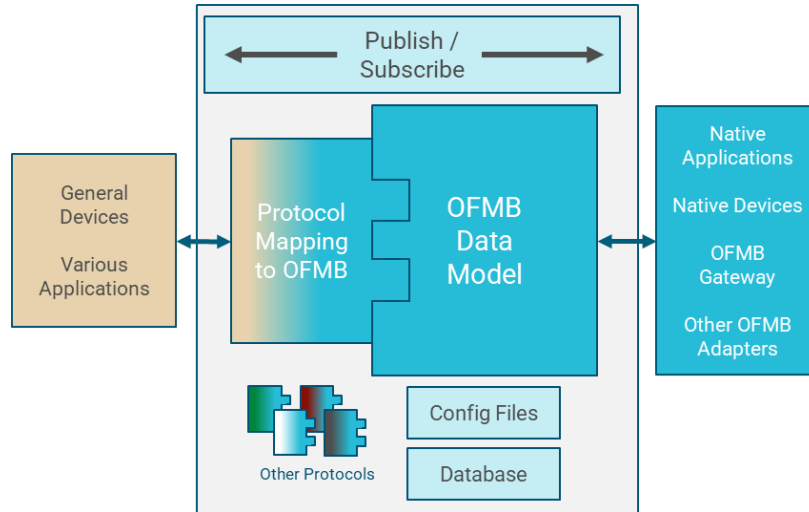


Figure 2.2: OpenFMB adapters.

The adapter utilizes the latest, published OpenFMB data model. In this case, that is 2.1, which included support for DER grid codes. The main protocols in distribution devices are DNP3 and Modbus, which the adapter supports. However, the OES adapter also currently handles ICCP, IEC 61850 GOOSE, OCCP 1.6j, OpenADR, and IEEE 2030.5. With each of these protocols, the adapter has a configuration file it uses to map from the protocol(s) used by the device to OpenFMB. This is what creates the interoperability between equipment and systems that speak different protocols. Within OpenFMB, there are different types of profiles (e.g., readings, statuses, events, and controls) to categorize communications. OpenFMB as a reference framework uses publish/subscribe (pub/sub) technology for sending/receiving these messages. The default pub/sub protocols used are Message Queuing Telemetry Transport (MQTT), Neural Automatic Transport System (NATS), and Data Distribution Service (DDS). Beyond these standard capabilities, the OES adapter also has a historian, security, logging, and capture/replay. Finally, the adapter is containerized which allows it to be completely self-contained as well as easily loaded and operated on a variety of different hardware and operating systems.

OpenFMB adapters enable communication between such varied protocols as: distributed network protocol 3 (DNP-3), Modbus, American National Standards Institute (ANSI) C12, message queuing telemetry transport (MQTT), data distributed service (DDS), IEC 61850, GOOSE messages, advanced message queuing protocol (AMQP), and the NATS protocol. The OpenFMB adapters have been developed, tested, and released as open-source [1].

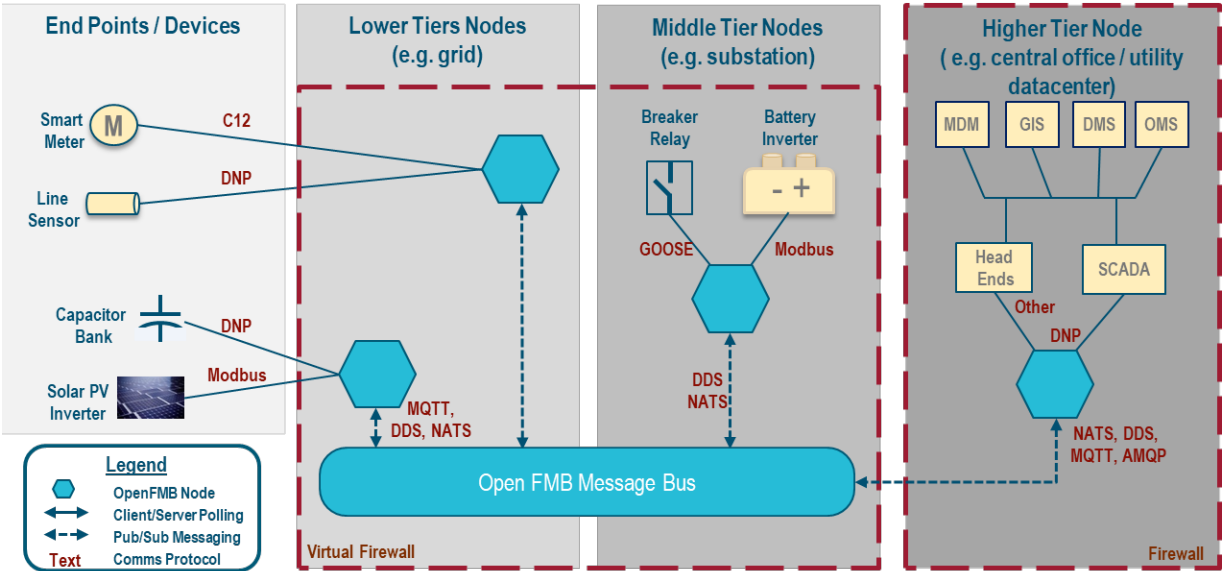


Figure 2.3: Layered architecture of OpenFMB control system.

In Figure 2.3, an example of an OpenFMB architecture is shown, allowing the simultaneous use of multiple protocols across multiple devices. This is essential in distributed control systems since multiple protocols are often used because of the range of device types. For example, electric distribution utilities in North America use DNP-3 for end-point devices, such as line sensors and shunt capacitors. However, the majority of PV and battery energy storage system (BESS) controllers use Modbus, and smart meters commonly use ANSI C12. As a result, the interoperability challenges associated with coordinating these devices can be significant, especially in real-time. OpenFMB is still evolving, and early implementations of OpenFMB-based distributed controls have provided lessons learned [2]:

- Open-source, lightweight message bus protocols are not difficult to implement on static embedded telemetry and have the following advantages:
 - Portability, reusability, and modularity.
 - Significant reduction in time and effort to deploy.
 - Greater interoperability between different vendors.
- A publish and subscribe (pub/sub) messaging pattern enables interoperability between different protocols, disparate legacy assets, and information technology (IT) enterprise systems, and has multiple advantages:
 - Agnostic of programming language, operating system (OS), and protocol(s).
 - Agnostic of physical communications medium, as long as performance requirements (latency, bandwidth, etc.) are met: Wi-Fi, Cellular, or power line carrier (PLC).
 - Decoupling of physical, network, and logic layers.

3.0 Overview of EPB Distribution Infrastructure

For the Citadels project, the considered system includes a number of EPB 12.47 kV distribution circuits, their substations, and the sub-transmission and transmission lines that interconnect them. While microgrids typically operate only at the distribution level, networked microgrid operations must consider interaction on a larger scale. Specifically, networked microgrid operations must consider the coordinated operations of microgrids that are not geographically co-located.

3.1 Overview of EPB System

EPB is supplied by 14 Tennessee Valley Authority (TVA) substations, seven 161kV/46 kV and seven 161 kV/12 kV. These 14 TVA substations supply 90 EPB owned substations, which serve 43 - 46 kV circuits, 204 - 12 kV circuits, and 91 - 4 kV circuits. The EPB distribution circuits operate at 12.47 kV and are a standard four-wire grounded-wye design. Distribution and sub-transmission systems are interconnected with a standard three-wire design at 46 kV and/or 161 kV.

In addition to the radially operated distribution system, EPB also operates a microgrid at their operations facility, as shown in Figure 3.1. The microgrid is primarily supplied by the 1.30 MW (DC) solar PV and supported by a 1.25 MW (2.50 MWh) Tesla battery. The peak load of this building is typically 45 kVA, which is normally supplied from within the MG boundary. During all field tests, it was operated at this level. In the unlikely event that involves a diesel generator failure, EPB has the capability to switch an additional 700 kVA to the Control Center Building. However, such an emergency is not anticipated.

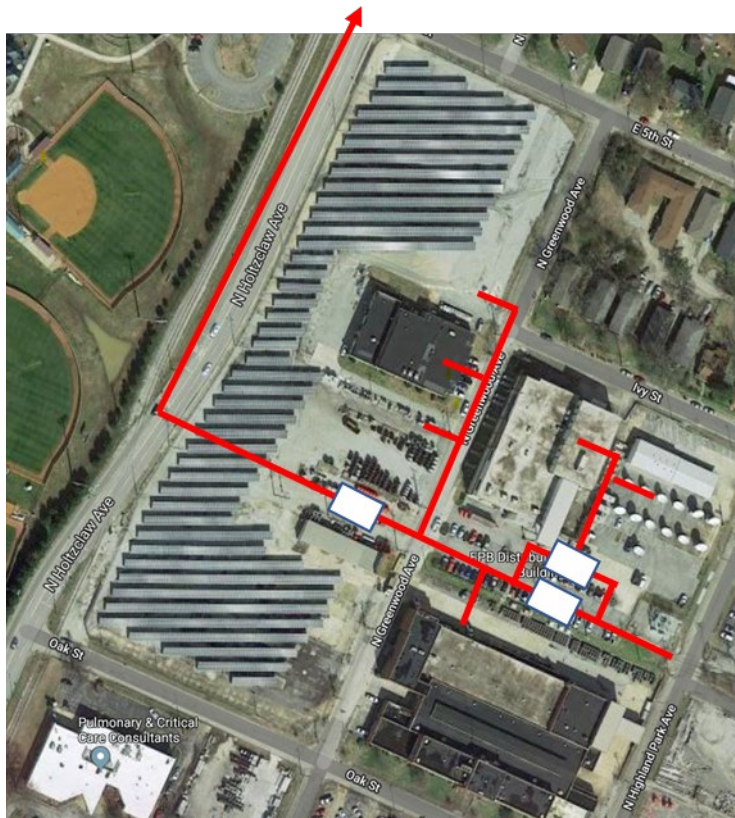


Figure 3.1: Aerial view of EPB microgrid, with one-line notional overlay.

In addition to electrical infrastructure, EPB also owns and operates a gigabit passive optical network (GPON) that supports all substations, pole top devices, and AMI communications. The GPON also supplies retail customers with internet, television, and phone services.

3.2 Local Control Systems

PV and energy storage systems are critical components of many microgrids. They often provide a significant portion of the energy needed to power local loads, especially in islanded mode. However, the variability and availability of these energy resources can make it challenging to effectively control and manage the microgrid system. This is why a combination of local and coordinated controls are typically used.

For the microgrid at the EPB control center, the solar PV locally implements a maximum power point tracking (MPPT) scheme to optimization power collection, and a grid-following (GFL) inverter for the inverter that connects the PV to the grid. The Tesla battery implements a range of proprietary controls for battery management and optimization, and a grid-forming (GFM) inverter, with a range of control modes, for the inverter that connects the battery to the grid.

Both the solar PV and battery are then connected to a Complete System level Efficient and Interoperable Solution for Microgrid Integrated Controls (CSEISMIC) microgrid controller, implemented as a containerized software application on an industry standard relay, for coordination as part of a microgrid. It is the microgrid controller that has the control functions that ensure that any variable PV resources and/or load can be mitigated by the battery energy storage, ensuring a stable frequency and voltage for the end-use loads.

3.3 System Operators and Other Involved Personnel

Personnel that most often interact with the system are the system operators and line crews. The system operators interact with the system via the DMS/SCADA using the fiber optic network. Line crews physically interact with the system by executing switching operations and maintenance tasks as instructed by the system operator. There are other EPB personnel who impact EPB's system indirectly, such as distribution system planners, protection engineers, customer service agents, and meter technicians.

4.0 Control Architecture

A key purpose of “grid architecture” is to help manage complexity and risk. To this end, a properly developed architecture is designed to illustrate a basic relationship between structures, and not to present a complete design. The relationships between elements may represent a range of interactions that can include, but are not limited to, the flow of power, control signals, data, regulatory interactions, and financial interactions. For the purposes of Citadels, the structure is created by showing the relationship between the key entities/elements that participate in the functions included in networked microgrid operations. Figure 4.1 illustrates the general architectural features for the planned implementation. The figure aggregates information from the more detailed diagrams associated with the operational use-cases, which are discussed in Section 7.0.

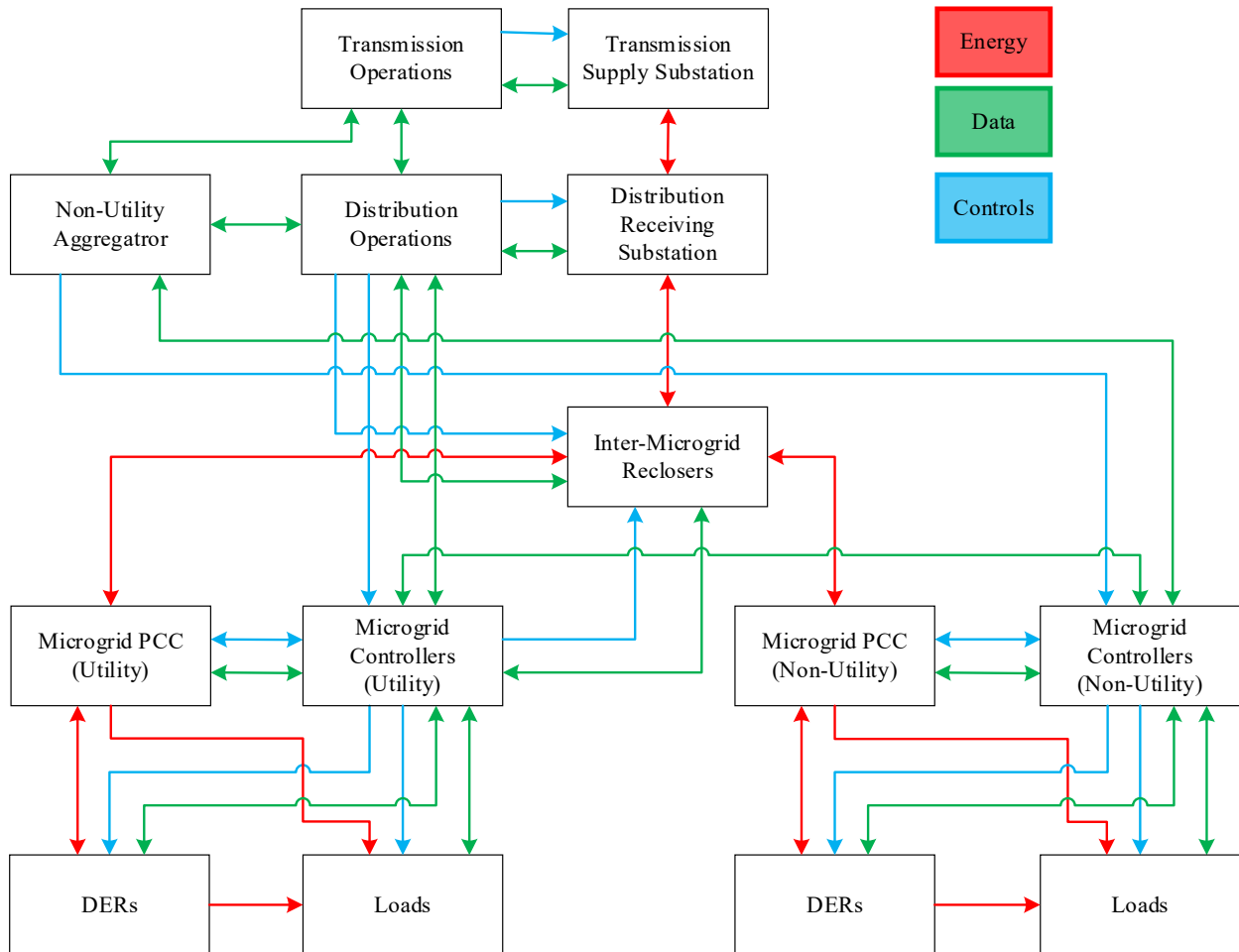


Figure 4.1: Conceptual control architecture for Citadels.

In Figure 4.1, the individual elements are connected by three types of lines, each indicating a different type of interaction. First, the red lines indicate the flow of electricity between entities or devices. Second, the blue lines indicate data/information flow between entities and/or devices. And third, the green lines indicate control signals.

One approach to managing the complexity of networked microgrid operations is to apply the principles of laminar decomposition. In this approach, an optimization problem and associated constraints are defined

and then decomposed into one or more layers of sub-problems that can be solved simultaneously in each layer. This approach is based on distributed control coordination techniques developed over the last several decades.

For this project, the details of the optimization problem(s) must be defined. In general, though, the problem is as follows: multiple individual microgrid controllers operate to achieve their local objectives informed by data and operational information from other microgrids. Details of the objectives, optimization, and consensus are reported in [7]. The first operational decision that an individual microgrid controller must make is to determine what “mode of operation” it is in, as discussed in Section 3.0. Once the “mode of operation” is determined, the execution of specific functions to achieve control goals must be met.

For the Citadels project, each microgrid locally decides its current mode of operation. The four modes of operation for Citadels are listed as follows. The typical transition between these four modes is shown in Figure 4.2.

- **Mode 1: Normal** – The microgrid is connected to the bulk power system and operating primarily for economic gains through demand side management. There are extensive examples in the literature for how microgrids can operate when grid-connected; examples may include providing ancillary services such as spinning reserve and/or coordinating the operation of distributed energy resources (DERs). Because of the range of potential operations, and the fact that they have been well studied, Citadels does not develop any additional control functions for grid-connected operations. Instead, the range of “normal” grid-connected options falls under the control mode heading of “Normal”.
- **Mode 2: Abnormal** - In the Abnormal Mode of Operation, the microgrid is grid-connected and operating to support the bulk power system under abnormal conditions such as a dynamic stability event or a pre-cursor to a voltage collapse. It should be noted that the Abnormal Mode of Operation is to an extent independent of the condition of the bulk power system. Specifically, it is possible for the bulk power system to be experiencing an abnormal operating condition, but for the microgrid to remain in the Normal Operating Mode; deciding when/if to support the bulk power system is a control decision the microgrid needs to make. Unlike the Normal Mode of Operation, there is less available literature on how microgrids can operate to support the bulk power system during abnormal events. For this reason, Citadels developed control functions for how a microgrid can support the bulk power system during abnormal operations.
- **Mode 3: Support critical load** – Supporting critical end-use loads is one of the primary reasons that utilities and end-use customers deploy microgrids. While the operational requirements for a single microgrid to support a critical end-use load is well understood, coordinating the operations of multiple microgrids in this role is not. Citadels examines the potential for multiple microgrids to coordinate their operations and interconnect as necessary to support critical end-use loads. The “self-assembly” of collections of microgrids is a far more complicated problem than the traditional distribution reconfiguration problem because radial assumptions may not be valid, connections may occur across sub-transmission systems, and because all microgrids may not operate with the same objectives.
- **Mode 4: Restoration** - Traditional power system restoration is a “top down” approach where the bulk power system is first restored, and then lower voltage distribution systems are energized. Microgrids allow for the potential of a “bottom-up” approach where microgrids energize lower voltage level distribution systems before the bulk power system. This strategy is being examined by other projects in the GMLC and is leveraged by Citadels. For this reason, Citadels also leverages other on-going work and does not develop new restoration or black-start capabilities.

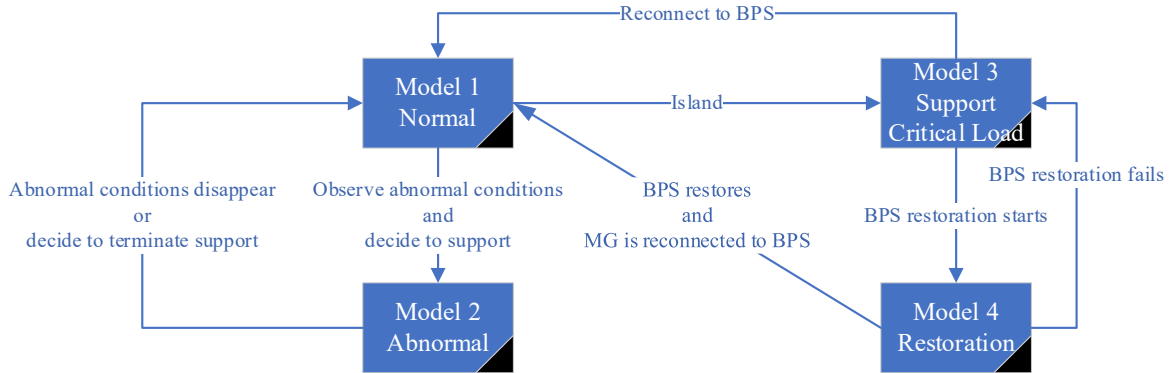


Figure 4.2: Typical transition of the four MG operation modes.

For Citadels, there were four layers to the control architecture. The layers are as follow:

- Layer 1: Individual device to microgrid controller

Individual devices including relays, controllers, and sensors communicate directly with the individual microgrid controller. This includes the exchange of information as well as control signals. Interactions at this layer could be a traditional centralized approach or a peer-to-peer implementation; either is feasible given the limited size of individual microgrids. For Citadels, individual devices are only able to communicate with their host microgrid controller, and no other microgrid controllers.

- Layer 2: Microgrid controller to microgrid controller

At this layer the individual microgrids exchange information, but not control signals. Interactions at this layer could be a traditional mapped Supervisory Control and Data Acquisition (SCADA) approach, but for scalability, a peer-to-peer approach would typically be more appropriate. For Citadels, Layer 2 operations are where most consensus algorithms are expected to apply.

- Layer 3: Microgrid controller to, via SCADA

At this layer, the utility's centralized DMS, via SCADA, has the ability to communicate with the microgrid controllers. This layer would only be active if there is a functioning communications infrastructure, and the centralized systems were performing a supervisory function. For a consensus algorithm, the centralized control is not needed to achieve a solution. Because some of the microgrids are privately owned, the DMS will only be able to communicate with utility owned microgrids.

- Layer 4: Microgrid controller to aggregator

Networked microgrids can enable aggregators to support transmission operation by allowing the aggregator to communicate with individual microgrid controllers at Layer 4 of the communication hierarchy. At this layer, the aggregator can exchange information with the microgrid controllers to facilitate the coordination of power generation and distribution. The aggregator can also provide services such as frequency regulation and load balancing to the transmission grid by aggregating the output of multiple microgrids.

However, in a mixed ownership environment, where microgrids are owned by both utilities and non-utilities, the aggregator may only be able to communicate with the non-utility owned

microgrids. This limitation may come from regulatory constraints and may be aimed at preventing the aggregator from having undue influence on utility-owned microgrids.

Despite this limitation, networked microgrids provide significant benefits to transmission operation by enabling the aggregation of DERs and enhancing the resilience of the grid. By leveraging the diverse and distributed nature of microgrids, aggregators can support transmission operation by optimizing the use of DERs and reducing the need for centralized generation. Overall, networked microgrids provide a valuable tool for enhancing the reliability and efficiency of the transmission grid, while also enabling the integration of renewable energy sources and inverter-based resources.

Aggregator operations were not considered as a core part of the Citadels project, but the work was developed to include the possibility of their participation. This reflects the changing operating structures in the utility industry where aggregators are expected to become a more common, and influence stakeholder.

These are conceptually modeled and shown in Figure 4.3 below. There are three laminar layers of controls, with each layer operating to achieve its own layer level goal(s) and managing the constraints and data exchange between layers.

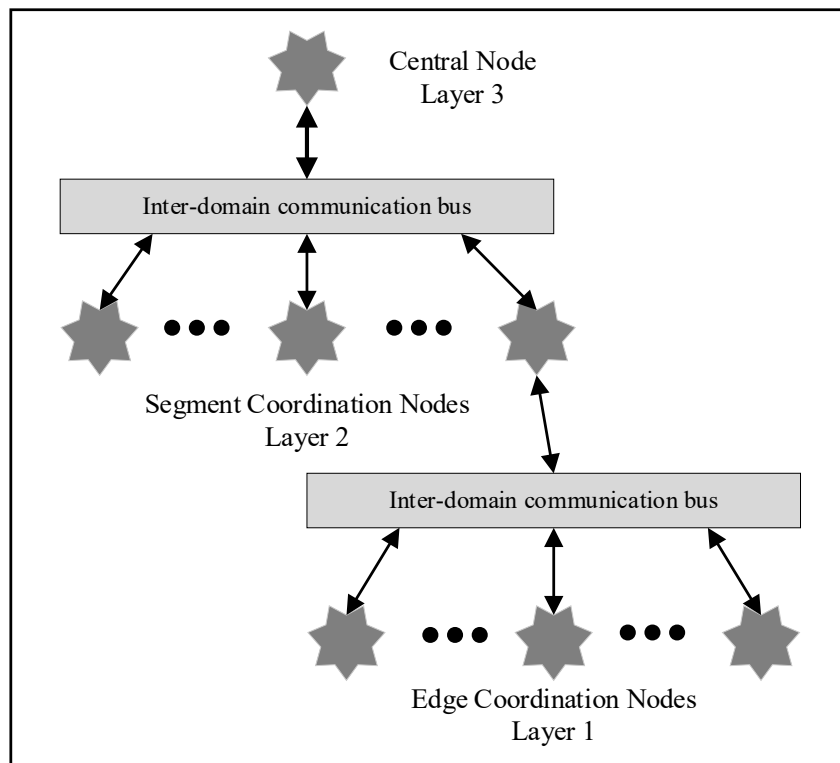


Figure 4.3: Citadels layered control architecture.

5.0 Consensus Algorithms

This section outlines the concept of using consensus algorithms and the specific implementation within collaborative autonomy (CA) that was used in this project. Consensus algorithms were chosen for this project as a means to coordinate information exchange and decision-making between heterogeneous, networked microgrids, in a potentially mixed-ownership environment.

Collaborative autonomy (CA) is a family of decentralized, parallel computational methods for use in unreliable computing environments. Indeed, any parallel algorithm that meets the following criteria can be included in the collaborative autonomy taxonomy: 1) it is decentralized 2) it includes resiliency considerations suitable for unreliable environments, where the unreliability may be hardware, communication links, etc. It should be noted that *distributed* algorithms are distinct in that there is still a centralized controller organizing the computation, where for *decentralized* algorithms there is no centralized controller, but a collection of decentralized, autonomous devices. Key features of many CA based applications include Byzantine fault tolerance, malicious data spoofing tolerance, low computing requirements, practical (time) convergences, and asynchrony.

Consensus algorithms are then a related subset of such algorithms used to come to an agreement on a value or objective. Having been successfully utilized in other domains, there is limited but growing application of consensus algorithms and multi-agent systems in the power system operations and control realm [4]-[6]. Algorithms used in a particular domain, such as power and energy, are dependent on the particular application, goals, and constraints of real-world challenges and implementation.

Additional details are provided in Sections 5.1 and 5.2 which describe the specific algorithms applied to the Citadels project use-cases, as well as the considerations that drove those selections and how the proposed algorithms achieve the project objectives. Lastly, a few comments on extensibility to other systems and considerations regarding mixed mode operations are provided.

5.1 Voltage Support Algorithm

This section describes the consensus-based voltage support methods developed to enable networked microgrids to support the bulk power system (BPS) during a low voltage event (Use-Case #2, Scenarios 3 and 4). The following algorithm leverages voltage measurements from the various microgrids and their collective communication/computation capabilities to detect and respond to an undervoltage (<0.95 pu) event at/near the BPS.

The key objectives that should be addressed include the following:

- Using (primarily) voltages measured at the microgrids, estimate the current state of the BPS. This may not be the *exact state* at a common point, but at the least a proxy that is representative of what is observed by the distributed microgrids.
- Determine if there has been a significant change in state (e.g., voltage droop).
- Identify outlier agents (e.g., measurements with a bias or Byzantine agents).
- Determine what collective action(s) should be taken, if any.

Consensus algorithms implemented in distributed devices are well suited for these tasks. For example, to determine the status of the BPS (assuming and knowing all microgrids are grid-connected), an averaging-based consensus is applied to the voltage measurements that the microgrids share with each other, peer-to-

peer. The resulting average is a *BPS voltage metric*. To determine if there has been a voltage droop at the BPS (and not just local) level, previous voltage measurements or metrics are compared to the current, or some pre-set threshold, like 0.95 pu. Further details are provided below.

There are many objective functions that can be used as criteria for when to provide grid support in a multi-microgrid scenario. What has been implemented for this project is described below:

$$G_k^* = \sum_k w_k \times \frac{V_{nom} - V_k}{V_{nom}} \quad (5-1)$$

The objective function, G_k^* , is the weighted sum of the total per unit voltage deviation measured by each microgrid, k , where a discussion on the determination of weights is provided in Section 5.1.1. The V_{nom} term is pre-determined and is to be representative of the normal operating condition, such as 1 pu. The purpose of the collaboratively determined corrective actions taken by each microgrid is to minimize G^* .

Each microgrid controller agent will attempt to take an action to support the grid based on its available resource, uncommitted volt ampere reactive (var) capacity $Q_{reserve_k}$ providing reactive power proportional to G_k^* , i.e. $Q_k \propto K_k \cdot G_k^*$ where Q_k represents the amount of reactive power injected into the grid from microgrid k .

$$Q_k = K_k[n] \cdot G_k^* \cdot Q_{reserve_k} \quad (5-2)$$

During the iterative process, the magnitude of each microgrid's var support gain parameter at step n , $K_k[n]$ can be adjusted, by observing the response of the system and global objective to the support action.

$$K_k[n] = f(K_k[n-1], G_k^*, \Delta G_k^*) \quad (5-3)$$

s. t. $Q_k < Q_{reserve_k}$

During regular operations (Mode 1), the microgrids share voltage measurements and determine the voltage metric using distributed averaging on an ongoing basis. During a voltage droop at the bulk power system, the collective observations of the distributed devices will verify that the current grid state needs support when the majority of microgrids observe the dip, i.e. the disturbance is not merely a local phenomenon. The microgrids then enter Mode 2: grid support mode and determine their available capacity to support the grid. For voltage support, this includes spare capacity that can be dispatched as vars or reactive power load that can be curtailed.

With each iteration, participating microgrids dispatch reactive power in proportion to the collectively determined objective function and the system response (change in voltage) is observed. In the next iteration, if the collectively computed objective is sufficiently small (or meets some other predetermined criteria, like maximum number of steps) the microgrids will return to normal operating mode, that is Mode 1.

This method leverages existing consensus building blocks, namely distributed averaging, to iteratively dispatch reactive power to support bulk power system objectives. Additional considerations for robustness to bad data or Byzantine agents is described in Section 5.1.1.

A similar methodology can be applied to frequency events (Use-Case #2, Scenarios 1 and 2), with a set frequency as the objective, as opposed to voltage, and active power dispatched to address the issue instead of reactive power, among other unique considerations.

5.1.1 Robustness

As referenced in (5-1), a trust metric, or relative weight, can be assigned to the information being shared by the various microgrid agents. These weights are incorporated into the collaborative decision-making process and can be used for detecting outlying information, which can then be down weighted in the collective. The properties which can inform the agent weights include the class (accuracy) of the sensors within the system managed by the agent, the ownership of the microgrid (such as whether it is utility or non-utility owned), and the location of the microgrid/agent.

There exist many ways to identify and reject outliers, to leverage the consensus building blocks of distributed averages. One simple method is presented in what follows. In this approach there are three types of weights based on the agent properties previously outlined. First, the sensor class weight is the inverse of the sensor measurement variance $w_{\sigma_k} = 1/\sigma_k^2$. Second, the trust/ownership weight is w_{T_k} , where the initial weight is based on assumptions made about the ownership but can change over time with a value of 0 corresponding to complete untrustworthiness and a value of 1 corresponding to complete trust. Third, the location-based weight w_{L_k} is defined to be inversely proportional to the agent's relative impedance from the point of coupling to what is intended to be the boundary of the bulk power system; in bulk system support scenarios this is intended to be a proxy for how sensitive an agent's measurements are to a given event source based on limited (i.e., not a full model) information on the system topology. Finally, the joint weight can be defined.

$$w_k = \frac{w_{\sigma_k} w_{T_k} w_{L_k}}{\sum_k w_{\sigma_k} w_{T_k} w_{L_k}} \quad (5-4)$$

Given the joint weight of (5-4), it is possible to calculate the weighted mean and variance in the following procedure which informs robustness to outliers for determination of the objective function. This method is most appropriate when there is strong correlation between the baseline measurements at the microgrids or if the deviation from nominal is assessed instead of the absolute (normalized) measurements. First the weighted mean and variance are determined. To perform outlier rejection, the z-score of each measurement is computed as well as the probability of such a measurement occurring, assuming a Gaussian distribution. Unlikely, measurements are rejected based on a previously determined probability threshold. Then, the trust weights associated with the rejected measurements are decreased while the trust weights associated with the accepted measurements are increased.

5.1.2 Field Implementation

The CA implemented for the field demonstration is Python-based and leverages the NATS protocol to communicate over the NATS Messaging Bus. Using this method, the different CA agents, containers deployed on COTS hardware, can communicate through a publish and subscribe model set forth by NATS with the formats defined by OpenFMB. In this way, the CA agents collaboratively make decisions based upon measurements at resources they are responsible for to move into Mode 2 for Voltage Support or remain/return to Mode 1 for persistent monitoring.

A unique feature of how NATS enables processing of communication between devices is that no device needs to know where another is; they only need to know where the NATS server is. From there, they can

publish and subscribe different tags against the messaging bus and can have full transactions with one or many devices also talking over NATS. With OpenFMB, tags can be specified, such as switches, regulators, and load types, which represent real field elements and aids in organization.

OpenFMB is used to communicate attributes of the microgrid resources that are required for the CA process. Namely, the SwitchReadingProfile and ResourceStatusProfile tags describe attributes about the CA and its associated microgrid resources through multiple StringEventAndStatus subtags. This enables sharing of vital information such as: the current operating mode, known neighbors (other microgrid-associated CA agents), and voltage status. The use of the NATS messaging bus for the OpenFMB protocol-enabled collaboration with less agent overhead and clearer and cleaner communication for devices. Implementing CA communication using OpenFMB over NATS allowed for streamlined analysis and verification using OES's OpenFMB Message Inspector, and the resulting architecture aligned with the goals and strengths of CA.

The deployed CA code has three main components: agent code, utility functions, and the voltage support algorithms. The responsibility of the agent code is to make sure each agent can send, receive, and parse data from the NATS bus. The messages each agent expects include information about the microgrid resource it is responsible for and information about other agents that are also talking on the NATS bus. From any microgrid, the agent collects the following information at a user-defined frequency, which should be informed by the rate of availability from the microgrid controller and operational needs:

- Microgrid voltage, phase (A, B, or C) and magnitude
- Microgrid frequency
- State of the point of common coupling to the feeder (PCC)
- Current reactive power draw/dispatch

From any agent, the following information can be collected from the messages:

- Agent's associated microgrid information (voltage, frequency, PCC state, reactive power)
- Agent's current mode (Mode 1 for monitoring, Mode 2 for Voltage Support)
- Agent MRID, name
- List of publications the agent has to offer

The default subjects which are *published* on by the agents are ResourceStatusProfile.* (this is subscribed to so the agent can see all messages published by all agents) and ResourceStatusProfile.<mrid> (this subject is so the agent can see information published for statuses meant for the specific agent). The default subjects *subscribed* to by the agents are so the agent can subscribe to values published by the microgrid controller/adaptor that it corresponds to (ResourceReadingProfile), send information to other agents (ResourceStatusProfile, this is the main publish/subscribe used by the agents and a building block of the collaborative algorithms), and may be manually overridden (ResourceDiscreteControlProfile, this enables manual override of the agent's current mode for testing purposes). These interactions are demonstrated in Figure 5.1.

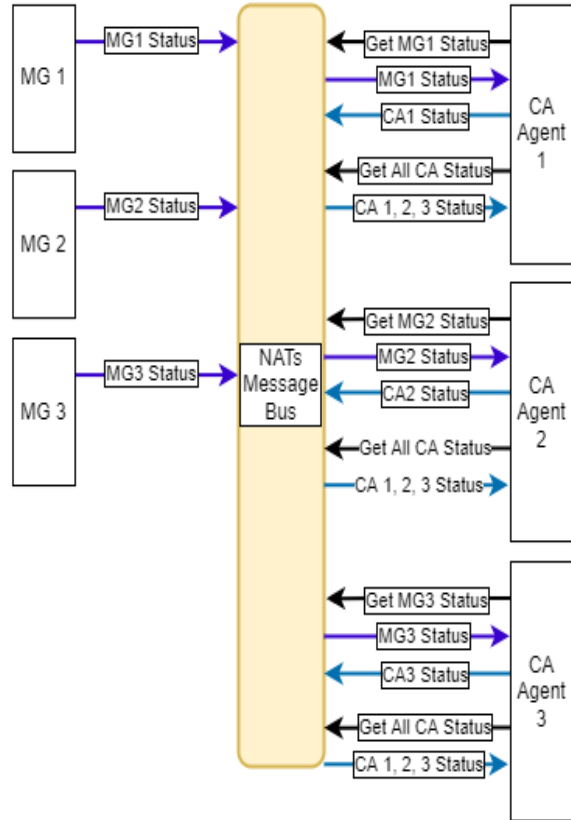


Figure 5.1: NATS interactions enable CA-agent capabilities.

Each agent is then able to identify which neighbors it knows, which publications each neighbor has, and the status for each neighbor’s microgrid. This gives each agent the ability to perform complex calculations with the neighborhood of collaborative agents without needing to consistently query other neighbors since each neighbor is already broadcasting its current status.

The voltage support algorithm agent implements the algorithm previously described in this report. In the deployed implementation, the voltage support agent extends the normal functionality of the basic agent by including additional information to be sent between agents for the voltage support calculations. This functionality (as depicted in Figure 5.2) requires additional subscription tags related to calculating the voltage metric, published and parsed similar to the agent information exchange depicted in Figure 5.1. Ultimately, the voltage support agent will request reactive power changes from its associated microgrid based on the consensus among the agents in its neighborhood. These are published as ResourceDiscreteControlProfiles messages. With the additions corresponding to the voltage support agent code, the interactions can be visualized as follows:

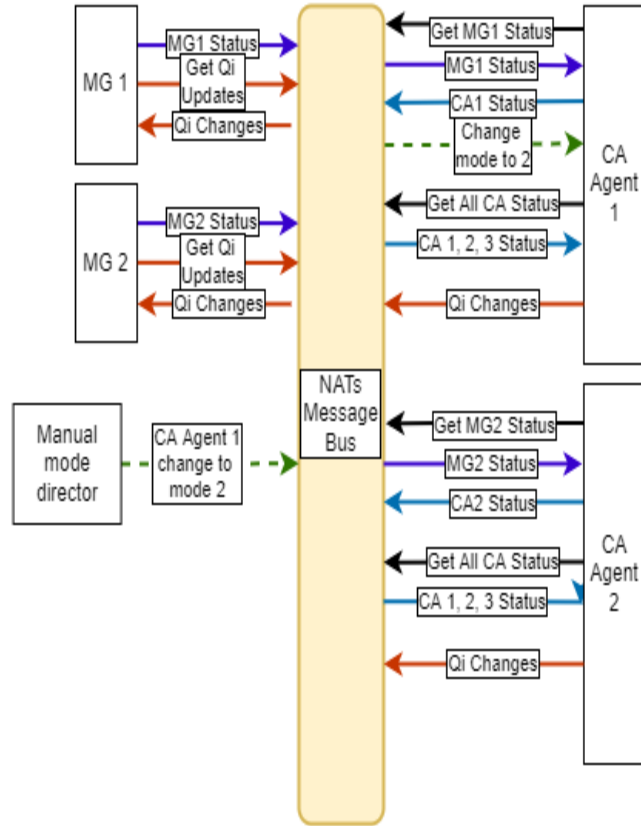


Figure 5.2: NATS interactions which enable voltage support capability.

5.2 Self-Assembly Algorithms

The concept behind the self-assembly of microgrids is at the crossroads of microgrid operations and distribution system reconfiguration, without strong central control. In addition to enabling the support of end-use loads within the microgrids, the microgrids may also pick up loads between microgrid PCCs as a result of the recommended switching operations. The proposed multi-step process for decentralized microgrid self-assembly is provided in Figure 5.3 with additional detail provided in the following subsections.

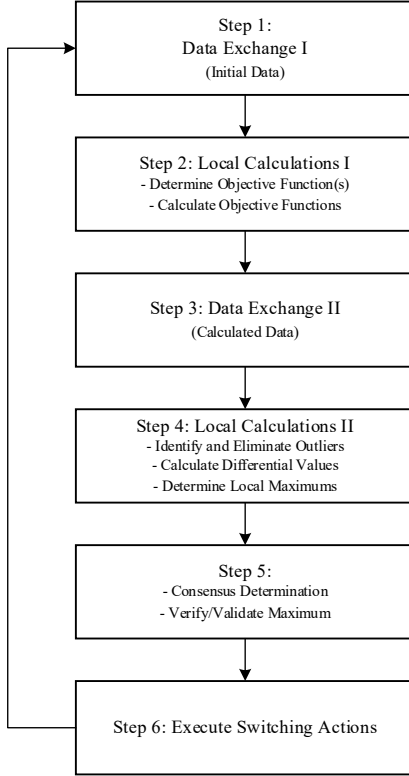


Figure 5.3: Six-step microgrid self-assembly process.

Without centralized control and data management, the microgrids will be required to exchange information peer-to-peer (Step 1), such as through OpenFMB. This is possible with the proposed architecture and also supports consensus objectives and implementation.

In Step 2, the fundamental question of which microgrids should connect and in what order comes to the forefront. While this could be addressed with a large and complex centralized optimization problem, the distributed set-up and potential mixed-ownership environment necessitate unique approaches for solving this problem. There are many potential objective functions that can be broken down into problems that can be solved in a distributed fashion. Here, each microgrid first calculates its internal critical load run time, as well as how long it can support the critical load when connected to each of the other microgrids to which it has a valid switching path. In Step 3, these calculated values (as well as an assertion of the quality of the provided estimates and a ranked list) are circulated among the collective of microgrids. A range of techniques support the objectives of Steps 4 and 5, which include identifying and eliminating outliers and coming to a consensus about what the next operational action is, such that the switching action can commence (Step 6). Then the algorithm returns to Step 1 to assess if/which additional microgrids should connect or disconnect to continue or end the restoration process.

5.2.1 Simple Consensus

A fundamental building block on consensus algorithms from functional programming is the concept of a *reduce function*, where some set of numbers is reduced to a smaller set of numbers via a function. *Allreduce* is one such reduction operation, in which every participant i holding some information x_i , receives the answer to the collective calculation of the reduction $\bar{x} = \otimes_i x_i$, where \otimes denotes any operation both commutative and associative. In this use-case, it is used to find the maximum over the pieces of data, as that is commutative and associative. In application, after each microgrid determines its local ranked list of

potential connection, the lists and critical load run-time estimates are shared among the microgrids. To determine the single best potential connection in a collaborative fashion, defined to be the maximum critical load run-time, each microgrid will select one connection and corresponding run-time estimate, the local maximum among what was shared with it, to submit to the global maximum *allreduce*. The set of local best connections are reduced to a singular connection-estimate pair, a copy of which has been distributed to each participating agent.

This method can be made more robust by including an information fusion step when the local best connection is being determined. Information fusion is the process of integrating or associating data from multiple sources to produce more useful or consistent information; hence, the fact that the combined total critical load run-time of the connection between two microgrids is independently assessed by both microgrids is leveraged. Each microgrid can compare the received estimates that correspond to potential connections for itself to the local ranked-list as shared by the microgrids in the ranked-list calculation phase. In the presence of heterogenous microgrids and/or estimate uncertainty, any two microgrids will likely not produce the exact same estimate. Therefore, rules can be provided to the microgrids regarding under what conditions discrepancies between estimates can lead to the rejection or acceptance of the assertion.

5.2.2 More Complex Capabilities

Without the additional checks and balances outlined above, the ring reduce method is not inherently robust to outliers. A method that is able to reject outlier data is the Cloture Vote approach which will achieve the consensus within a fixed number of iterations, specifically $t+1$, where t is the number of faulty processes or agents. This is implemented using the Phase King Algorithm and described in detail in the project high-level paper [7].

LLNL has also developed additional complex algorithms leveraging mixture model synthesis and a Bayesian Markov Chain Monte Carlo approach to improve the robustness to and down weighting of Byzantine or greedy actors trying to influence the consensus. While these algorithms are not published yet, they are listed in Section A.4.

5.3 Extensibility to Other Systems and Mixed Mode Operations

Throughout the development of the proposed algorithms, ensuring that the concepts are appropriate even in mixed ownership and mixed mode operations was a consideration. In general, the work stived to minimize the amount and specificity of data required to achieve the bulk power system support objectives and leveraged consensus concepts to ensure that even if there are differences in ownership, resource mix, and internal resource optimization, the decision making aggregated at the microgrid control level can still move toward the pre-determined global objective. This provides the flexibility for these concepts to be deployed in various regions, despite differences, such as regulatory.

6.0 OpenFMB Harness

The Architecture shown in Section 4.0 shows operations at a conceptual level. However, the concept needs to be implemented in physical reality, supported by software. The work presented in this final project report was conducted, as a reference architecture, using an OpenFMB Harness. An example is illustrated in Figure 6.1, and is the physical instantiation of the OpenFMB architecture.

The Harness can be accessed by utility and non-utility assets to share information in the pub/sub-system. The communications infrastructure for the Harness utilizes the same network that the participating entities use. For utility assets, the connection to the Harness is made using hardened SEL computers running open-sourced translation nodes. These open-sourced nodes were connected to utility SCADA via DNP3 connection using an SEL RTAC.

For non-utility assets, the connection to the Harness is made using open-sourced nodes developed by OES. Other connection options include VOLTTRON™ nodes [8] as shown in the figure below. VOLTTRON is an open-source technology developed by the Department of Energy to be a flexible, scalable, economical, and secure solution to operate the Internet of Things (IoT). The assets that may interact via an open-sourced node may include inverters, microgrid assets, microgrid controllers, and potentially Building Energy Management Systems (BEMS). While it would be technically possible to directly interconnect this equipment, using open-source nodes are usually more cost-effective and, at the time of this report, no production equipment has been developed with native OpenFMB support.

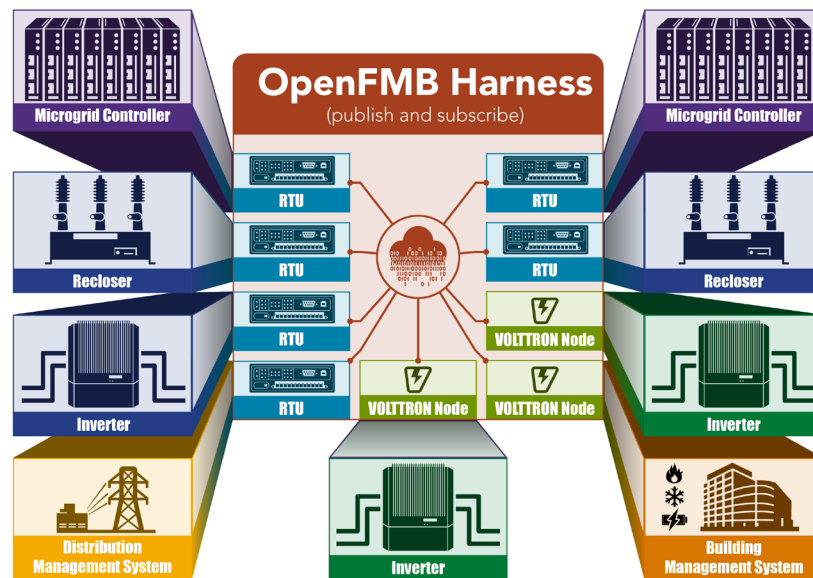


Figure 6.1: Structural view of the OpenFMB Harness being deployed on the Duke Energy circuits.

The Harness demonstrates the ability of an open-source node to act as the connection that enables the communication between both a utility's system and a privately operated system. NATS has been used as the pub/sub communication protocol between the OpenFMB and the non-utility DERs, which enables peer to peer communication among the devices. Each device can receive data based on the subscription topics. This peer-to-peer idea reduces the latency of direct communication between the system and devices.

7.0 Operational Use-Cases

The OpenFMB Harness described in Section 6.0 is a control system that enables a wide range of communications and operations. This section presents use-cases, detailing how the OpenFMB Harness enables operations that coordinate the centralized and distributed resources. The use-cases in Table 7-1 were used as the basis for the project and were the framework for the execution of work by the team members. This includes the control architecture, consensus algorithms, modeling and emulation, and field demonstration. Each use-case provides a sequence of operations for various events to represent how the electrical system, and operators are expected to respond to various conditions. Details of use-cases and scenarios are reported in CONOPS and are not repeated in this section. While these use-cases do not reflect the specific scenarios that were used in the final field validation, all work conducted in the project is traceable to one or more elements in the use-cases and/or the field demonstration. Details of the modeling and the field validation are presented in Section 8.0 and Section 9.0, respectively.

Table 7-1: List of Use-Cases and Scenarios

Use-Case	Scenario
Use-Case #1: Base Case Operations	Scenario 1: Operations when Grid-Connected
	Scenario 2: Operations when Supporting Critical End-Use Loads
Use-Case #2: Operations when Grid Connected and Supporting Bulk Power Systems	Scenario 1: All Microgrids (frequency event)
	Scenario 2: Some Microgrids Support (frequency event)
	Scenario 3: All Microgrids (voltage event)
	Scenario 4: Some Microgrids Support (voltage event)
Use-Case #3: Operations when Islanded to Support Critical End-use Loads	Scenario 1: Self-Assembly all Microgrids Participate
	Scenario 2: Self-Assembly Some Microgrids Participate
Use-Case #4: Dark-Sky Event	Scenario 1: Examine of BPS frequency support when communication is lost
	Scenario 2: Example of BPS voltage support when information is incorrect

8.0 Modeling and Emulation

This section summarizes the modeling and emulation efforts of PNNL, LLNL, SNL, WSU, and ORNL for different research needs. The real distribution system model from EPB was converted by PNNL for running in the open-source tool GridLAB-D. The model of GridLAB-D is then shared with other partners as references and is the base version. LLNL modified and expanded the model for co-simulation to test their consensus algorithms. WSU also revised the model to establish a similar co-simulation environment, in which the communication systems are well modeled and consensus algorithms are investigated. The co-simulation of LLNL does not include the detailed model of communication systems but is focused on the interaction among agents and the data transfer between GridLAB-D and agents. In addition, the study of LLNL on consensus algorithms covers the Byzantine agents, while WSU's work does not. The research of SNL and ORNL is on the modeling of inverters and testbed emulation, respectively. They both involve hardware devices and hardware-in-the-loop (HIL) tests.

8.1 PNNL Distribution Modeling

This subsection provides background information on the model conversion tools and techniques that convert utility data into GridLAB-D models for simulation. The accuracy of the converted model is also reported. Details are also reported in [9].

8.1.1 Unbalanced Dynamic Simulations: GridLAB-D

As an open-source power system simulation tool, GridLAB-D was initially developed for steady state study in phasor representation [10]. It provides valuable information to users who design and operate electric power transmission and distribution systems, and to utilities that wish to take advantage of the latest smart grid technologies. GridLAB-D incorporates advanced modeling techniques with high-performance algorithms. The end-use load modeling technology is integrated with three-phase unbalanced power flow and retail market systems. Historically, the inability to effectively model and evaluate smart grid technologies has been a barrier to adoption. GridLAB-D is designed to address this problem. The user documentation and source code are reported in [11] and [12], respectively.

8.1.2 Model Conversion Tools and Scripts

Utility companies typically provide model and data exported from their power engineering software, e.g., Synergi Electric and CYME. These real model and data need a conversion process to generate the model files for GridLAB-D. There are multiple tools and scripts that provide this model conversion functionality and/or assistance. Two of these are developed by PNNL. They have been used by authors to successfully convert models from several utilities, including: Duke Energy, Seattle City Light, EPB of Chattanooga, Portland General Electric, Avista, and ComEd. First, CIMHub is a tool set for translating electric power distribution system models between various formats, using the IEC Standard 61970/61968 Common Information Model (CIM). The source code and guidance of CIMHub are reported in [13]. Second, a set of Python scripts that converts CYME into GridLAB-D model is available in the repository of GridLAB-D tools [14]. Overall, each conversion tool/script has its advantages and disadvantages, e.g., the inputs and outputs of CIMHub [13] cover multiple formats, while the Python scripts [14] can convert CYME model into GridLAB-D format only. However, the Python scripts require less installations and settings. Benefits and/or needs of model conversion may include: 1) avoidance of license costs; 2) utilization of specific functionalities of different simulation tools; 3) pursuit of performance and/or compatibility in operating system; and 4) requirements of clients and/or sponsors.

8.1.3 Model Conversion Accuracy

In this study, CIMHub was used to convert the model exported from CYME into the GridLAB-D format. This involves the following steps: 1) convert the CYME into OpenDSS [15] model; 2) export the CIM model from OpenDSS model; and 3) export the GridLAB-D model from the CIM model. The numbers of components of these two selected feeders in CYME are listed in Table 8-1. Service transformers are replaced as closed switches in the GridLAB-D model.

There are 6 feeders, 4 distribution substations, and 3 sub-transmission substations. The bulk power system involves 2 swing nodes at 161 kV. Transformers of sub-transmission substations bring the voltage down to 46 kV. Five feeders are at 12.47 kV, while one feeder (FDR4) is at 12.00 kV. The geographic display and feeder topologies are not shown for data privacy. However, a high-level one-line diagram is shown in Figure 8.1. FDR6 is a short feeder, which is not included in Figure 8.1 and most studies. It was converted as a backup, as it has two tie-switches for the interconnection with FDR5. The conductor operating temperature is set at 77°F. Line capacitances are included in the GridLAB-D model for an optional feature of considering the line charging. Python scripts that convert constant power load objects into ZIP loads are uploaded to this repository [16]. The Recloser 5c does not exist in the original EPB system, while it is added in the GridLAB-D model for establishing an interconnection path between MG2 and MG3.

To validate the converted model, power flow results of both GridLAB-D and CYME are compared. As the maximum deviation on the voltage magnitude is less than 0.009%, the accuracy of converted GridLAB-D model is very high. In the authors' experience, the accuracy of model conversion is typically impacted for longer and/or heavier feeders. For instance, round-off errors can be accumulated gradually along the length of a feeder. In addition, heavier loads contribute more currents, which can magnify the small deviations on models and solvers between different simulation tools.

Table 8-1: Numbers of Components of Two Selected Feeders in CYME

Feeder ID	Number of Nodes	Number of Spot Loads	Number of Overhead Lines	Number of Underground Cables	Number of Service Transformers	Number of Switches	Number of Reclosers	Number of Fuses
FDR1	932	110	671	54	119	23	10	54
FDR2	18	1	14	1	1	1	0	0
FDR3	1536	267	1155	51	233	28	12	60
FDR4	1063	183	785	44	163	18	9	49
FDR5	953	172	616	71	167	21	9	75
FDR6	17	1	5	7	1	3	0	0
Total of F1-F6	4519	734	3246	228	684	94	40	238

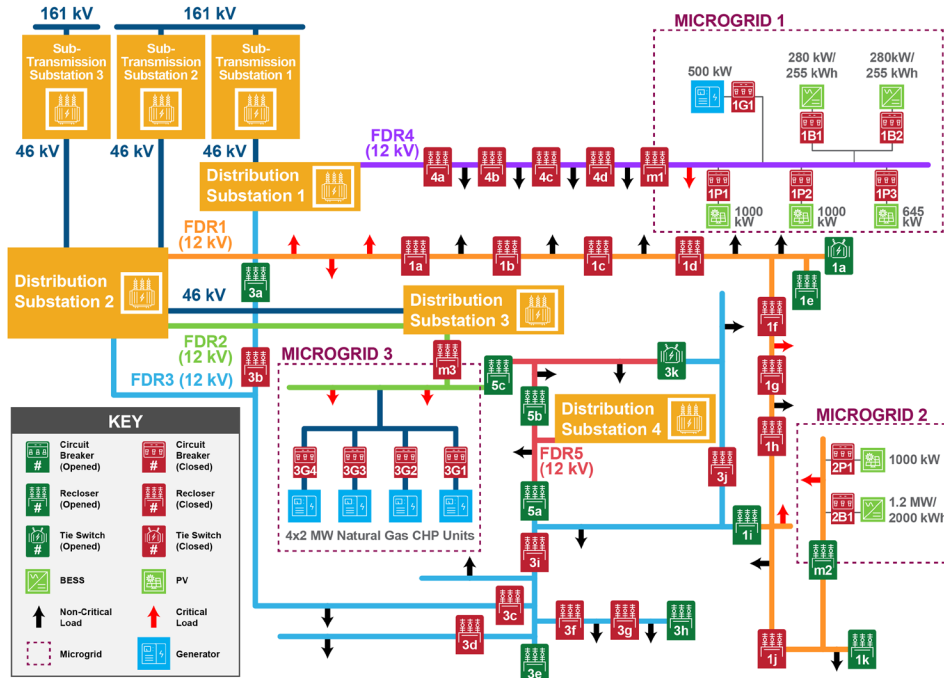


Figure 8.1: One-line diagram of model in GridLAB-D.

8.2 LLNL Collaborative Autonomy Modeling

To simulate the voltage support algorithm before the field deployment, an isolated portion of the provided EPB GridLAB-D model was used, with additional proxy microgrids to simulate a collective. The simulations were conducted using the GridLAB-D simulation environment. The Deltamode in GridLAB-D enables unbalanced dynamic simulations to simulate a BPS voltage drop and assumed that reactive power could be requested as soon as the algorithm solved (multiple times a second), though in operations those requests would be made at lower frequency. During the test, the grid source connected at the sub-transmission level was regulated down to 0.96 pu. Voltage was measured at the five “microgrids” and used as the values shared among the collective in the algorithm. Battery energy storage was available in the microgrids to provide reactive power support. For the simulation it was assumed that the battery energy storage could provide up to 1.25 Mvar to support voltage control, while for the field demonstration, we limited the maximum requested support to 500 kvar, per operator request, though the battery maximum output was about 1.00 Mvar. During the forced voltage drop, the microgrid agent did the following: observed and confirmed the event, transitioned to Mode 2, collaboratively determined the global voltage metric, and requested proportional reactive power support from their internal resource. Over a few iterations, this mitigated the voltage drop, both at the metered locations and at the point of interconnection to the sub-transmission grid, as seen in Figure 8.2.

With respect to performance, even with some loss of communication, the global voltage metric can be converged to from the available information and the voltage successfully moved towards nominal. The incremental adjustments will persist, iterating until either the voltage drop is no longer observed, the voltage metric is determined to be above the pre-determined acceptable minimum, or all the reactive power sources have reached their maximum output. For a system of this size, set points can be collaboratively calculated multiple times a second, though a delay was added for the field test such that commands and system response could propagate before recalculation. For the field demonstration, tunable parameter K in (5-2) was set such that there would be convergence (in this case, maximum reactive power dispatch) within two iterations, per operator request, and the algorithm successfully increased the voltage and maintained it (see 9.2.8).

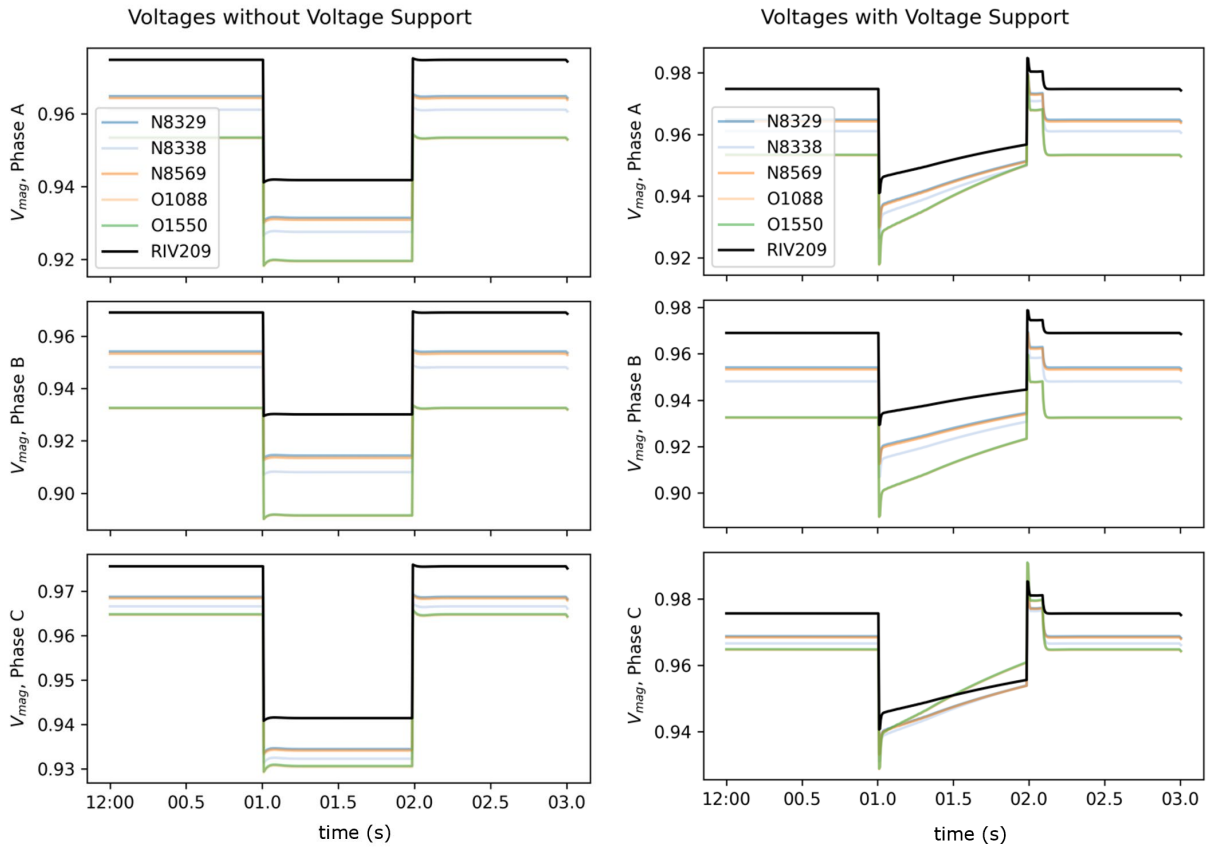


Figure 8.2: Meter voltage from GridLAB-D, without (left) and with (right) the voltage support algorithm.

8.3 SNL Inverter Modeling and Testing

Participation of Sandia National Laboratories focused mostly on experimental testing of inverters, either: grid-following (GFL) or grid-forming (GFM) [17]. Also, the interactions between a GFM inverter and a diesel genset were tested. Such experiments were conducted with the main objective of gaining some insights regarding the fault behavior [18], [19] and transient dynamics involved while testing commercially available equipment. The results were used to validate, or further improve the available simulation models [20], [21].

A good majority of the available GFL inverter models tend to become unstable as the grid reactance increases, which makes the power system weaker in terms of the Short Circuit Capacity Ratio (SCCR) [22], defined by:

$$SCCR = \frac{1.5 \frac{V_{PCC}^2}{\omega_0 L_{grid}}}{VSC_{capacity}} \quad (8-1)$$

The first experiment was intended to verify the stability of a commercially available, single-phase GFL inverter. The testing setup is depicted in Figure 8.3, where the GFL inverter (SMA Sunny Boy) is tested under different values of the interface inductor L (5mH, 10mH, 15mH). The GFL inverter is rated 3 kVA operating at rated voltage of 240V. Under a stiff grid condition ($L=0$), the power amplifier provides the voltage reference for the PLL of a GFL inverter, and the dynamics of the PLL are decoupled from the inverter's control scheme. As the interface inductor increases, the coupling between the PLL and the inverter's control scheme increases. Such coupling has the potential to affect the internal stability of the inverter as the grid stiffness reduces. From (8-1), the corresponding SCCR values for each inductor value used are shown in Table 8-2.

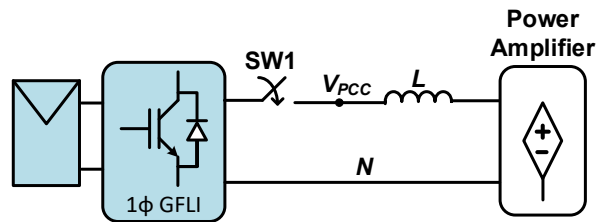


Figure 8.3: Experimental setup for the GFL inverter.

Table 8-2: Inductor Values and Corresponding SCCR

Inductor Value (L)	SCCR
5 mH	15.2
10 mH	7.6
15 mH	5.1

For each experiment, the GFL inverter was set to deliver rated power at unity power factor. Figure 8.4 and Figure 8.5 show the experimental results of the voltage and current traces for the different values of the interfacing inductor. Notice from both figures that with $L=0$ (no inductor) and $L=5$ mH, the GFL inverter connects and maintains stability without noticeable transient dynamics. However, for the largest available inductor value ($L=15$ mH), the inverter makes two interconnection attempts with noticeable transient dynamics (voltage spikes) before the final interconnection, on which stability was maintained.

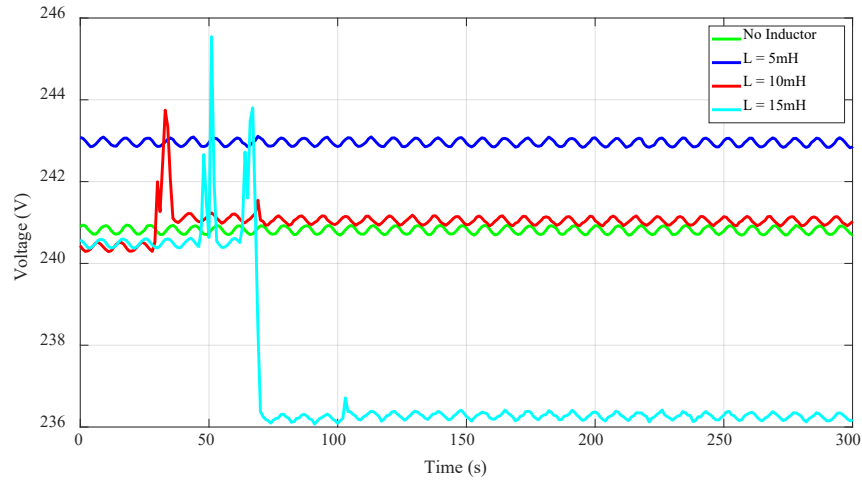


Figure 8.4: Voltage traces at PCC for each value of L .

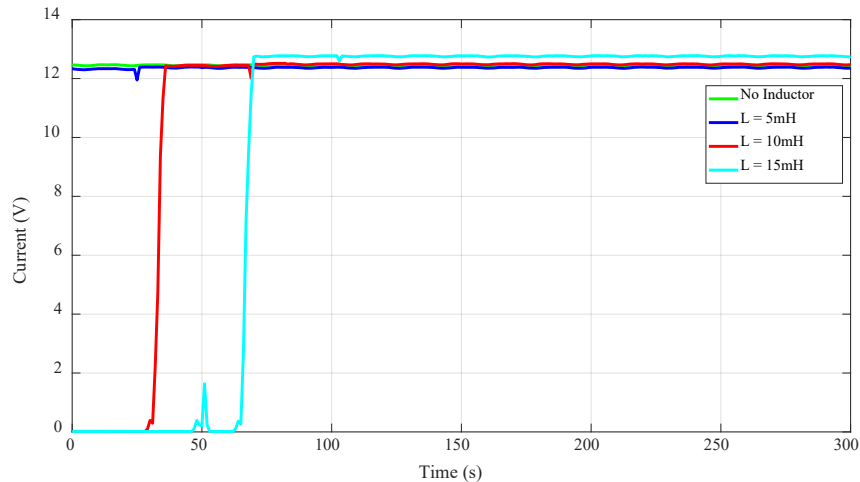


Figure 8.5: Current traces for each value of L .

For the SCCR values tested, the internal stability of the inverter was maintained. However, as the SCCR of the system was reduced by increasing the value of L , the inverter showed noticeable voltage spikes as if it attempted to adjust the PLL dynamics before making a successful interconnection. Of further interest is the analysis of these dynamics shows correlation to either: a PLL's parameters adjustment or a control scheme (using adaptive, or robust control) that considers the dynamics of the PLL.

Regarding GFM inverters, the inverter under test was the PCS100 from ABB, which uses the Virtual Generator Mode (VGM) while operating in grid-forming mode. The inverter interacts with the grid emulating a synchronous generator by presenting a low-impedance voltage source to the grid. Because of the lack of spinning mass, this behavior is emulated through power electronic control, and the physical inertia is emulated within the PCS100 control scheme, providing a damping response to the grid frequency through the energy storage device connected on the DC side [23]. While in VGM, the GFM inverter can be operated in either: PQ power flow control mode, where the converter operates with set-points for active and reactive power; or Vf control, where the converter operates with fixed voltage and frequency set-points

allowing islanding. These two control modes can switch while the GFM inverter is running. Figure 8.6 shows the control block diagram of the PCS100 while in grid-forming mode.

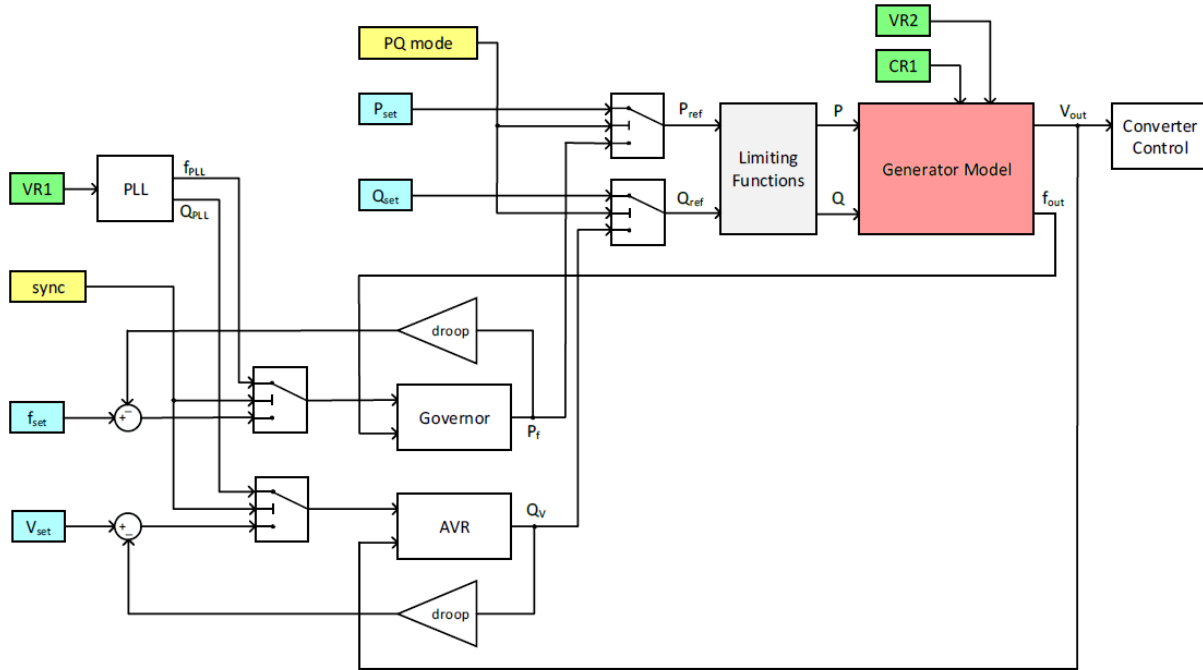


Figure 8.6: Control block diagram of PCS100 (courtesy of ABB PCS100 user’s manual) [23].

The dynamic equations of the synchronous generator are embedded inside the generator model block in Figure 8.6, where the only parameter available for the user to modify is the inertia time constant (H) of the swing equation. The range for H goes from 10 ms to 10000 ms.

According to ABB technical services, testing the effect of H is best done using PQ power flow control mode (disconnects the governor) and setting P_{ref} while grid connected, and then opening the grid connection. The output frequency of the inverter will then rise/fall dependent upon P_{ref} sign, and the system will trip finally on over/under frequency. For this test, P_{ref} was set to 10 kW, and the over-frequency upper limit was set to 69 Hz. The voltage waveforms were captured and post-processed to extract the frequency dynamics using a fast response, synchronous reference frame PLL with $K_p=100$ and $K_i=500$. The plots of the frequency dynamics for different values of H are shown in Figure 8.7, where evidently for larger values of H the dynamics are slower. Of special attention is the magnified area in Figure 8.7, where the initial slope of each curve seems to be very similar during the first 20 ms after the grid connection was removed.

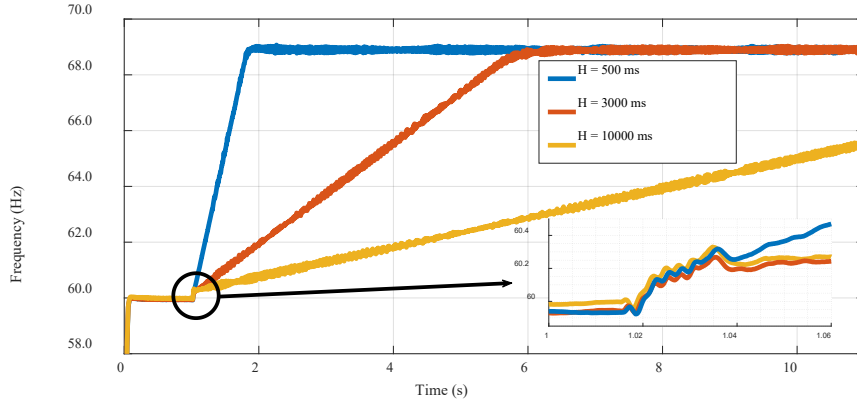


Figure 8.7: Frequency dynamics for different values of H.

This similar initial ramp seems to dominate the dynamics during small frequency deviations as the ones present in stiffer power systems. Whereas, for weaker systems, the second ramp related to the corresponding value of H, must have a significant impact on the frequency dynamics. This type of impacts on system dynamics can be studied by interfacing the GFM inverter in power hardware-in-the-loop (PHIL) [24], [25].

Furthermore, comparisons between GFM and GFL inverters were made to investigate their frequency responses under different droop values [26]. For the GFL inverter, the AC source the inverter was connected to was programmed to ramp to 61 Hz at various rates. Figure 8.8 shows the inverter’s response for a rate of 100 Hz/s. Something to note is that the response of the GFL inverter is very linear, with the power ramping down over the span of around 500 ms, with a slight undershoot before reaching steady state. More experimental data and tables for different rate of change of frequency (ROCOF) are discussed in [26].

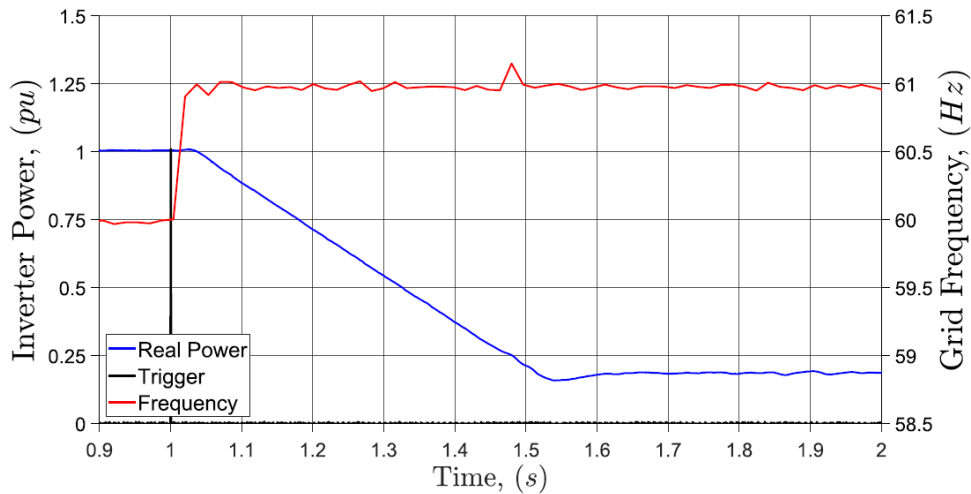


Figure 8.8: GFL inverter frequency response (100 Hz/s ramp to 61 Hz).

The GFM inverter was first interconnected to the grid simulator to see its response to different ROCOF values at a fixed frequency droop of 2%. Another important parameter that needs to be set in the GFM inverter is the Inertia Time Constant (ITC), which emulates the very same ITC present in synchronous machines. Figure 8.9 shows the response of the inverter. Notice how the frequency settling time is significantly faster than the GFL inverter. Additionally, to slow down the frequency response time, higher

droop setpoints are required, and thus larger changes in frequency are observed. This can be detrimental to sensitive loads such as motor loads if low frequencies are sustained. For further experimental information regarding different ITC values consult [26].

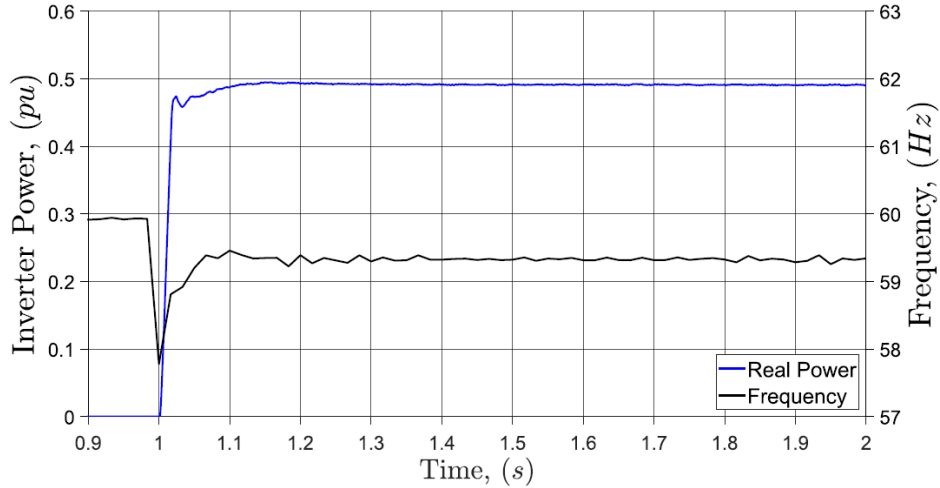


Figure 8.9: GFM inverter islanded frequency response (2% droop, 1000 ms inertia time constant).

Finally, experiments related to the dynamic interactions between a diesel genset and a GFM inverter were conducted. Both devices shared a 60-kW load. The GFM inverter was left at default inertia settings, set to VSI-VF with 1% frequency droop, and 5% voltage droop. The genset was operated in isochronous mode, which constrains the power sharing in the steady state and forces the power contribution from the inverter to almost zero. The results of this test are shown in Figure 8.10. Notice how the genset power overshoot (blue trace) is mostly absorbed by the inverter (red trace). Also notice that the steady state frequency (pink trace) goes back to nominal due to the lack of droop in the genset.

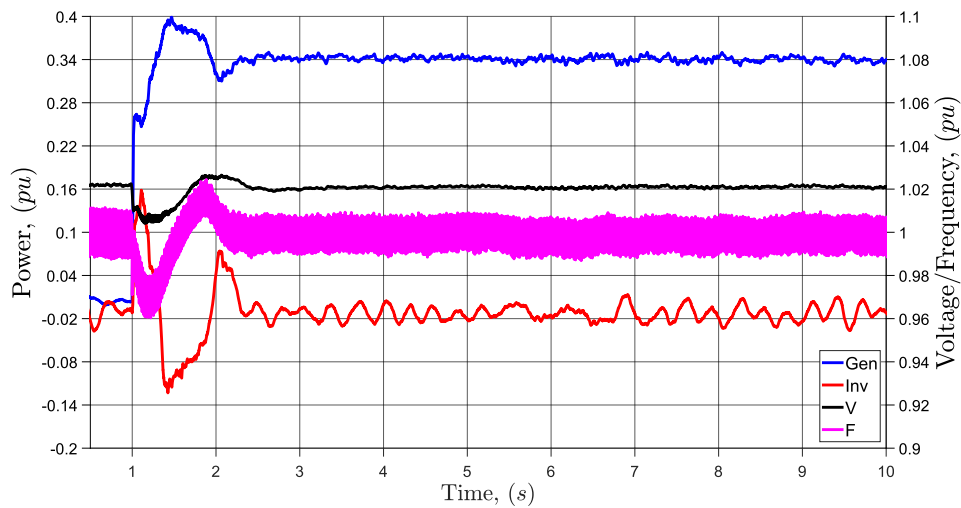


Figure 8.10: GFM inverter and genset responses.

8.4 WSU Co-Simulation

The following sections contain the technical details for the co-simulation work that was conducted.

8.4.1 Power-Communication-Control Co-simulation Development

The goal of the Co-Simulation Platform is to enable the analysis of distributed algorithms for the networked microgrid control in an electric power distribution system. The platform uses the Hierarchical Engine for Large-scale Infrastructure Co-Simulation (HELICS) [27] at its core to coordinate several different simulation programs. The physical power system is simulated using GridLAB-D [10], the communication system is simulated with ns-3 [28], and the controllers and other logical agents are separate python programs.

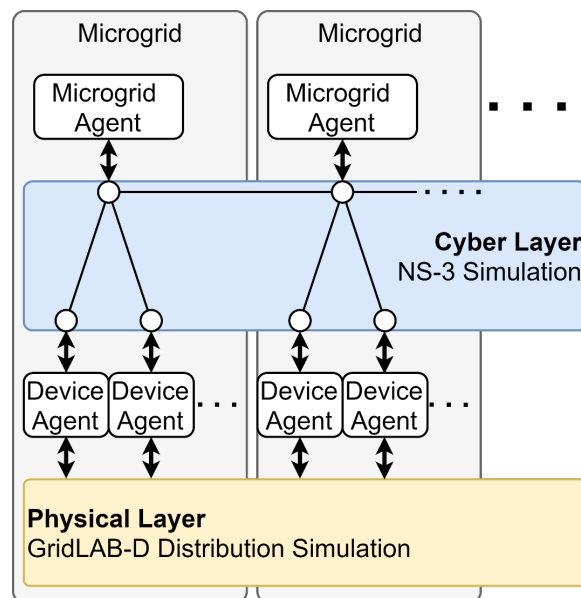


Figure 8.11: Cyber-physical co-simulation platform.

8.4.1.1 Physical Layer

The power system model is simulated using GridLAB-D. The physical system model includes distributed generators with smart inverters capable of four quadrant operation. Multiple microgrids (MGs) may be integrated with the distribution system; however, the entire system is simulated as a single system in GridLAB-D. Though each MG is physically interconnected as one system, each MG has a single microgrid control agent (MGC) which can only observe and control assets within the boundaries of the local MG. The physical layer is depicted as the lowest box in Figure 8.11. It interfaces with the cyber layer through device agents which parse received commands and format measurement data to send to the local MGC.

8.4.1.2 Cyber Layer

The cyber layer of the co-simulation platform is composed of the communication network model simulated in ns-3 environment. It is integrated with microgrid control agents modeled using Python 3. The MGCs (Microgrid Controllers) are shown as the highest block in Figure 8.11. The MGC agents include the

control/optimization algorithm needed for the coordination of the networked microgrids. The MGCs receive measurements from metering devices, send commands to controllable devices, and communicate key information to other MGCs according to the distributed algorithm.

All communication between agents is passed through the communication network, which is simulated in ns-3 [28]. In the ns-3 simulation, point-to-point links, which represent fiber optic links, connect all the communication nodes, and have predefined data-rates in bits per second (bps) and time-delays in milliseconds (ms). The ns-3 simulation uses global centralized routing for routing packets through the network [29]. This routing method is based on the Open Shortest Path First (OSPF) protocol, which is a type of commonly used Interior Gateway Protocol (IGP) [30]. This protocol routes packets through the path with the least number of links without consideration for actual travel time.

8.4.1.3 HELICS

HELICS is the core of the co-simulation platform. It manages all the disparate simulations (known as federates), keeping them coordinated and facilitates message passing between federates. Connections between the GridLAB-D federate and the Python-based device agents use HELICS publications and subscriptions. Connections to the ns-3 communication network use HELICS endpoints.

8.4.2 Distributed Coordination in IEEE Test System

IEEE test systems were run using the HELICIS platform for co-simulation analysis.

8.4.2.1 Co-Simulation Using IEEE Test Systems

A variety of case studies were conducted using the IEEE-123 bus system. The system was divided into 4 areas or microgrids (MGs). The IEEE-123 bus system is a three-phase unbalanced systems. Simulations were conducted using variants of the IEEE-123 bust system with different arrangements of distributed energy resources (DERs) in the system. In one arrangement, 10 three-phase buses with DERs and smart inverters (nodes: 15, 23, 30, 37, 49, 50, 51, 67, 78, 107) are simulated. Another variant simulated another arrangement with higher DER penetration, having 30 nodes with smart inverters (nodes: 3, 9, 15, 20, 23, 25, 30, 37, 44, 49, 50, 51, 56, 59, 62, 65, 67, 78, 88, 93, 95, 99, 101, 102, 103, 107, 110, 119, 120). By default, each inverter had a capacity of 60kVA per-phase (50kW active power capacity per-phase). An additional use-case with 48kVA per-phase, and 40kW active power capacity per-phase was conducted.

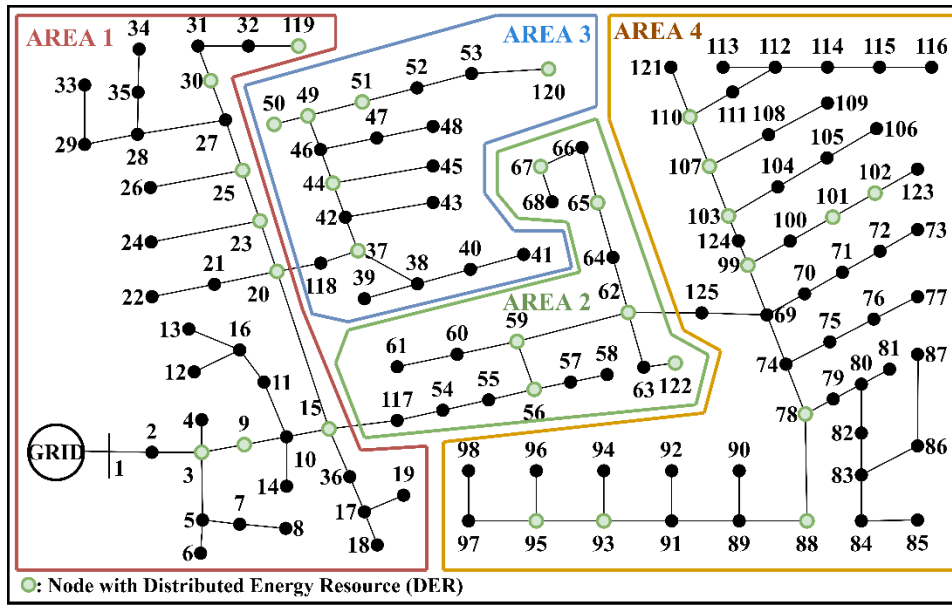


Figure 8.12: IEEE 123-bus test system divided into four areas.

8.4.2.2 Algorithms Implemented

For networked microgrid coordination, the distributed optimal power flow algorithm (D-OPF) called Equivalent Network Approximation method (ENApp), developed by WSU [31] was used. The distributed algorithm decomposes the optimization problem into several sub-problems, that model the local OPF problem for each area. The D-OPF algorithm then solves each local problem and utilizes the local OPF solutions to obtain the system-wide solution.

The algorithm works in the following way. A computing agent, or microgrid controller (MGC), is assigned to each area. Each agent models downstream areas as constant loads and the upstream area as the voltage source and independently minimizes the objective function only for its area. Once the OPF is solved, each agent shares the solved bus voltages (at the area boundary) with the downstream areas and the solved power flow (active and reactive) with the upstream area. In next iteration, each agent updates the values used for their source voltage and loads based on received values from the neighbors. Within the co-simulation platform, MGCs run a linear approximated model to solve the optimization problem [32]. The linear model does not account for power losses and may result in errors in voltage and power flow solutions. To account for these errors, the implemented optimal solutions obtained from the D-OPF to the GridLAB-D model of the system. Then the voltage and power flow values obtained from the GridLAB-D simulator are transmitted to the neighboring MGCs. The GridLAB-D corrector model is referred to as a digital twin (DT).

In [31], implementation of the algorithm is validated on the co-simulation platform. They show results for two different objectives, loss minimization and DER maximization and compare the results achieved using different methods. Results in Table 8-3 show that both linear D-OPF methods, which use the co-simulation platform, produce solutions very close to the Nonlinear OPF which uses a nonlinear solver to get an exact solution. Furthermore, the method using DT to correct the power flow solutions obtained from approximated D-OPF resulted solutions closer to the nonlinear D-OPF model.

Table 8-3: Loss Minimization and DER Maximization Results Using Different Methods.

Method	Loss Minimization		DER Maximization	
	Loss (kW)	Communication Round	Generation (MW)	Communication Round
No OPF	53.338	-	5.4	-
Linear C-OPF	26.508	0	5.135	0
Linear D-OPF	26.546	5	5.135	7
Linear D-OPF+DT	27.238	5	5.163	5
Nonlinear OPF	27.16	-	5.18	-

8.4.2.3 Effects of Communication on Algorithm Output

To verify the robustness of the proposed D-OPF algorithm when subjected to poor communication network conditions, the algorithm with the DT is tested with two different communication network topologies (each for three different data-rates) for the loss minimization problem and for the DER maximization problem. The two topologies include an ideal topology and a circle topology. In the ideal topology, each area controller has a direct link with its immediate neighbors and a direct link with devices (inverters and meters) in its own area. In the circle topology all devices and controllers are connected in a single large loop without regard to physical location. The purpose of the circle topology is not to be realistic, but rather to show how different topologies can have an impact on the system operations. Each link between network nodes is a point-to-point link with a negligible delay and a bandwidth of 3kbps, 2kbps, or 1kbps. These bandwidths were chosen because they test the lower limit functionality for the algorithm.

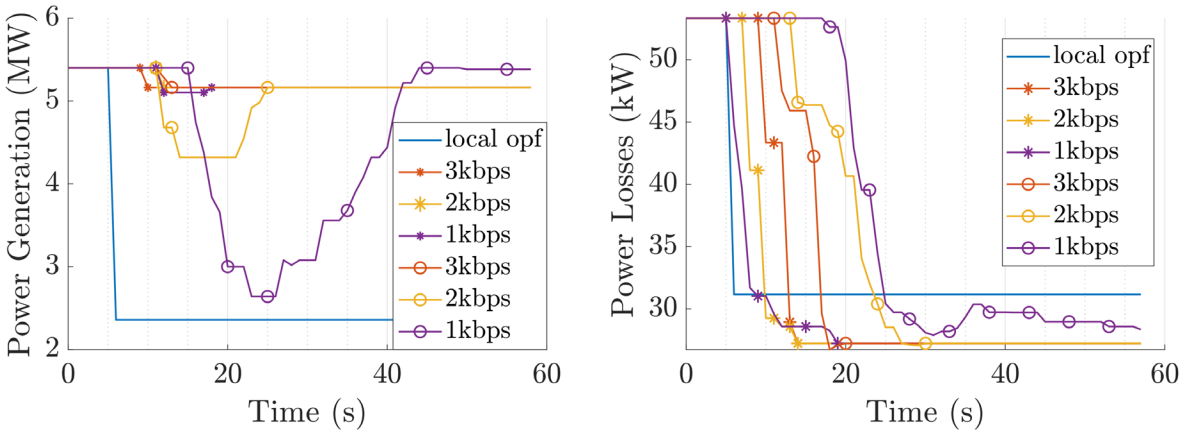


Figure 8.13: Communication stress test.

The plots of Figure 8.13 show how the objective values, as measured, change as the optimization runs. The lines marked with circles indicate results run with the circle topology and lines marked with a star indicate the ideal topology. The blue line in each plot, marked "local opf" in the legend, shows the results if no communication is allowed between controllers and the controllers have perfect communication links with local devices. In both figures, it can be seen that even the worst cases were still more optimal than the "local opf" case.

There are several effects of poor communications to be observed:

- If a controller doesn't receive data from any of the neighboring areas because of data delays, it will falsely assume convergence and dispatch the inverters prematurely. When the delayed data does arrive, it will continue to iterate.
- Dispatch commands sent to different inverters in an area may not arrive simultaneously.
- If meter data takes too long to get to controllers, it cannot be used to enable a warm start for optimization.
- Delayed communication between areas does not prevent convergence except in extreme cases.
- The quality of the resulting solution, as measured after settling, is not impacted by the communication delays.
- Extreme communication delays may prevent the system from settling at the solution.

8.4.3 Co-Simulation Model Development for EPB System and Validation

PNNL developed and validated the GridLAB-D version of the EPB models. The model consists of: 3 sub-transmission substations, 4 distribution substations, and 5 main feeders. The model also contains microgrids 1, 2, and 3 as depicted in Figure 8.1.

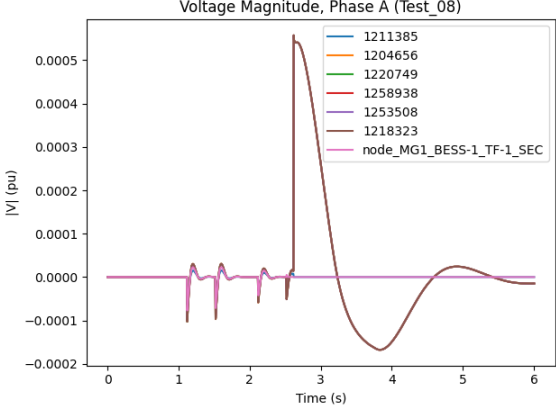
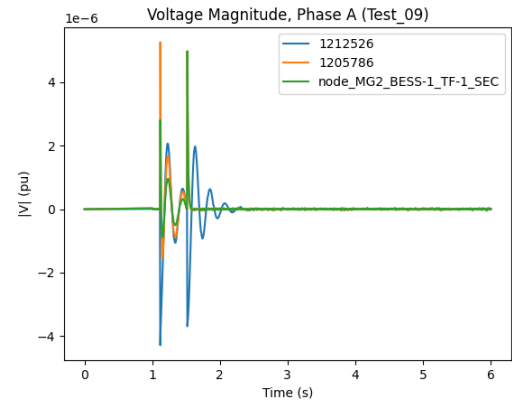
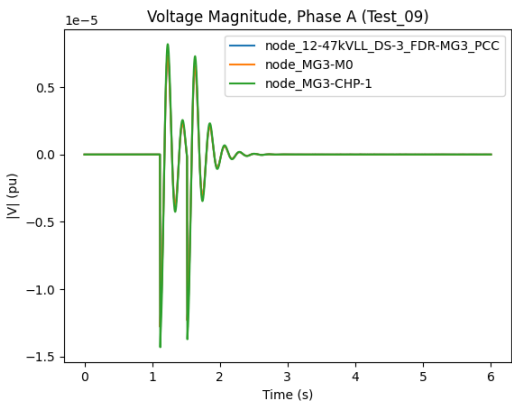
The goal in this section is to validate the co-simulation model for the EPB system. To this end, the project developed a power-communication co-simulation model using HELICS platform. Additionally, the collaborative autonomy algorithm developed by LLNL in the co-simulation platform was validated. The architecture of the co-simulation was the same as described in Section 8.4.1. A simplified communication system model with a hub and spoke architecture was used. The main EPB control center is the hub, and all other nodes are connected to it via a point-to-point link.

8.4.3.1 Test Case Replication on Co-Simulation Platform

PNNL produced a series of test cases for validation of the GridLAB-D models. WSU replicated several of these test cases using the co-simulation platform for validation. Initial tests were run to validate that the co-simulation platform could produce the same results that PNNL got using GridLAB-D. The results of the comparison between the original GridLAB-D tests and the tests run on the platform are shown in Table 8-4. The plots in the table show the validation error on select nodes calculated as co-simulation result minus pure GridLAB-D result. In all of the tests the errors are small and largely the result of small timing differences.

Table 8-4: Validation of EPB Co-Simulation

Test Name	Description Summary	Time Step	Difference in the simulation results obtained using GridLAB-D simulation and Co-Simulation Model
Test 5	Disconnect MG3-CHP-3, MG2-BESS-1	10ms	<p>Voltage Magnitude, Phase A (Test_05)</p> <p>The plot shows voltage magnitude V (pu) on the y-axis (ranging from -0.0006 to 0.0000) versus Time (s) on the x-axis (ranging from 0.0 to 3.0). A red horizontal line at 0.0000 pu represents node_MG3-CHP-3. Other nodes (1212526, node_12-47kVLL_DS-3_FDR-MG3_PCC, node_MG2_BESS-1_TF-1_PRI) show a sharp negative spike at approximately 1.2s, followed by a gradual decay towards zero.</p>
Test 6	Disconnect MG1-PV-1,2,3, MG1-BESS-1	10ms	<p>Voltage Magnitude, Phase A (Test_06)</p> <p>The plot shows voltage magnitude V (pu) on the y-axis (ranging from -0.00025 to 0.00005) versus Time (s) on the x-axis (ranging from 0.0 to 3.0). A purple horizontal line at 0.0000 pu represents node_1253508. Other nodes (1211385, 1204656, 1220749, 1258938) show a sharp negative spike at approximately 1.2s, followed by a gradual decay towards zero.</p>
Test 7	Disconnect MG1-PV-1,2,3, MG1-BESS-1, MG2-BESS-1	10ms	<p>Voltage Magnitude, Phase A (Test_07)</p> <p>The plot shows voltage magnitude V (pu) on the y-axis (ranging from -0.00025 to 0.00005) versus Time (s) on the x-axis (ranging from 0.0 to 3.0). A purple horizontal line at 0.0000 pu represents node_MG1_BESS-1_TF-1_SEC. Other nodes (1211385, 1204656, 1220749, 1258938, 1253508, node_MG2_BESS-1_TF-1_SEC) show a sharp negative spike at approximately 1.2s, followed by a gradual decay towards zero.</p>

Test 8	Island MG1	5ms	
Test 9	Island MG2	5ms	
Test 10	Island MG3	5ms	

8.4.3.2 Collaborative Autonomy Implementation on Co-Simulation Platform (EPB System)

The EPB co-simulation platform was also tested against LLNL’s CA Algorithm. This test was designed to demonstrate the ability of the platform to run a control algorithm with the EPB distribution system model. The goal was to provide voltage support to the distribution system using controllable resources from the microgrids. Specifically, the simulation implemented the CA algorithm developed by LLNL to control the reactive power supplied by microgrids to improve the distribution systems voltages in the event of a low-voltage condition, triggering a Mode 2 operation for the networked microgrids. The simulations also

demonstrated how the performance of the algorithm changes with change in communication system parameters especially under stressed communication system conditions. The simulation testcase is described next. The EPB system (Figure 8.1) is simulated with the source voltage to Sub-Transmission Substation 3 (STS 3) held at 0.96 pu voltage (Figure 8.14). Since Distribution Substation 2 (DS 2) is fed from STS 2 as well, the low voltage does not propagate to DS 2. At $t=1.01s$ the switch connecting STS 2 to its source is opened. This allows the low voltage to propagate downstream to FDR 1 (highlighted in Figure 8.14). The same switch closes at $t=2.01s$ bringing the system voltage back to normal. Also note, the switch connecting Microgrid 3 (m3) is disconnected throughout the test, preventing the CHP units from interfering with the test. Multiple load nodes within FDR1 were used to measure voltages. Note that FDR1 does not have any resources to provide reactive power support, thus has $Q_{reserve}=0$. Microgrid 2 (MG 2) is controlled to provide reactive power from its battery storage unit (with a $Q_{reserve}=2,368,543$ var). The communication network used had link delays of 0.05ms and bandwidths of 100 Gbps. Each agent has a direct link to the DMS node and a link to the local controllable devices.

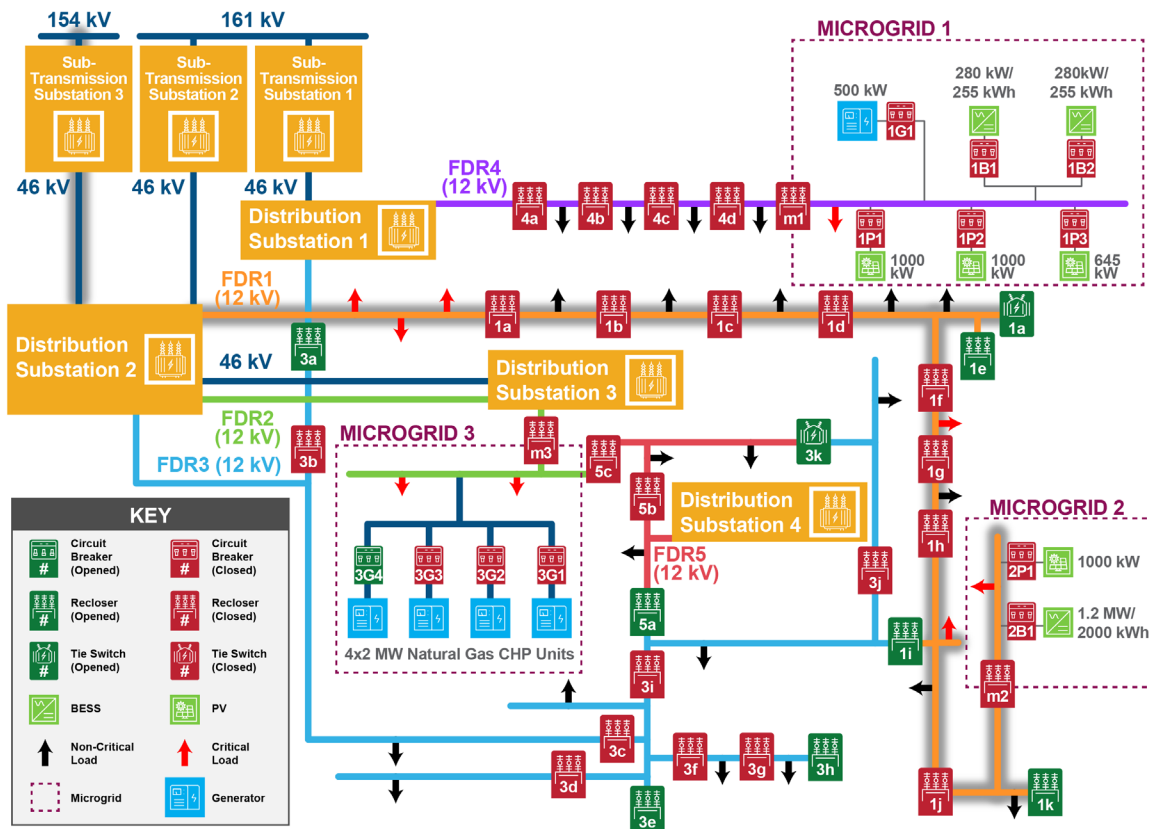


Figure 8.14: EPB systems test case simulation.

Parameters used:

- Each voltage measuring agent was given an equal weight of 0.2.
- Gains were initialized as $K=3$.
- The threshold for determining if a voltage drop has occurred was set at 0.94 p.u.
- After activating Mode 2 (voltage support mode), the goal of the control algorithm is to raise the bus voltages by providing the reactive power support.

- Once the low voltage event is mitigated, i.e. voltage > 0.95 pu, the system returns to normal mode, i.e. Mode 1.
- The simulation time step is set to 0.1s.

Timing:

- Overall time step: 0.1s.
- Voltage measurements from FD1 are sent at $t+0.01s$.
- Reactive power control decision sent at $t+0.02s$.
- Reactive power is dispatched at $t+0.03s$.

Test cases:

- Case 0: No support
- Case 1a: Replication of LLNL study, implementation of collaborative autonomy.
- Case 1b: Network stress test – Same as Case1a except bandwidth of network links is reduced to 750 kbps.
- Case 2a: Additional controllable asset introduced by replacing MG3 with an inverter having the same capacity as the battery inverter in MG2. The new inverter starts with zero output.
- Case 2b: Added voltage measurement point to MG3. The new voltage measurement has the same weight as others in the algorithm.
- Case 2c: MG3 voltage measurement point has double the weight assigned to others.

8.4.3.3 Co-Simulation Results

In all cases, the algorithm was successful in detecting the low voltage event and was able to provide reactive power to raise the voltage while the low voltage event was taking place. Additionally, when the low voltage incident was mitigated (i.e. system restored to Mode 1), the algorithm successfully detected a return to the normal state. The plot in Figure 8.15 shows the phase-B voltage on DS 2 throughout the test for each test cases.

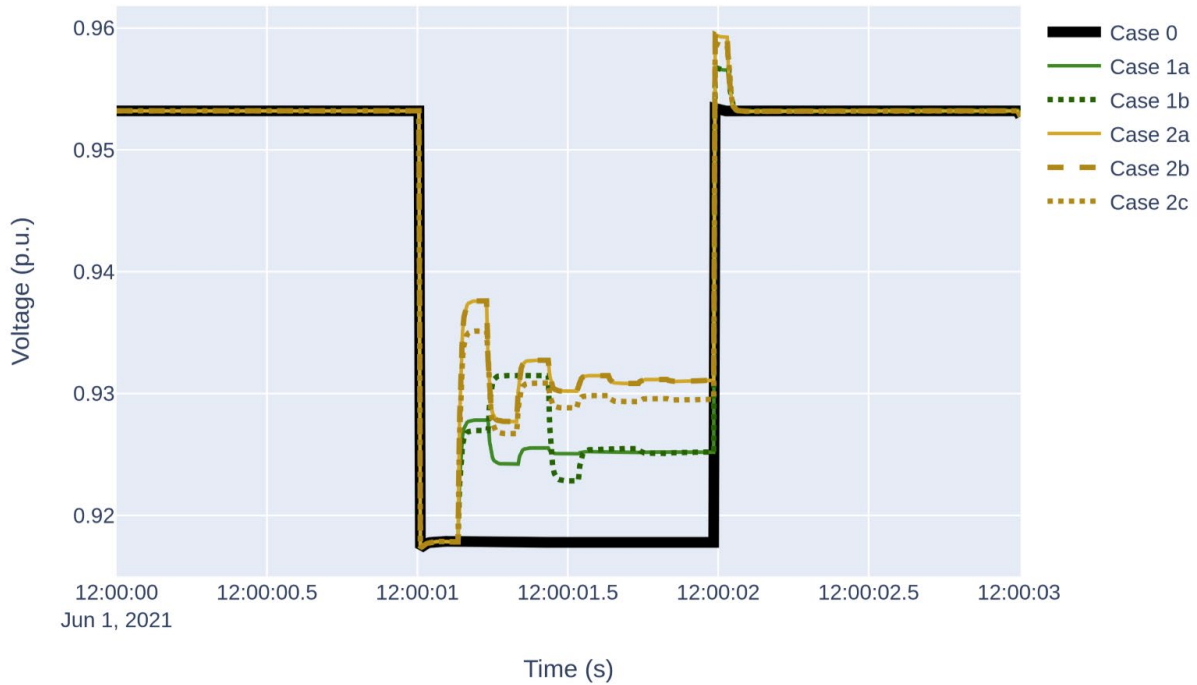


Figure 8.15: Voltage control using collaborative autonomy on EPB test systems.

Discussion on Case 1: Compared to Case 1a, Case 1b shows how the undervoltage mitigation is impacted when the communication bandwidth is reduced to 750kbps. The effect of data delays on the functioning of the algorithm depends strongly on how the algorithm is designed to handle missing or delayed transmissions. In the current implementation there are few checks to manage missing data. A more robust implementation could run with bandwidth values much lower than 750 kbps. This could be achieved in a few ways. One method would be to allow all the agents to wait up to a maximum time delay to allow more data to arrive. Additionally, old data could be used up to a maximum age, and contingencies for missing data could be implemented.

Case 2, as expected, provides more support since additional reactive power is available from MG3. In Case 2b, an additional voltage measurement point is added at MG3, however, since this voltage is much higher than the other voltage measurements, it is rejected as a bad data point. In Case 2c the MG3 measurement is assigned double the weight of other measurements, to incentivize the algorithm to trust this measurement. As a result, in case 2c, the new measurement is not rejected. Since the average voltage is closer to the desired voltage, the algorithm requests lesser reactive power from both microgrids, MG2 and MG3, resulting in overall lesser voltage support.

8.5 ORNL COMMANDER Testbed Emulation

In the field, it is challenging to find a set of multiple microgrids in close electrical proximity to one another through which research on co-dispatch and consensus can be performed. Furthermore, there are operational considerations and limitations on the types of experiments that can be performed on field systems, including customer outages, faults, and system flexibility. To compensate for these limitations, ORNL built the Coordinated Management of Microgrids and Distributed Energy Resources (COMMANDER) testbed.

As depicted in Figure 8.16, COMMANDER implements 3 microgrids in hardware for the testing and validation of various aspects of microgrid and DER integration including: optimization, controller interactions, reconfiguration dynamics, power quality, as well as others. Each microgrid includes 2 DC supplies and inverters, a motor-genset, a load, and 2 reclosers – 1 for a grid connection, 1 for reconfiguration. Currently, in each microgrid 1 DC supply drives a commercial PV inverter, and the other drives a V/f capable commercial energy storage inverter. Each microgrid has about 100 kW of total generation and load, bringing the full testbed rating to nearly 300 kW. There also exists a grid simulator acting as the grid connection for each microgrid. This simulator allows us to test various grid conditions such as low/high voltage, and certain types of transients.

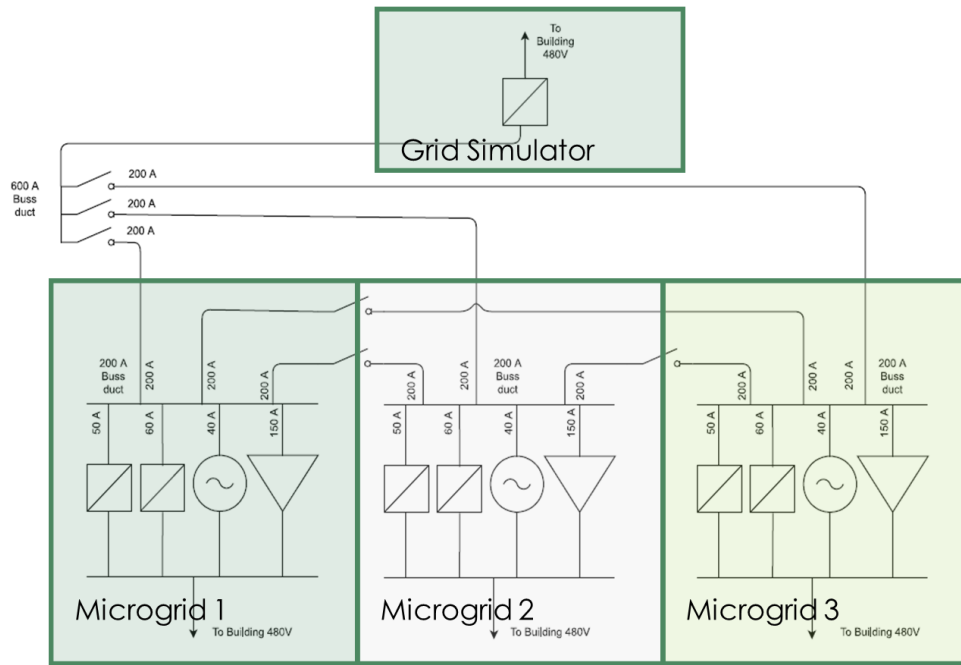


Figure 8.16: One-line diagram of COMMANDER testbed.

Each microgrid within the COMMANDER testbed has its own microgrid controller. The controllers handle all the device communication, startup/shutdown, optimization, dispatch, and forecasting for the microgrids. Different optimization algorithms can be performed by the controller to achieve grid functions, such as: voltage support, economic dispatch, islanding, black start, and others. Also, each controller has the capability to accept direct commands externally, such as real and reactive power requests. The controller will then dispatch the DER within the microgrid to try and reach the requested setpoint at the point of interconnection. For this project, the microgrids and their controllers were leveraged to implement the collective autonomy algorithms.

9.0 Field Demonstration

9.1 Field Demonstration Summary

This section contains excerpts from the Citadels Integrated Assessment Plan (IAP), which defined the procedure and events that were used to demonstrate, in a physical setting, the concepts developed over the course of the Citadels project. The field demonstration was carried out during the week of September 26, 2022, in the vicinity of EPB of Chattanooga’s central headquarters, in Chattanooga, TN. Teams of individuals from EPB, PNNL, ORNL, LLNL, and OpenFMB participated onsite at EPB headquarters and at the ORNL “Commander” microgrid testing facility.

The field demonstration was comprised of 12 events grouped into three categories: Steady State, Event Based, and Failure Events. Table 9-1 tabulates and provides details of each event. Steady State events (1-5) were designed to test to what extent networks of autonomous microgrids could mesh their operations into the well-established methods under which the grid is operated today. Event Based events (6-9) tested how well microgrids could regulate their own actions under autonomous operations. Failure Events (10-12) tested microgrids’ abilities to contend and mitigate common failures that could occur in the system.

Table 9-1: Field Demonstration Events

	Number	Event	Importance	Difficulty	Risk
Steady State	1	Verify pub/sub data exchange between all architecture components (at all five microgrids)	High	Low	Low
	2	Verify that each authorized controller can execute commands on field devices	High	Low	Low
	3	Coordinate protection settings between grid edge controllers, SCADA, and breakers/reclosers	Medium	Medium	Low
	4	Verify that grid edge controllers can distinguish between line clearances and hot line work permits	Medium	Medium	Low
	5	Verify that change in topology, as indicated by reclosers, is observed and changes tracked	High	Low	Low
Event Based	6	Add and drop authorized controller and verify how the consensus is affected (add/drop a laboratory microgrid controller)	High	Medium	Medium
	7	Microgrid controllers able to determine the mode of operation and coordinate with other controllers	Medium	Medium	Low
	8	Consensus that results in voltage/reactive power change (at EPB microgrid)	High	Medium	Medium
	9	Black start of a microgrid (at EPB microgrid)	Medium	Medium	Low
Failure Events	10	Failure of one or more sensors (at laboratory microgrid)	Medium	Low	Low
	11	Loss of communication to a microgrid (at laboratory microgrid)	High	Low	Low
	12	Byzantine Actor (at laboratory microgrid)	High	Medium	Low

For each of the events in Table 9-1, there is an indication of “Importance”, “Difficulty”, and “Risk”. These indicate how important the event is to the field validation, how difficult it will be for the team to operationally execute the event, and what the perceived risk with respect to safety and service interruptions. Because there are not clear metrics for quantifying these values, each was assigned “Low”, “Medium”, or “High” designation as part of the planning process in the IAP.

9.2 Description of Field Demonstration Events

This section provides more detail about the 12 events that were carried out in the field demonstration.

9.2.1 Event 1: Verify Pub/Sub Data Exchange between All Architecture Components

Event 1 was considered high importance, a low level of difficulty, and a low level of risk.

9.2.1.1 Event 1: Overview

This event established a baseline of the full solution by verifying proper configuration and commissioning of all the advanced technology elements: OpenFMB, CSEISMIC microgrid controller, and consensus algorithms. In a Blue-Sky situation, it was important to make sure that accurate data was flowing between affected systems and their intended origins/destinations, and that everything was working as expected.

For this event, there were two elements. First, SCADA values for each device were measured, and using the OpenFMB Message Inspector, compared with messages published by the corresponding adapter. For each subscribing adapter and device, the values received by the device were compared with Message Inspector values. Second, for publishing and subscribing to the two main systems, data from the sending system/device were compared with the data at the receiving system.

As expected, both the OpenFMB Visualization Tool and the Message Inspector were used to verify data flow and troubleshooting as needed.

Consensus Algorithms that send and receive consensus data from collaborative agents were similarly compared.

9.2.1.2 Event 1: Initial Operating State

This test began with the system in a steady state condition under Blue Sky conditions with all microgrids operating in Mode 1.

The field had the CSEISMIC microgrid controller speaking directly to devices. Communications with collaborative agents or devices outside the microgrid were accomplished through OpenFMB.

The microgrids in the Commander test bed were OpenFMB-enabled, so all communications that originated or received in the Commander testbed flowed through OpenFMB.

With that in mind, each of the microgrid nodes were verified for proper configuration, and their connectivity with devices and other microgrid nodes was verified before beginning the test. Therefore, all microgrids were connected to the OpenFMB Harness, and each one was capable of participating in consensus decisions.

9.2.1.3 Event 1: Initiating Condition

Because this event was a steady state event, it was initiated with the beginning of data collection.

9.2.1.4 Event 1: Anticipated System Response

As intended, there was no active response resulting from running this scenario. The intent was only to verify the passive publish and subscribe data exchange between affected devices.

9.2.1.5 Event 1: Results

Table 9-2: Field Demonstration Event 1 Results

Event #	Affected Microgrids	Event Switching and Execution Steps	Data Collection Point	Results
1	Lab and Field Microgrids	None	CA: All CA containers transmitting modes and are consistent across all agents. OpenFMB: OpenFMB messages seen from devices on all nodes. Messages verified using the OpenFMB Message Inspector.	* Retrieved screenshot(s) from Open FMB that shows typical data point values.

9.2.2 Event 2: Verify that Each Authorized Controller Can Execute Commands on Field Devices and Topology Changes are Tracked by Subscribed Controllers and Consensus Algorithms

Event 2 was considered high importance, a low level of difficulty, and a low level of risk.

9.2.2.1 Event 2: Overview

The purpose of this event was to verify that controllers executed commands on operational devices in the field, with the key aspect being that commands issued from distributed controllers did not conflict with other distributed controllers. This operation was tested by changing the position of a normal open. A normal open is a point on a distribution feeder(s) where one section of the feeder is physically isolated from the other. The normal open is usually established by an open switch or reclosing device. The nomenclature is suggestive of the normal state of the switch or recloser, being in an open configuration. There are three types of testing that were completed:

- CSEISMIC data exchange with Field Devices (directly via DNP3), Lab Devices (via OpenFMB, and SCADA.

9.2.2.2 Event 2: Initial Operating State

The event began with the system under Blue Sky conditions in a nominal configuration. Microgrids were grid-connected and in Mode 1. All microgrids were connected to the OpenFMB Harness, with the ability to participate in consensus decisions.

9.2.2.3 Event 2: Initiating Condition

The normal open recloser was commanded by the microgrid controller to close, paralleling the two feeders. A 30-second delay was observed for the system to stabilize, after which the new normal recloser was sent a command by the microgrid controller to open, establishing the new normal open.

9.2.2.4 Event 2: Anticipated System Response

The affected reclosers were cycled open and closed as commanded by the controlling microgrid. All subscribed devices reported the action through the OpenFMB Harness using pub/sub protocols.

9.2.2.5 Event 2: Results

Table 9-3: Field Demonstration Event 2 Results

Event #	Affected Microgrids	Event Switching and Execution Steps	Data Collection Point	Results
2	Field Microgrid	EPB microgrid controller - command present normal open CLOSED	Log that all agents logged change in EPB system topology.	1) Time 9:55 Eastern - Closed recloser, SCADA Logged change, all agents logged change
		EPB microgrid controller - command new normal open recloser OPEN	Log that all agents logged change in EPB system topology. OpenFMB: Verify position change in OpenFMB status message.	1) Time 9:58 AM Eastern - Opened recloser, SCADA logged change. All agents logged change.

9.2.3 Event 3: Verify that Change in Topology, as Indicated by Reclosers, is Observed and Changes Tracked

Event 3 was considered high importance, a low level of difficulty, and a low level of risk. Event 2 and Event 3 occurred simultaneously. Event 2 verified that a microgrid controller could issue switching commands and Event 3 verified that changes were transmitted across OpenFMB and all subscribed devices tracked changes in system topology.

9.2.3.1 Event 3: Overview

This event verified that changes in system topology were reflected on the OpenFMB Visualization Tool, and that the microgrid controllers received the updated information.

9.2.3.2 Event 3: Initial Operating State

This event began with the system in a steady state condition under Blue Sky conditions with all microgrids operating in Mode 1, connected to the OpenFMB Harness, and with the ability to participate in consensus decisions.

9.2.3.3 Event 3: Initiating Condition

This event was initiated with Event 2

9.2.3.4 Event 3: Anticipated System Response

Beyond the change in system topology, no significant response was expected.

9.2.3.5 Event 3: Results

Table 9-4: Field Demonstration Event 3 Results

Event #	Affected Microgrids	Event Switching and Execution Steps	Data Collection Point	Results
3	Field Microgrid	No explicit action - log change in EPB topology when present normal open recloser CLOSED.	Log that all agents logged change in EPB system topology. OpenFMB: Verify position change in OpenFMB status message.	All agents logged change.
		No explicit action - log change in EPB topology when new normal open recloser is OPEN.	Log that all agents logged change in EPB system topology. OpenFMB: Verify position change in OpenFMB status message.	

9.2.4 Event 4: Coordinate Protection Settings Between Grid Edge Controllers, SCADA, and Breakers/Reclosers

Event 4 was considered of medium importance, a medium level of difficulty, and a low level of risk.

9.2.4.1 Event 4: Overview

This event ensured that microgrid controllers could issue commands to reclosers to change protection profiles. EPB’s reclosers were preprogrammed with four protection settings, and this event issued commands from a microgrid controller to a recloser to transition from one profile to another. Therefore, this event required no additional protection setting calculations. Instead, this event ensured that generated commands will not place the system in a mis-coordinated condition.

EPB’s pre-programmed protection profiles were applied in the forward and reverse current directions. The profiles had been configured based upon prior fault current analysis and coordination with other devices. Per their design, changing the protection profiles on the reclosers were normally accomplished by issuing manual commands through SCADA.

Based on experience with the Airport microgrid, EPB chose to create an islanded protection profile for reclosers that was based on voltage measurements. For reclosers in a series configuration and during an islanded configuration, the trip settings were created to first isolate the sections farthest away from the DERs to clear faults. For the Airport microgrid, this issue arose due to the low fault current supplied by inverter-based resources.

With grid connected microgrids interconnecting across the distribution system and having autonomous control over system protection devices and their operation, a future method is needed so that updated protection settings are coordinated and published over OpenFMB as the system topography changes. The coordination should be seamless between SCADA-enabled protection devices, central distribution control systems, and all microgrid controllers.

For Citadels testing purposes, a microgrid controller was forced to issue a command to a recloser to change its protection setting profile until a more autonomous method is developed.

9.2.4.2 Event 4: Initial Operating State

This test began with the system in a steady state condition under Blue Sky conditions with all microgrids operating in Mode 1. All microgrids were connected to the OpenFMB Harness with the ability to participate in consensus decisions.

9.2.4.3 Event 4: Initiating Condition

The command was executed by an authorized microgrid controller. The test was carried out according to the following steps:

- Issue command to test recloser to change its protection profile from Profile 1 to Profile 4.
- The other prescribed devices should register the protection setting change.

9.2.4.4 Event 4: System Response

The expectation was that the recloser under test would transition to the new protection setting profile and publish its new settings across OpenFMB, with other subscribed devices and CA registering the change in the protection profile.

9.2.4.5 Event 4: Results

Table 9-5: Field Demonstration Event 4 Results

Event #	Affected Microgrids	Event Switching and Execution Steps	Data Collection Point	Results	Agent Notes
4	Field Microgrid	Microgrid controller issued command to test recloser through SCADA to move from protection Profile 1 to Profile 4.	System operator reads value from SCADA OpenFMB: Verify change in OpenFMB status message (action presently not able to complete, may add later if time permits)	Received DNP3 error for 1st attempt, compiling a new image. Reloaded new image. New command sent 11:00 AM Eastern after new image load, received error again. Translator problem occurred. Successful after 2nd attempt	CSEISMIC – Needed to disable auto-restore on test recloser

9.2.5 Event 5: Verify Grid Edge Controllers Can Distinguish between Line Clearances and Hot Line Work Permits

Event 5 was considered medium importance, a medium level of difficulty, and a medium level of risk.

9.2.5.1 Event 5: Overview

The purpose of this event was to demonstrate that grid edge controllers, specifically the consensus algorithms and the CSEISMIC controllers could identify when a recloser was under a clearance or work permit. This was necessary to protect against a microgrid controller issuing a command to operate a device that was operationally out of service for maintenance and/or a safety issue.

It is regular industry practice for line clearances to be issued if work is to be performed with the affected section of grid deenergized and isolated from the grid. The deenergized section of grid is rendered safe and clear by isolating it with airgap switches at either end of the cleared section. Some utilities place manual clearance tags on the poles where the air gap switches are installed; other utilities perform lock-out, tag-out procedures. Therefore, the clearance requires switching orders and manual switching operations in the field. As an added precaution, both ends of the cleared section of grid are usually grounded. The line clearance is the safest way to perform manual work and usually carries severe repercussions if the terms of the clearance are neglected.

Hot line work permits are issued for simpler maintenance tasks in which line personnel work on the affected grid section while energized; they wear protective gear meant to insulate them from electric shock. Because the lines are energized, the risk of electrical shock and injury are increased over the deenergized clearance case; therefore, the reclosing function of upstream auto-reclosing devices is deactivated to protect line personnel in case contact is made with energized components or conductors.

Although physical safeguards (such as local grounding) are in place to protect line personnel from harm, the microgrid controllers should be able to recognize when field devices are involved and restricted under a clearance or hot line work permit, be aware that restricted devices cannot be involved in reconfiguring the system or in participating in self-assembly, and avoid taking any action on restricted devices either at the isolation points or within the confines of the clearance or hot line work permit.

9.2.5.2 Event 5: Initial Operating State

This test began with the system in a steady state condition under Blue Sky conditions with all microgrids operating in Mode 1. All microgrids were connected to the OpenFMB Harness, with the ability to participate in consensus decisions.

9.2.5.3 Event 5: Initiating Condition

The test proceeded as followed:

- The system operator issued a **HOT LINE TAG** through SCADA to test recloser.
- The change in status of the recloser propagated over OpenFMB to all subscribed controllers; a system check verified that subscribed devices logged the change.
- The EPB system operator verified through SCADA that the recloser under test was **OPEN**.

- The **CSEISMIC OPERATOR** issued a command through *the EPB microgrid controller* to **CLOSE** test recloser.
- As expected, the EPB microgrid controller refused to execute the **CLOSE** command due to an active **Hot Line TAG**.

9.2.5.4 Event 5: System Response

After a hotline tag was issued to the recloser under test, all system devices should log the change.

The microgrid controller did not comply with the close command from CSEISMIC.

9.2.5.5 Event 5: Results

Table 9-6: Field Demonstration Event 5 Results

Event #	Affected Microgrids	Event Switching and Execution Steps	Data Collection Point	Results
5	Lab Microgrids	1. The system operator issued a HOT LINE TAG through SCADA to test recloser.	1. Record that HOT LINE TAG was acknowledged across all subscribed devices, CSEISMIC, and CA.	Hot line tag issued from SCADA 11:50
		2. EPB system operator verified through SCADA that test recloser was in the OPEN position.	1. Record the current state of test recloser to be OPEN.	Open and verified
		3. CSEISMIC OPERATOR issued a command to EPB microgrid controller to CLOSE test recloser.	Log result - EPB controller DENIED close command due to HOT LINE TAG.	Hot line tag issued from SCADA 11:50 and close command was denied by controller. HLT not showing on subscribed devices. ORNL to perform fix. 2:02 PM-HLT applied, and status shows on subscribed devices.

9.2.6 Event 6: Add and Drop Authorized Controller and Verify How the Consensus is Affected (Add/Drop a Laboratory Microgrid Controller)

Event 6 was considered high importance, a medium level of difficulty, and a medium level of risk.

9.2.6.1 Event 6: Overview

The purpose of this event was to validate that the consensus algorithm could properly operate when microgrid controllers are added to, and removed from, the microgrid collaborative. In particular, the goal was to verify that the consensus algorithms could continue to function when the number of controllers was changed.

9.2.6.2 Event 6: Initial Operating State

This test initiated with the system in a steady state condition under Blue Sky conditions with all microgrids operating in Mode 1. All but one microgrid was connected to the OpenFMB Harness, with the ability to participate in consensus decisions.

9.2.6.3 Event 6: Initiating Condition

Lab personnel configured a lab controller and commanded its consensus agent to request admittance to the consensus collective of grid-connected microgrids following the prescribed protocol across the OpenFMB system.

The event’s procedure was verified by plugging the communications cable of the controller requesting admittance into its receptacle after the controller was configured.

9.2.6.4 Event 6: System Response

The already networked consensus agents received and processed the lab microgrid’s request to join the consensus collective, verified the lab microgrid’s request, and admitted the lab microgrid to the consensus.

Each microgrid consensus agent periodically published the identifiers of the other microgrid controllers in the consensus group; OpenFMB Message Inspector was used to verify the pre- and post-authorization set of participating controllers.

As expected, there was no expected active system response.

9.2.6.5 Event 6: Results

Table 9-7: Field Demonstration Event 6 Results

Event #	Affected Microgrids	Event Switching and Execution Steps	Data Collection Point	Results
6	Lab and Field Microgrids	ORNL personnel prepared lab microgrid #2 for admittance into an existing consensus of microgrids.	Record lab microgrid controller. CA: Record which microgrids are part of the collective with selected microgrid disconnected.	Lab Microgrid 2 All ORNL Pods and EPB Microgrids

		ORNL personnel connected communications cable of lab microgrid #2 to comm port.	CA: Record which microgrids are part of the collective with selected microgrid connected. Record Resource Status Profile values from lab controller #2.	CA shows admittance of Oak Ridge Microgrid #2
--	--	---	--	---

9.2.7 Event 7: Microgrid Controllers Able to Determine the Mode of Operation and Coordinate with Other Controllers

Event 7 was considered high importance, a medium level of difficulty, and a medium level of risk.

9.2.7.1 Event 7: Overview

This event tested a controller's ability to determine an operating mode given specific criteria and operating conditions.

For this project, microgrids were conceptualized to operate in one of five modes according to circumstances such as grid health, weather, economic goals, and efficiency. Although a consensus of microgrids may agree on operating mode, there are times when they may operate in different modes depending on their own operational goals, such as those related to reliability.

This test determined if the microgrids could determine in which mode they should be operating and if the self-assembled microgrids could continue to operate if some microgrids were operating in different modes. The test was carried out by virtually inducing conditions using a grid simulator that warranted a mode change. The test proceeded according to two cases:

1. A forced case commanded the EPB microgrid controller to move from Mode 1 to Mode 2 and the system was observed for stability.
2. An induced case used a grid simulator to produce a depressed system frequency reading in the laboratory microgrid, after which the laboratory microgrid was expected to respond by transitioning from Mode 1 to Mode 2.

9.2.7.2 Event 7: Initial Operating State

This test began with the system in a steady state condition under Blue Sky conditions with all microgrids operating in Mode 1. All microgrids were connected to the OpenFMB Harness with the ability to participate in consensus decisions.

9.2.7.3 Event 7: Initiating Condition

For the induced change, virtual sensors in the substation(s) detected a serious and consistent frequency depression on the high side, indicating a frequency excursion event on the BPS. The frequency event affected all the connected microgrids. However, the event was designed such that the microgrids

collectively supported the local distribution system and mitigated the local frequency. For the purpose of this test, the grid simulator was used in the ORNL lab and simulated a frequency depression of 59.9 Hz.

9.2.7.4 Event 7: System Response

For the induced case involving a frequency excursion event on the BPS, all the microgrids detected the change either by direct sensing or by notification over OpenFMB. The controllers also recognized through consensus that the threat affected the BPS, and thus the local distribution system and all the participating microgrids. Therefore, all microgrids should have immediately entered Mode 2.

The laboratory CA containers received the frequency data either by direct measurement or by communication over OpenFMB. The three lab controllers entered Mode 2; however, since the EPB microgrid is a field deployed controller, it could not sense the simulated frequency values directly. Therefore, the EPB microgrid controller entered Mode 2 after being alerted to the frequency event over OpenFMB.

After the mode change from Mode 1 to Mode 2 was observed, the grid simulator value was returned to normal, and all laboratory controllers returned to Mode 1.

9.2.7.5 Event 7: Results

Table 9-8: Field Demonstration Event 7 Results

Event #	Affected Microgrids	Event Switching and Execution Steps	Data Collection Point	Results
7	Forced Case: One field microgrid and one lab microgrid	Open FMB operator issued command to EPB microgrid controller to move from Mode 1 to Mode 2.	Log result of mode change from field microgrid to all other subscribed controllers.	9:00 - Forced case complete
		After result of mode command was observed, returned field microgrid to Mode 1.	OpenFMB: Issue message to return CA to Mode 1. Verify CA status message accurately reports mode.	
	Induced Case: All lab microgrid controllers	To begin induced case, Commander operator simulated depressed frequency value of 59.9 Hz in substation using the grid simulator.	Record frequency value as indicated by all subscribed controllers and CA. Record when connected microgrid controllers changed from Mode 1 to Mode 2. Verify OpenFMB messages report frequency and CA mode.	9:00 - Began moving frequency to 59.8 9:04 - all devices moved to Mode 2 including CA
		Returned EPB field controller to Mode 1 (normal).	OpenFMB: If needed, issue OpenFMB message to return CA to Mode 1 and verify CA status message accurately reports mode.	9:10 – returned to normal frequency (60 Hz)

9.2.8 Event 8: Consensus that Results in Voltage/Reactive Power Change (at EPB Microgrid)

Event 8 was considered high importance, a medium level of difficulty, and a medium level of risk.

9.2.8.1 Event 8: Overview

The purpose of this event was to verify the operation of a microgrid controller in Mode 2 participating in a collaborative collective. A microgrid controller was prompted to increase reactive power output by increasing the lower system voltage threshold, which initiated an increase in reactive power output and subsequent change in system voltage toward a desired value.

For this event, the voltage at multiple locations and the reactive power output of the microgrids in Mode 2 was monitored to ensure the anticipated outcome.

9.2.8.2 Event 8: Initial Operating State

This test began with the system in a steady state condition under Blue Sky conditions with all microgrids connected, operating in Mode 1, and capable of participating in consensus decisions.

9.2.8.3 Event 8: Initiating Condition

For this test, the microgrids were prompted to enter Mode 2 by changing the lower voltage threshold from 0.95 to 1.02, altering the acceptable voltage range from 1.02 to 1.05. Consequently, the CA determined that the system operating voltage was low, which prompted a transition to Mode 2 and a calculation of a revised reactive power setpoint.

To accomplish the new voltage range of 1.02 to 1.05, the software container with the initial threshold value was stopped, and a new, pre-built container with the new voltage range was initiated. This was to prevent corruption to the original container. Per actual EPB system constraints, CA was limited to an ~1-Volt change and was restricted to three iterations in reactive power output settings. Although the EPB battery could supply up to 1,250 kvar, CSEISMIC and CA were restricted to 500 kvar out of safety and system stability concerns.

Upon completion of the test, the new container was stopped, and the container with the original thresholds (0.95 to 1.05) was restarted.

9.2.8.4 Event 8: System Response

One field microgrid and one lab microgrid entered Mode 2 and transmitted the change over OpenFMB. Using the system information (voltage) shared over OpenFMB, the microgrids collaboratively determined their updated reactive power output. These values were sent to their respective microgrid controllers over OpenFMB, and CSEISMIC and CA supervised the adjustment. The resulting changes in reactive power output and voltage were monitored by the team to verify proper operation.

Operations confirmed that the correct microgrids entered Mode 2 and adjusted their reactive power output, resulting in a voltage change in the desired direction.

9.2.8.5 Event 8: Results

Table 9-9: Field Demonstration Event 8 Results

Event #	Affected Microgrids	Event Switching and Execution Steps	Data Collection Point	General Notes
8	Lab and Field Microgrids	Recorded pre-event system voltage at test recloser and verified it was below the lower testing threshold of 1.02.	1. Record system voltage at test recloser before starting new CA container. OpenFMB: Verify OpenFMB message is accurately reporting voltage	The team conducted a pre-event test whereby manual commands were sent from CSEISMIC to verify that the battery could be controlled and that a reactive power setpoint would initiate a change in voltage. Team injected 400 kvar from the battery that consequently resulted in a positive change in system voltage. Quantity was around 0.5 volts.
		Communicated test recloser's voltage reading to laboratory personnel and simulated actual system voltage value for all laboratory microgrids.		
		Stopped default CA container(s) and verified stability.	OpenFMB: Stop CA with normal voltage bounds. Verify that all other containers are still running, and messages are still being published.	
		<i>Wait 5 minutes for system to stabilize</i>		
		Started new CA containers for all microgrids with new thresholds of 1.02 to 1.05 and verify stability. Monitored CA, CSEISMIC, and system behavior as CA determined new reactive power output and transmitted new setpoint command to CSEISMIC.	1. Record system voltage at test recloser throughout this step 2. Record reactive power setpoint commands from CA and timestamps 3. Record reactive power output from Tesla battery OpenFMB: Start CA container with updated low voltage bounds. Verify other containers are still	11:43 - The message inspector indicated message traffic from CA to CSEISMIC to alter reactive power output. Consensus was reached on all five microgrids as to reactive power setpoint.

Event #	Affected Microgrids	Event Switching and Execution Steps	Data Collection Point	General Notes
			running and messages are still being published. Verify CA accurately reports status.	
		Returned to default CA containers.	<p>1. CA: Record Agents' Mode (should return to 1)</p> <p>OpenFMB: Stop modified CA container. Ensure other containers are still running and messages are still being published. Restart CA with normal voltage bounds. Verify all other containers are still running and messages are still being published.</p>	

9.2.9 Event 9: Black Start of a Microgrid (at EPB Microgrid)

Event 9 was considered medium importance, a low level of difficulty, and a low level of risk.

9.2.9.1 Event 9: Overview

The purpose of this event was to test whether the EPB microgrid could start its own critical loads and establish a stable islanded condition behind the PCC. The test took place at EPB's microgrid with the EPB microgrid grid-connected and operating in Mode 1. To black start the critical loads, the microgrid and loads were islanded behind the PCC, simulating an unintentional island.

9.2.9.2 Event 9: Initial Operating State

This test began with the system in a steady state condition under Blue Sky conditions with all laboratory microgrids operating in Mode 1 and the EPB control center microgrid shut down. All laboratory microgrids were connected to the OpenFMB Harness with the ability to participate in consensus decisions.

The EPB battery's state-of-charge was verified to be at least 50% before the test began.

9.2.9.3 Event 9: Initiating Condition

The exercise began after the EPB microgrid was islanded by opening the recloser at the EPB microgrid's PCC.

9.2.9.4 Event 9: System Response

The EPB microgrid controller detected the loss of grid support and unintentional island condition and consequently tripped the loads behind its PCC. The controller then begin the process of reenergizing the microgrid by initiating its black start protocol.

CSEISMIC was be started, detected the dead bus, and began the black start protocol. CA was in a monitoring posture during the black start test.

9.2.9.5 Event 9: Results

Table 9-10: Field Demonstration Event 9 Results

Event #	Affected Microgrids	Event Switching and Execution Steps	Data Collection Point	Results
9	Field Microgrid	Issued SCADA command to islanding recloser to create island behind the EPB microgrid PCC.	Record that the EPB controller tripped all its critical loads. Record if CSEISMIC began its black start protocol. Record if CA logged the system change.	2:43 PCC recloser Opened, however voltage was observed on PCC at 2:50. CSEISMIC was left in safe mode so command to move into black start was blocked. Error was discovered and safe tag removed. System black-started after.
			Critical loads are energized.	Critical loads were black started.

9.2.10 Event 10: Failure of One or More Sensors (Laboratory Microgrid)

Event 10 was considered medium importance, a medium level of difficulty, and a low level of risk.

9.2.10.1 Event 10: Overview

The purpose of this event was to assess if a consensus of microgrids could effectively operate around a faulty sensor. This test was conducted in the ORNL lab to minimize risk to EPB’s system. The test introduced noise to interfere with the voltage readings of one of the lab’s reclosers, and thus produced erroneous values to the consensus processes. CA determined if the sensor’s readings were abnormal, and down-weighted the impact of the abnormality in the collaborative decision-making functions. The consensus agents used system knowledge and similar sensor readings from other devices and reclosers to determine the validity of the sensor readings.

Before the test, lab personnel determined to what extent they could affect the ability of the sensors to accurately read the voltage and frequency and determine the degree in which they should affect the sensors output.

9.2.10.2 Event 10: Initial Operating State

This test began with the system in a steady state condition under Blue Sky conditions with all microgrids operating in Mode 1. All microgrids will be connected, with the ability to participate in consensus decisions.

9.2.10.3 Event 10: Initiating Condition

Lab personnel adjusted the connected grid simulator to induce a change in the lab microgrids from Mode 1 to Mode 2 by reducing grid emulator voltage level. Lab personnel will then introduce noise, as previously determined to the affected recloser, and observe the change in the output to the collaborative agents.

9.2.10.4 Event 10: System Response

The change in signal values were broadcast over the OpenFMB system. The consensus of controllers logically deduced if the signals were indicative of an actual change or the product of a faulty sensor. Any decision-making consensus computations minimized involvement of data from the faulty sensors, and instead, voltage and frequency readings from functioning recloser sensors were be prioritized. The consensus had the latitude to request changes in the P/Q settings if the requests were reasonable and unaffected by the faulty sensor’s input.

9.2.10.5 Event 10: Expected Final Operating State

The lab controllers began in Mode 2. There were changes in reactive power and voltage due to microgrid actions, but the system remained in the original configuration.

9.2.10.6 Event 10: Terminating Conditions

The test would have been terminated if the consensus does not identify the faulty sensor data and begins recommending changes to the system based on the erroneous information.

9.2.10.7 Event 10: Results

Table 9-11: Field Demonstration Event 10 Results

Event #	Affected Microgrids	Event Switching and Execution Steps	Data Collection Point	Results	Agent Notes
10	Laboratory Microgrid	Induced a mode change from Mode 1 to Mode 2, reducing grid emulator voltage level.	Verified all agents moved to Mode 2.	Voltage at 0.95 pu. Did not immediately move into Mode 2. Eventually, all ORNL and EPB controllers saw the change in voltage and moved to Mode 2. ----- Run 2: All PODS minus EPB moved to Mode 2 (EPB is excluded for Run -----	CA - EPB did not immediately go to Mode 2 but the consensus decided that given the conditions all should be in Mode 2. 2nd Run: The population of controllers were too small for the CA to identify

				Run 3: All agents left in Mode 1, therefore the cluster of the controllers were closely positioned around the weighted average.	outliers, therefore running 3rd time.
		Lab personnel introduced random noise to laboratory recloser for the Pod 1 microgrid by adding 10% random noise to Va on PCC.	<p>Logged magnitude of noise.</p> <p>Verified that the change in signal values was broadcast across OpenFMB.</p> <p>Verified that the consensus downgraded the erroneous microgrid.</p> <p>Log any changes in reactive power settings and reactions of consensus agents to the generated noise. Consensus agents should provide new reactive power set points.</p>	<p>CA downgraded all phases on Pod 2, the correct pod.</p> <p>-----</p> <p>Run 2: The CA did not target the erroneous POD sensor due to insufficient thresholds, will rerun with tighter thresholds.</p> <p>-----</p> <p>Run 3: Team did not introduce noise but multiplied the actual Pod phase A voltage by a factor of 1.1 and the CA identified the erroneous Pod and the correct measurement (phase A).</p>	CA- After closer inspection, CA picked the EPB controller as the outlier and downgraded its contribution to the consensus. EPB was outside the envelope of what was judged acceptable to the consensus. The test will be run again with the EPB excluded from the collective.

9.2.11 Event 11: Loss of Communication to a Microgrid (Laboratory Microgrid)

Event 11 was considered high importance, a low level of difficulty, and a low level of risk.

9.2.11.1 Event 11: Overview

The purpose of this event was to investigate the performance of collaborative microgrid consensus if one controller lost communication with the remaining controllers over both OpenFMB and SCADA. It was expected that the remaining controllers would proceed to form a consensus group based on their respective modes and carry out the expected objective(s) based on each group's mode, without being derailed by the lost microgrid.

The investigation was carried out in the lab to reduce risk to EPB's system, as it is unknown how the remaining microgrids will react.

9.2.11.2 Event 11: Initial Operating State

This test began with the system in a steady state condition under Blue Sky conditions with all microgrids operating in Mode 1. All microgrids were connected, with the ability to participate in consensus decisions.

9.2.11.3 Event 11: Initiating Condition

The exercise initiated when the OpenFMB node's communications cable was removed from one of the controllers to simulate a communications outage.

9.2.11.4 Event 11: Anticipated System Response

The expectation was that the loss of communication to one microgrid would not affect the physical system in a dramatic way, and the other microgrids should remain in Mode 1. When the collaborative agent corresponding to the disconnected microgrid agent determined that it lost communication to the microgrid controller, it would cease to publish (to be subscribed to by the other collaborative agents) that it is in Mode 1. By the same means that the publish/subscribe data exchanges were verified in Event 1, it can be verified that the disconnected microgrid was not included in the Mode 1 group.

9.2.11.5 Event 11: Results

Table 9-12: Field Demonstration Event 11 Results

Event #	Affected Microgrids	Event Switching and Execution Steps	Data Collection Point	Results
11	Laboratory Microgrids	Removed one microgrid's communication cable from the communication port to simulate a communications outage.	Log if the remainder of the microgrids remained in Mode 1 and any other changes indicative of the comm loss. Log that all CA containers observed that communication has been lost to the microgrid. Log that CA continues to monitor for mode changes despite the lost microgrid (i.e., CA does not "hang" or get stuck because of the loss).	Pod 2 comm cable was removed. All remaining microgrids remained in Mode 1. No other Mode changes were observed.

9.2.12 Event 12: Byzantine Actor (Laboratory Microgrid)

Event 12 was considered medium importance, a medium level of difficulty, and a low level of risk.

9.2.12.1 Event 12: Overview

The purpose of this event was to test the response of the collaborative microgrid consensus to the action of a Byzantine Actor, which broadcasts erroneous data and signals either resulting from malfunction or

malicious intent. This test was achieved using the same method used in Event 10 to generate noise and affect a sensor’s ability to accurately report voltage and frequency, except that the noise was induced not randomly but in opposition to the expected desired action. The controller should have been flagged as a Byzantine Actor and heavily down-weighted in the proceeding consensus computations. The noise was severe enough to produce values that are sufficiently departed from the norm and appear fabricated, or the product of a severely malfunctioning controller. This test occurred at the ORNL lab.

9.2.12.2 Event 12: Initial Operating State

This test began with the system in a steady state condition under Blue Sky conditions with all microgrids operating in Mode 1. All microgrids were connected to the OpenFMB Harness, with the ability to participate in consensus decisions.

9.2.12.3 Event 12: Initiating Condition

Lab personnel adjusted the connected grid simulator to induce a change in the lab microgrids from Mode 1 to Mode 2. ORNL personnel introduced noise to one controller and observed erroneous readings from the affected sensor.

9.2.12.4 Event 12: System Response

The collaborative agents responded by identifying the compromised controller as a Byzantine Actor and the data shared by this controller and the information exchanged by its corresponding collaborative agent were down-weighted in the consensus algorithm.

9.2.12.5 Event 12: Results

Table 9-13: Field Demonstration Event 12 Results

Event #	Affected Microgrids	Event Switching and Execution Steps	Data Collection Point	Results
12	Laboratory Microgrids	Lab personnel adjusted the connected grid simulator by reducing nominal voltage to induce a change in the lab microgrids and CA from Mode 1 to Mode 2.	Record that all agents moved from Mode 1 to Mode 2.	*See Event 10, same procedure was carried out here except the Pod 2 Va value was multiplied by 0.95.

		<p>The voltage level at the point of common coupling for the Pod 1 microgrid sent the inverse delta from nominal voltage, therefore producing an erroneous value (e.g., actual voltage 0.95 pu, measured voltage 1.05 pu).</p>	<p>Record voltage level being sent from Byzantine Actor and that value is acknowledged from all agents.</p> <p>Verify that the weight associated with the Byzantine Actor signal is down-weighted.</p> <p>Verify that CA continues to provide reasonable reactive power setpoints despite the Byzantine signal.</p>	<p>Observed lower voltage value for Va and the command line output that Va was being down-weighted.</p> <p>The microgrids were left in Mode 1, so there were no reactive power changes observed.</p>
--	--	--	---	--

10.0 Lessons Learned and Concluding Comments

Overall, the Citadels project was a success, as validated in the final field validation and associated simulation and analysis. This section contains the lessons learned, final comments, and need for future work in this area.

10.1 Lessons Learned

Because the work in this project ranged from foundational research to applied engineering, there was an array of lessons learned.

10.1.1 Modeling and Simulation

- For any research project that will utilize multiple simulation types, there needs to be a consensus on the “source” for the system model. For this project, the co-simulation model and the HIL models for this project both used the EPB CYME model as the data source.
- When a single source is being used for different models, there must be a defined process for migrating from the source data to the individual model. For this project, there was a defined process for how to create the co-simulation, dynamic, and HIL models. This included rules for model reduction, validation, and comparison to ensure that results from different models could be compared. For example, nodes that were control points, such as a DER, could not be reduced. The process used was adopted from a previous GMLC project at Duke Energy.
- Even though a project can have different simulation types, they must be cross-validated for consistency. For this project, co-simulation, dynamic, and HIL models were compared in steady state to ensure fundamental agreements. This allows for cross-coordination for more complicated simulation results, and comparison. For example, electromechanical dynamic simulations were directly compared to HIL simulations to validate control performance. This enabled detailed high-fidelity HIL simulations to support larger scale co-simulation for transactive controls.

10.1.2 Hardware and Software Containerization

- Managing distributed, containerized control applications requires orchestration beyond what is provided by container-focused tools such as Docker and Kubernetes. While these tools provide powerful management of the containers themselves, they do not provide much in the way of application management and multi-container sequencing (e.g., start-up and shut-down sequence, and application error handling).

10.1.3 Consensus Algorithms

- The consensus algorithms implemented were very effective, but also relatively simple. There is still significant work to be done exploring the full range of operational capabilities that consensus algorithms can provide.

10.1.4 Sustainability of Deployment

- A standards-based approach is essential to ensure long term sustainability. This is especially true over time as system elements (hardware and software) are replaced and as new equipment is added.

- Operationally, the work must align with legacy operational practices. Additionally, operational staff should be consulted during the development phase to ensure that developed solutions are practical.
- Given the number of unique actors and containers operating in a system, a strong method of managing and updating software is critical to long-term sustainability of the system.

10.1.5 Distribution and Bulk Power Systems

- The work of Sec. 8.3 contributes to the support of bulk power system using microgrids. While the focus of this research is mainly on distribution systems, it does not necessarily preclude the investigation of bulk power behaviors such as ROCOF and frequency regulation. In fact, these behaviors are relevant to both distribution and bulk power systems, as they relate to the stability and reliability of the power grid as a whole.
- With respect to the black start, there are differences between restoring an individual microgrid and black starting a bulk power system. For instance, a microgrid typically has a smaller capacity and may rely more heavily on DERs such as batteries. In contrast, a bulk power system typically has a much larger capacity and rely more on traditional power generation sources such as hydropower plants. Additionally, bulk power system restoration schemes typically involve numerous utilities.
- Bulk system restoration strategies are examined by other projects in the GMLC and is leveraged by Citadels, which leverages other on-going work and does not develop new restoration or black-start capabilities for distribution and bulk systems.
- In general, the application space of this research encompasses both distribution and bulk power systems, as both types of systems are critical components of the larger power grid. By investigating the challenges and opportunities associated with microgrids and their interaction with bulk power systems, it is expected to improve the overall resilience and reliability of the power grid as a whole.

10.1.6 Field Demonstration

- The 12 events of the field demonstration designed to simulate various scenarios that a microgrid could encounter in real-world operation, such as grid outages, equipment failures, and changes in load demand. By testing these scenarios, EPB and participated national laboratories were able to evaluate the performance of the microgrid system and identify areas for improvement. These can be referred and studied by other utilities too.
- Any effective field demonstration must include events that are related to the use cases used for the supporting research. For the Citadels field demonstration, the 12 events in Section 9.0 were divided into three categories, steady state, event based, and failure based. While the 12 events were specific to the research needs of Citadels, any field demonstration should include events from all three categories. This ensures that new systems will operate effectively under normal, abnormal, and extreme events. This is especially important as new systems become more complex.
- The results of these tests provide valuable information that can be used to inform the design and operation of microgrids in other locations with different utility distribution systems. By applying the lessons learned from these tests, microgrid operators can better prepare for a variety of possible events and improve the resilience and reliability of their systems.

10.2 Concluding Comments and Specific Outcomes

As stated in the introduction, the primary goal of this GMLC project was to increase the operational flexibility of power systems by engaging microgrids distributedly, coordinated using consensus algorithms. The primary goal was divided into three areas as shown below, each of which was accomplished.

- Implement peer-to-peer control between microgrid controllers using the Open Field Message Bus (OpenFMB) approach.
- Develop and implement consensus algorithms on commercially available hardware that allows a group of microgrids to distributedly implement operational controls.
- Develop the architectures and controls to enable groups of microgrids to coordinate their operations to support the bulk power system during abnormal events, and end-use loads in the event the bulk power system fails.

Specific tasks within the project developed the architectural design for a layered control structure that enables the coordination of microgrids with consensus algorithms. Simulations were conducted in various platforms (including co-simulation, steady state, HIL, and emulation) that examined various operational use-cases under normal and abnormal conditions. This included evaluations of supporting the bulk power system during abnormal conditions and microgrid self-assembly when there is a loss of the bulk power system. A physical instantiation of the OpenFMB framework was created in the OpenFMB Harness, which allowed for the evaluation of interoperability and cyber security issues. This work was coordinated with EPBs microgrid deployment. An integrated assessment plan was developed for a final field validation that was successfully completed. Specific outcomes of the project included:

- The Citadels project was a proof of concept that successfully demonstrated microgrid controllers can be coordinated using consensus algorithms on a secure pub/sub network, using OpenFMB.
- Using distributed control, via OpenFMB, it is possible to implement a distributed control architecture that is cyber-secure.
- Groups of microgrid controllers can distributedly support bulk power system operations without central control.
- Groups of microgrid controllers can distributedly coordinate to execute self-assembly operations.
- The computer hardware and communication architecture deployed and commissioned during the Citadels project will support efforts under the ORNL COMMANDER project.
- The EPB microgrid commissioning (BESS, PV, switchgear, etc.) performed under the Citadels project will be utilized in future CSEISMIC work under the COMMANDER project.

As part of the Citadels project there are a number of capabilities that were developed and can be made accessible to researchers and the industry. While it is not possible to share all details because of operational considerations, accessible resources and the applicable point of contact include:

- Dynamic simulation capabilities, inverter models for unbalanced electromechanical dynamic simulations, and Architectural work: PNNL POC.
- Consensus algorithms used during the field demonstration : LLNL POC.
- Hardware emulation, CSEISMIC microgrid controller, and the COMMANDER testbed: ORNL POC.
- In the laboratory inverter testing, including controls and model validation: SNL POC.

- Co-simulation of power and communications systems: WSU POC.
- Open-source OpenFMB adaptors used during the field demonstration : OES POC.
- Utility perspective and follow-on operations: EPB: POC.

10.3 Potential Follow-on Research Areas

Overall, the Citadels project successfully demonstrated each of the three areas of the primary goal. However, Citadels was only a first step in understating how peer-to-peer communications could enable mixed-ownership microgrids to coordinate operations. Future work could include, but not be limited to:

- Extend the framework to include additional objective functions to represent a broader range of potential stakeholders. This could include emerging concepts such as community microgrids, virtual power plants, third party aggregators, and rural deployments.
- Citadels implemented a relatively simple cloture voting approach, but there are much more complex, and capable, consensus algorithms that could be explored. These could include consensus algorithms that can account for multi-objective optimizations and multiple Byzantine agents.
- Further explore layered architecture and power electronics devices. Because power electronics can exist at multiple levels, exploring their coordination with respect to stability and reliability issues is needed. This could include an expanded range of battery and storage inverter controls, electric vehicle charging infrastructure (light duty, medium duty, and fleet), and solidate state substation technologies.
- Apply the lessons learned in the field demonstration to the microgrids and/or distribution systems of utilities with different infrastructure, operating procedures, and operational objectives.

11.0 References

- [1] OpenFMB Repository. Accessed: Jan. 2019. [Online]: <https://openfmb.gitlab.io/>
- [2] A. Smallwood, S. Laval, J. Gibson, and F. Goodman, “Managing renewables and DERs with open field message bus,” *Proc. DistribuTECH*, 2018, pp. 1–6.
- [3] Anderson Sports and Entertainment Center. [Online]: <http://www.andersonevents.com/>
- [4] N. Jacobs, A. Sumemrs, S. Hossain-McKenzie, D. Calzada, H. Li, Z. Mao, C. Goes, K. Davis, K. Shetye, “Next-Generation Relay Voting Scheme Design Leveraging Consensus Algorithms,” *IEEE Power and Energy Conference at Illinois*, 2021, pp. 1-6.
- [5] I. Aravena, S. J. Chapin, C. Ponce, “Decentralized Failure-Tolerant Optimization of Electric Vehicle Charging,” *IEEE Transactions on Smart Grid*, vol. 12, no. 5, pp. 4068-4078, 2021.
- [6] J. Xie and C.-C. Liu, “Multi-agent systems and their applications,” *Journal of International Council on Electrical Engineering*, vol. 7, no. 1, pp. 188–197, 2017.
- [7] K. P. Schneider et al., “A Framework for Coordinated Self-Assembly of Networked Microgrids Using Consensus Algorithms,” *IEEE Access*, vol. 10, pp. 3864-3878, 2022.
- [8] S. Katipamula, J. Haack, G. Hernandez, B. Akyol, and J. Hagerman, “VOLTTRON: An open-source software platform of the future,” *IEEE Electrification Magazine*, vol. 4, no. 4, pp. 15–22, Dec. 2016.
- [9] J. Xie, et al., “Impact analysis of future electric vehicles using model of real distribution feeders”, *IEEE ISGT North America*, Washington, D.C., USA, Jan. 2023.
- [10] D. P. Chassin, K. Schneider, and C. Gerkenmeyer, “GridLAB-D: An open-source power systems modeling and simulation environment,” *IEEE PES Transmission and Distribution Conference and Exposition*, Chicago, IL, USA, Apr. 2008.
- [11] “GridLAB-D User Documentation,” [Online]. Available: <http://gridlab-d.shoutwiki.com/> (Accessed Sep. 2, 2022).
- [12] “GridLAB-D Source Code,” [Online]. Available: <https://github.com/gridlab-d/gridlab-d> (Accessed Sep. 2, 2022).
- [13] T. E. McDermott, “CIMHub Source Code,” [Online]. Available: <https://github.com/GRIDAPPSD/CIMHub> (Accessed Sep. 2, 2022).
- [14] H. Wang and A. Fisher, “Python Scripts - CYME to GridLAB-D,” [Online]. Available: https://github.com/gridlab-d/tools/tree/master/conversion_scripts (Accessed Sep. 2, 2022).
- [15] R. C. Dugan and T. E. McDermott, “An open source platform for collaborating on smart grid research,” *IEEE Power and Energy Society General Meeting*, Detroit, MI, USA, Jul. 2011.
- [16] J. Xie, “GridLAB-D Tool Scripts,” [Online]. Available: https://github.com/gridlab-d/tools/tree/master/python_scripts (Accessed Sep. 2, 2022).
- [17] N. S. Gurule, J. H. Alvidrez, M. J. Reno, and J. Flicker, “Multiple Inverter Microgrid Experimental Fault Testing,” Nov. 2022, pp. 0578–0583. doi: 10.1109/PVSC48317.2022.9938676.
- [18] N. S. Gurule, J. Hernandez-Alvidrez, M. J. Reno, A. Summers, S. Gonzalez, and J. Flicker, “Grid-forming Inverter Experimental Testing of Fault Current Contributions,” in *Conference Record of the IEEE Photovoltaic Specialists Conference*, Jun. 2019, pp. 3150–3155. doi: 10.1109/PVSC40753.2019.8980892.
- [19] N. S. Gurule, J. Hernandez-Alvidrez, R. Darbali-Zamora, M. J. Reno, and J. D. Flicker, “Experimental Evaluation of Grid-Forming Inverters under Unbalanced and Fault Conditions,” in *IECON Proceedings (Industrial Electronics Conference)*, Oct. 2020, vol. 2020-October, pp. 4057–4062. doi: 10.1109/IECON43393.2020.9254562.

- [20] J. Hernandez-Alvidrez, N. S. Gurule, R. Darbali-Zamora, M. J. Reno, and J. D. Flicker, “Modeling a Grid-Forming Inverter Dynamics under Ground Fault Scenarios Using Experimental Data from Commercially Available Equipment,” in *Conference Record of the IEEE Photovoltaic Specialists Conference*, Jun. 2021, pp. 1517–1523. doi: 10.1109/PVSC43889.2021.9518794.
- [21] N. S. Gurule, J. A. Azzolini, R. Darbali-Zamora, and M. J. Reno, “Impact of Grid Support Functionality on PV Inverter Response to Faults,” in *Conference Record of the IEEE Photovoltaic Specialists Conference*, Jun. 2021, pp. 1440–1447. doi: 10.1109/PVSC43889.2021.9518953.
- [22] M. Davari and Y. A. R. I. Mohamed, “Robust Vector Control of a Very Weak-Grid-Connected Voltage-Source Converter Considering the Phase-Locked Loop Dynamics,” *IEEE Trans Power Electron*, vol. 32, no. 2, pp. 977–994, Feb. 2017, doi: 10.1109/TPEL.2016.2546341.
- [23] ABB, *PCS100 ESS Grid Connect Interface for Energy Storage Systems User Manual*, 1st Editio.
- [24] J. Hernandez-Alvidrez, A. Summers, M. J. Reno, J. Flicker, and N. Pragallapati, “Simulation of Grid-Forming Inverters Dynamic Models using a Power Hardware in the Loop Testbed,” in *46th IEEE Photovoltaic Specialists Conference*, 2019, no. July.
- [25] J. Hernandez-Alvidrez, N. S. Gurule, M. J. Reno, J. D. Flicker, A. Summers, and A. Ellis, “Method to Interface Grid-Forming Inverters into Power Hardware in the Loop Setups,” in *Conference Record of the IEEE Photovoltaic Specialists Conference*, Jun. 2020, vol. 2020-June, pp. 1804–1810. doi: 10.1109/PVSC45281.2020.9300804.
- [26] N. S. Gurule, J. H. Alvidrez, M. J. Reno, W. Du, and K. Schneider, “Grid-Forming and Grid-Following Inverter Comparison of Droop Response,” Nov. 2022, pp. 0190–0196. doi: 10.1109/PVSC48317.2022.9938666.
- [27] B. Palmintier, D. Krishnamurthy, P. Top, S. Smith, J. Daily, and J. Fuller, “Design of the HELICS high-performance transmission-distribution-communication-market co-simulation framework,” in *2017 Workshop on Modeling and Simulation of Cyber-Physical Energy Systems (MSCPES)*, Pittsburgh, PA, Apr. 2017, pp. 1–6. doi: 10.1109/MSCPES.2017.8064542.
- [28] ns-3, “NS-3 Network Simulator.” Accessed: Nov. 03, 2020. [Online]. Available: <https://www.nsnam.org/>
- [29] “Routing overview — Model Library.” <https://www.nsnam.org/docs/models/html/routing-overview.html#global-centralized-routing> (accessed Aug. 12, 2021).
- [30] “Interior Gateway Protocols,” IBM Documentation, Mar. 22, 2021. <https://prod.ibmdocs-production-dal-6099123ce774e592a519d7c33db8265e-0000.us-south.containers.appdomain.cloud/docs/en/zos/2.1.0?topic=terminology-interior-gateway-protocols> (accessed Aug. 10, 2021).
- [31] Rabayet Sadnan, Nathan Gray, Anjan Bose, and Anamika Dubey, “Simulation-Integrated Distributed Optimization for Unbalanced Power Distribution Systems,” submitted to *IEEE Transactions on Power Delivery*, Nov 2022.
- [32] R. R. Jha, A. Dubey, C.-C. Liu, and K. P. Schneider, “Bi-Level Volt-VAR Optimization to Coordinate Smart Inverters With Voltage Control Devices,” *IEEE Trans. Power Syst.*, vol. 34, no. 3, pp. 1801–1813, May 2019, doi: 10.1109/TPWRS.2018.2890613.

Appendix A: Complete List of Project Publications

This appendix includes a complete list of project publications, including published conference papers, published journal papers, and manuscripts in preparation/review.

A.1 Published/Accepted Conference Papers

- [1] J. Hernandez-Alvidrez, N. S. Gurule, M. J. Reno, J. D. Flicker, A. Summers, and A. Ellis, "Method to Interface Grid-Forming Inverters into Power Hardware in the Loop Setups," *IEEE Photovoltaic Specialists Conference (PVSC)*, 2020.
- [2] J. Hernández-Alvidrez, N. S. Gurule, R. Darbali-Zamora, M. J. Reno, and J. D. Flicker, "Modeling Grid-Forming Inverters Dynamics Under Ground Fault Scenarios Using Experimental Data From Commercially Available Equipment," *IEEE Photovoltaic Specialists Conference (PVSC)*, 2021.
- [3] R. Darbali-Zamora, N. S. Gurule, J. Hernandez-Alvidrez, S. Gonzalez, and M. J. Reno, "Performance of a Grid-Forming Inverter Under Balanced and Unbalanced Voltage Phase Angle Jump Conditions," *IEEE Photovoltaic Specialists Conference (PVSC)*, 2021.
- [4] A. Poudyal, A. Dubey, and S. Poudel, "A Risk-Driven Probabilistic Approach to Quantify Resilience in Power Distribution Systems," *Probabilistic Methods Applied to Power Systems (PMAPS)*, 2022.
- [5] N.S. Gurule, J. Hernandez-Alvidrez, M. Reno, W. Du, and K.P. Schneider, "Grid-Forming and Grid-Following Inverter Comparison of Droop Response," *IEEE Photovoltaic Specialists Conference (PVSC)*, 2022.
- [6] R. Sadnan, N. Gray, A. Dubey, and A. Bose, "Distributed Optimization for Power Distribution Systems with Cyber-Physical Co-simulation," *IEEE PES GM*, 2021.
- [7] R. Sadnan, A. Dubey, "Real-Time Distributed Control of Smart Inverters for Network-Level Optimization," *IEEE SmartGridComm*, Nov. 11-12, 2020.
- [8] R. Sadnan, A. Dubey, "Online Distributed Optimization in Radial Power Distribution Systems: Closed-Form Expressions," *IEEE SmartGridComm*, Oct. 24-28, 2021.
- [9] N. Grey, R. Sadnan, A. Dubey, and A. Bose, "Effects of Communication Network Topology on Distributed Optimal Power Flow for Radial Distribution Networks," *NAPS*, 2021.
- [10] R. Sadnan and A. Dubey, "Distributed Optimization in Distribution Systems with Grid-Forming and Grid-Supporting Inverters," *PES General Meeting*, 2022.
- [11] R. Sadnan, A. Dubey, "Distributed Computing for Scalable Optimal Power Flow in Large Radial Electric Power Distribution Systems with Distributed Energy Resources", *Hawaii International Conference on System Sciences (HICSS-56) Conference*, 2023.
- [12] Vu T., L.D. Marinovici, K.P. Schneider, J. Xie, C. Klauber, and A. Dubey, "Coordination of Networked Microgrids for Supporting Voltages of Bulk Power Systems," *PES General Meeting*, 2023.

A.2 Published/Accepted Journal Papers

- [1] K. P. Schneider *et al.*, "A Framework for Coordinated Self-Assembly of Networked Microgrids Using Consensus Algorithms," *IEEE Access*, vol. 10, pp. 3864-3878, 2022.
- [2] R. Sadnan and A. Dubey, "Distributed Optimization Using Reduced Network Equivalents for Radial Power Distribution Systems," *IEEE Transactions on Power Systems*, vol. 36, no. 4, pp. 3645-3656, July 2021.
- [3] R. Sadnan, S. Poudel, A. Dubey, and K. P. Schneider "Layered Coordination Architecture for Resilient Restoration of Power Distribution Systems," *IEEE Transactions on Industrial Informatics*, May 2022.
- [4] R. R. Jha, A. Inaolaji, B. D. Biswas, A. Suresh, A. Dubey, S. Paudyal, S. Kamalasan, "Distribution Grid Optimal Power Flow (D-OPF): Modeling, Analysis, and Benchmarking," *IEEE Transactions on Power Systems*, Oct 2022.

A.3 Published Technical Reports

- [1] K. P Schneider, H. Nagarajan, A. Pratt, M. J Reno, B. Ollis, et al., “Preliminary Design Process for Networked Microgrids,” Pacific Northwest National Laboratory, PNNL-30066, 2020.

A.4 Manuscripts in Preparation or under Review

- [1] C. Klauber, *et al*, “Robust Coordinated Self-Assembly of Networked Microgrids using Collaborative Autonomy,” to be submitted to *IEEE Open Access Journal of Power and Energy*.
- [2] J. Xie *et al.*, “Distributed Consensus Weighting Protocol to Support Network Microgrid Operations,” to be submitted to *IEEE Access*.
- [3] W. Dawson, *et al*, “Effective Cooperation in the Presence of Bad Actors,” to be submitted to *IEEE Transactions of Pattern Analysis and Machine Intelligence*.
- [4] R. Sadnan, N. Grey, A. Dubey, T. L. Vu, J. Xie, and C. Klauber, “Comparative Analysis of Distributed Algorithms for Bulk-Grid Voltage Support,” to be submitted to *IAS annual meeting*.
- [5] Y. Luo, R. Sadnan, B. Krishnamoorthy, and A. Dubey, “Convergence Guarantees of a Distributed Network Equivalence Algorithm for Distribution-OPF,” submitted to *IEEE Transactions on Smart Grid*.
- [6] R. Sadnan, N. Grey, A. Bose, and A. Dubey, “Simulation-Integrated Distributed Optimization for Unbalanced Power Distribution Systems,” to be submitted to *IEEE Transactions on Sustainable Energy*.
- [7] R. Sadnan, N. Grey, A. Dubey, and A. Bose, “Effects of Communication Systems Attributes on Distributed Microgrid Coordination for Bulk-grid Services,” to be submitted to *IEEE Transactions on Industrial Informatics*.

Appendix B: LLNL Emulation Methodology

As it is not feasible to implement *all* the above operations in a field demonstration at this time, the various events were intended to be used to validate *building block* functions spanned by all the operating modes. For example, Mode 2 cannot be fully tested without initiating a voltage collapse on the bulk power system and Mode 3 cannot be fully tested without inducing a customer outage.

Event 1 (Verify pub/sub data exchange between all architecture components): Among the values verified to be passed between architecture components were CA specific values including the microgrid Mode. Microgrid CA containers must also receive values from CSEISMIC and share values with each other. The distributed approach enabled the exchange of information sans a central controller/broker. Status and value changes were successfully transmitted and updated, validating that distributed pub/sub would be an appropriate alternative.

Event 6 (Add and drop authorized controller and verify how the consensus is affected) For this event, a lab microgrid controller was shut down and restarted. The CA continued to share values and assess the current operating conditions (as evidenced by CA status messages continuing to stream on the command line interface), not getting blocked waiting for information that previously had been there but was no longer. This validates that CA can function in an operationally dynamic environment, such as where the number of participants is changing.

Event 7 (Microgrid controllers able to determine the mode of operation and coordinate with other controllers) For this event a low frequency was induced in the lab testbed using the grid simulator. As the resulting frequency values were shared among the CA agents, they will observe and verify the change and determine that the mode should be changed from Mode 1 to Mode 2. This was observed in the CA status messages, verifying that multiple controllers can exchange information, validate measurements, and agree on a group action.

Event 8 (Consensus that results in voltage/reactive power change) This event built on Event 7 in that in addition to verifying that multiple controllers can exchange information, validate measurements and agree on a group action, in Event 8 that action was executed, resulting in an operational impact. This demonstrated, for the first time, that consensus can be used in operations in electric industrial control systems. At steps along the way, some of the values that were verified, demonstrating the aforementioned building blocks, include the CA agent modes (they should all transition from Mode 1 to Mode 2), the before and after voltage measured at a particular recloser (the voltage increased, as intended), and the desired reactive power setpoints from the CA and the actual reactive power output (the setpoint as determined by CA should be passed to CEISMIC and implemented in operations).

Event 10 (Failure of one or more sensors) To validate the building blocks that support operating through failure of one or more sensors, the plan was to introduce noise on the emulator voltage and for the CA to identify and down-weight that particular measurement. The CA outlier detection methodology assumes that there are a certain number of measurements electrically connected to ensure identification of outlier. As the lab microgrids were independent from the EPB microgrid, the failing sensor proxy (noise) had to be quite large for the CA to identify it. In future work, additional measurement points or alternative algorithms may increase the success of such tests.

Event 11 (Loss of communication to a microgrid) Though very similar to Event 6 in effect, in this event, a communication outage was induced by disconnecting a microgrid's communication cable. As expected, the remaining microgrids and corresponding CA agents continued to share information and remained in Mode 2. The loss of communication is acknowledged in the following log (Figure B.1) and does not prevent the

CA from continuing to step through its processes. This again verifies that CA is robust to a “dead” controller or communications issue and will continue to pursue the operational objectives.

NAME	MRID	MODE	NEIGHBORS	LAST SEEN	2022-09-28 08:58:03.584872
ca_epb	c4bbbc82-28b9-4758-8385-c810bc1b8bfb	2	pod1_ca, pod2_ca, hil_ca, pod3_ca	2022-09-28 08:49:20.492761	(DEAD)
pod1_ca	58eaf678-7ab4-4318-b1d2-8aeb3e743b8d	2	ca_epb, pod2_ca, hil_ca, pod3_ca	2022-09-28 08:49:34.546852	(ALIVE)
pod2_ca	33794989-46be-445d-887e-08ddff18c175	2	pod1_ca, pod3_ca, ca_epb, hil_ca	2022-09-28 08:49:34.774899	(ALIVE)
pod3_ca	e237415c-3386-4955-b427-886ccb08e989	2	pod2_ca, pod1_ca, hil_ca, ca_epb	2022-09-28 08:49:34.558782	(ALIVE)
hil_ca	9ab7e0a8-a463-4a6f-9b38-e9a9692e7803	2	pod2_ca, pod1_ca, pod3_ca, ca_epb	2022-09-28 08:49:34.551764	(ALIVE)

Figure B.1: CA container status monitoring during Event 11.

Event 12 (Byzantine Actor) Event 12 is quite similar to Event 10, demonstrating that the approach is robust to Byzantine behavior and that outlying information will not sway the consensus or cause other algorithm problems, an essential characteristic for systems with many distributed devices and actors. Figure B.2 shows selected lines from a CA container log during Event 12. In it, the spoofed input (PHV_A_MAG: 0.8915...) is rejected, down-weighted in the consensus determination, and the process does not progress to Mode 2 (“There is no need for support”) even though that value is less than the voltage lower bound that should trigger a move to Mode 2 (0.95 pu).

```

pod2_ca_log.txt - Notepad
File Edit Format View Help
2022-09-28 20:04:21.235 INFO ca.agent:print_microgrid_status:708 - PHV_A_MAG: 0.8915242472986729
2022-09-28 20:04:21.235 INFO ca.agent:print_microgrid_status:710 - PHV_B_MAG: 0.9905171033073807
2022-09-28 20:04:21.235 INFO ca.agent:print_microgrid_status:712 - PHV_C_MAG: 0.9887123359872341
2022-09-28 20:04:21.236 INFO ca.agent:print_microgrid_status:718 - PCC_STATUS: True
2022-09-28 20:04:21.236 INFO ca.agent:print_microgrid_status:719 - FREQ: 59.98
2022-09-28 20:04:24.659 WARNING ca.voltage_support:needs_support:374 - [Phase a ] Down weighting / Rejecting pod2_ca --> 33794989-46be-445d-887e-08ddff18c175
2022-09-28 20:04:28.732 INFO ca.voltage_support:needs_support:390 - V_lower = 0.95
2022-09-28 20:04:28.733 INFO ca.voltage_support:needs_support:429 - Exiting Early for phase a. There is no need for support.
2022-09-28 20:04:32.580 INFO ca.voltage_support:needs_support:390 - V_lower = 0.95
2022-09-28 20:04:32.581 INFO ca.voltage_support:needs_support:429 - Exiting Early for phase b. There is no need for support.
2022-09-28 20:04:40.969 INFO ca.voltage_support:needs_support:390 - V_lower = 0.95
2022-09-28 20:04:40.970 INFO ca.voltage_support:needs_support:429 - Exiting Early for phase c. There is no need for support

```

Figure B.2: Log file excerpt identifying Byzantine actor during Event 12.

Appendix C: Selected Tests of GridLAB-D Model

This appendix provides simulation results of selected tests on the GridLAB-D model, which is converted from the EPB real distribution system model in CYME. The first test (Test-01) is performed mainly for testing the interconnection of MG2 and MG3 using the “sync_check” [1] and “sync_ctrl” [2] objects in a short period. The second test (Test-02) is conducted for the islanding operation of MG3.

[1] http://gridlab-d.shoutwiki.com/wiki/Spec:sync_check

[2] http://gridlab-d.shoutwiki.com/wiki/Spec:sync_ctrl

C.1 Test-01: Operations of Interconnected MG2 and MG3

The one-line diagram of interconnected MG2 and MG3 is shown in Figure C.1. The preparation includes switching operations completed before closing R3k for the interconnection of MG2 and MG3:

- Open m3
- Connect CHP-4 initially
- Close 1i
- 3j remains closed
- 5a remains open
- Open 5b
- Close 5c

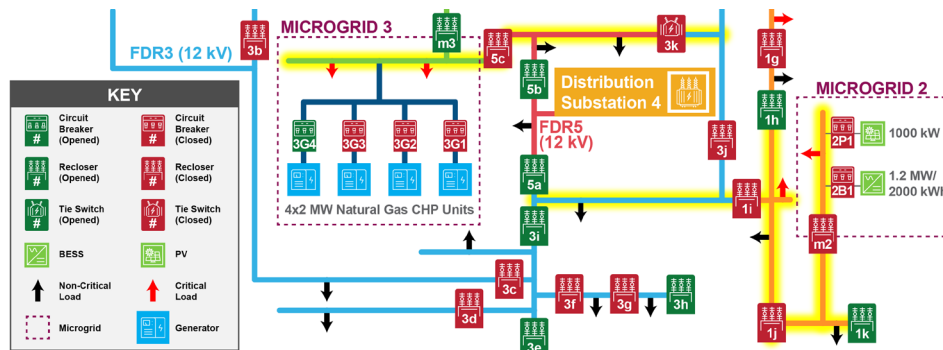


Figure C.1: One-line diagram of interconnected MG2 and MG3 (Test-01).

Settings of the “sync_check” and “sync_ctrl” objects are listed as follows:

sync_check

- name "sync_check_R3k";
- parent "rec_Recloser_XX";
- armed false;
- volt_compare_mode SEP_DIFF;

- frequency_tolerance 0.6 Hz;
- voltage_magnitude_tolerance_pu 0.035;
- voltage_angle_tolerance 5 deg;
- metrics_period 0.02 s;

sync_ctrl

- name "sync_ctrl_R3k";
- armed false;
- sync_check_object "sync_check_R3k";
- controlled_generation_unit "dg_MG3-CHP-1";
- controlling_period 0.2;
- monitoring_period 15;
- frequency_tolerance_ub_hz -0.7;
- frequency_tolerance_lb_hz -0.0;
- pi_freq_kp -2;
- pi_freq_ki -0.2;
- voltage_magnitude_tolerance_pu 0.05;
- pi_volt_mag_kp -2;
- pi_volt_mag_ki -0.2;
- sct_volt_cv_arm_flag true;
- pi_volt_mag_ub_pu 1.65;
- pi_volt_mag_lb_pu 1.00;
- sct_freq_cv_arm_flag true;
- pi_freq_ub_pu 1.0;
- pi_freq_lb_pu 0;

The simulation results are shown in Figure C.2 to Figure C.9.

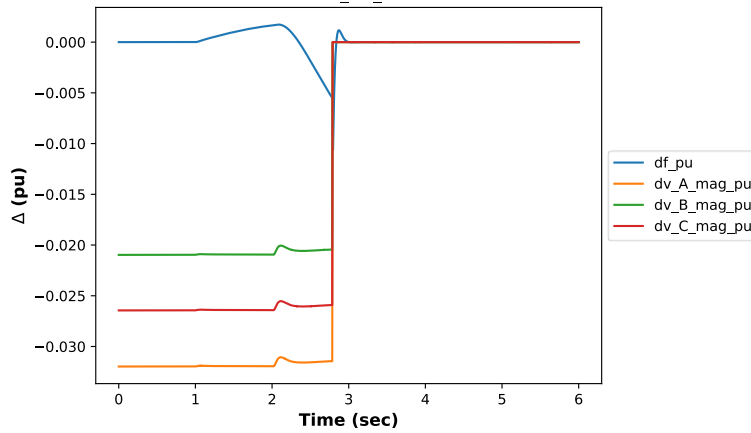


Figure C.2: Deviation between the “from” and “to” nodes of the “sync_check” object (Test-01).

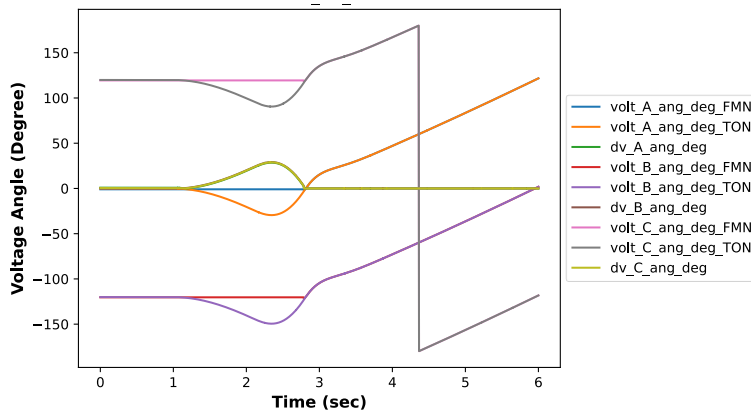


Figure C.3: Measurements of the “from” and “to” nodes of the “sync_check” object (Test-01).

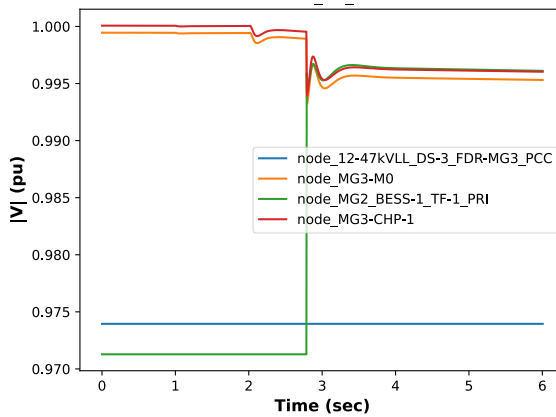


Figure C.4: Voltage magnitude of Phase A of selected nodes (Test-01).

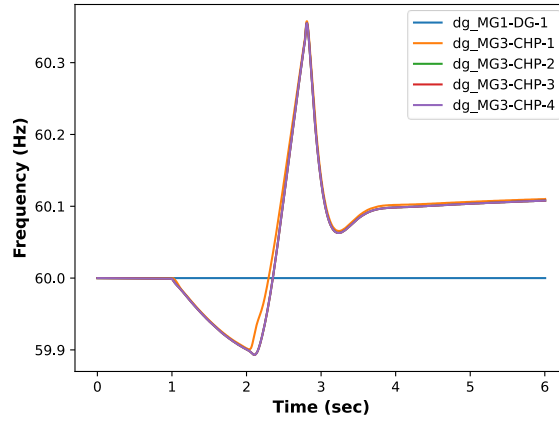


Figure C.5: Frequency of DGs (Test-01).

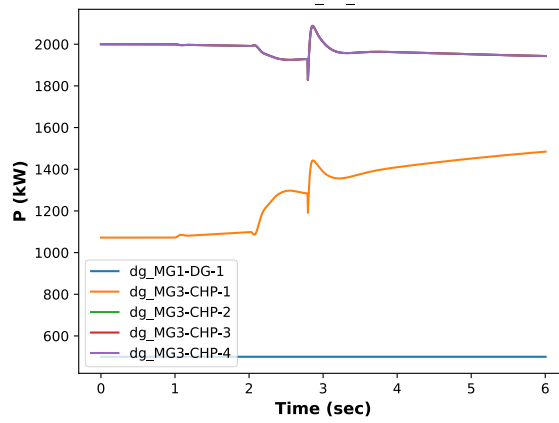


Figure C.6: Active power outputs of DGs (Test-01).

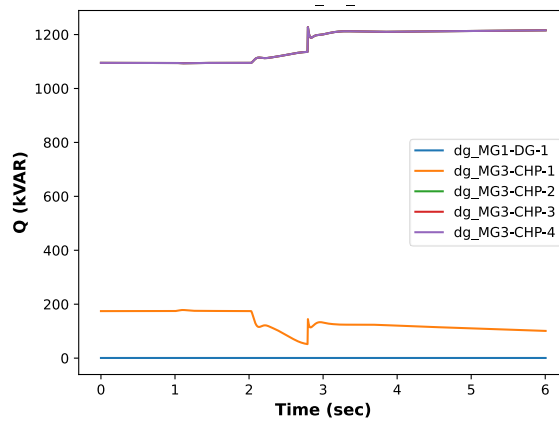


Figure C.7: Reactive power outputs of DGs (Test-01).

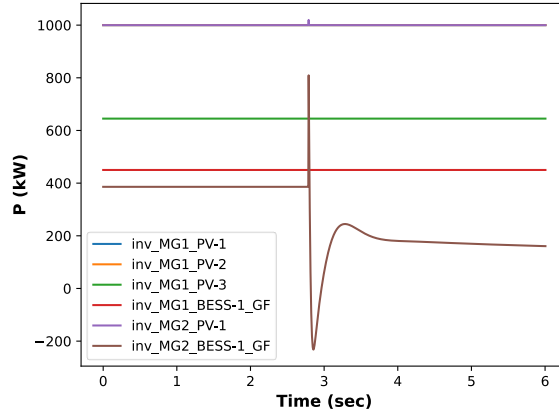


Figure C.8: Active power outputs of inverters (Test-01).

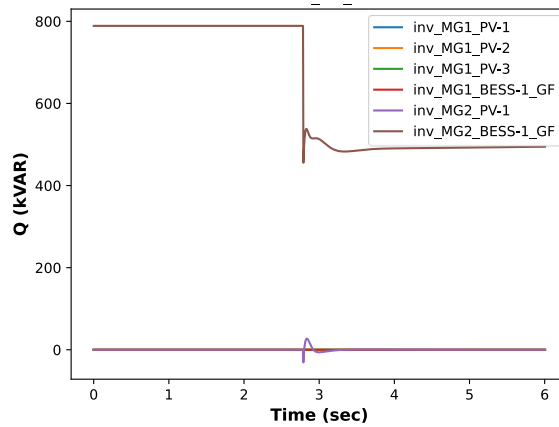


Figure C.9: Reactive power outputs of inverters (Test-01).

C.2 Test-02: Islanding Operation of MG3

The one-line diagram of islanded MG3 is shown in Figure C.10. MG3 is disconnected at 1.52 sec in the simulation by opening the switching device at PCC of MG3. Simulation results are shown in Figure C.11 to Figure C.16.

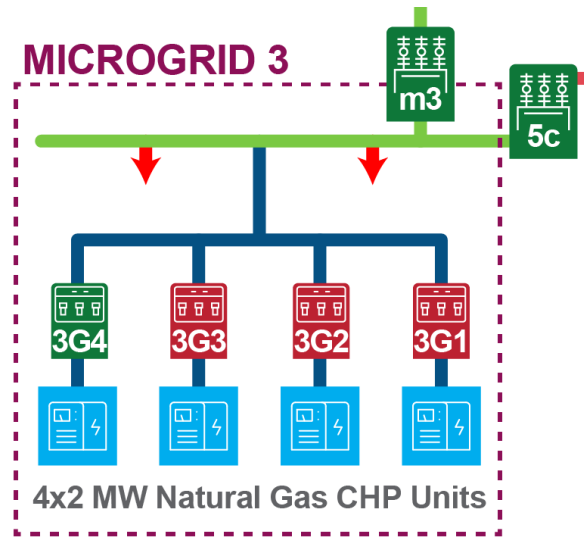


Figure C.10: One-line diagram of islanded MG3 (Test-02).

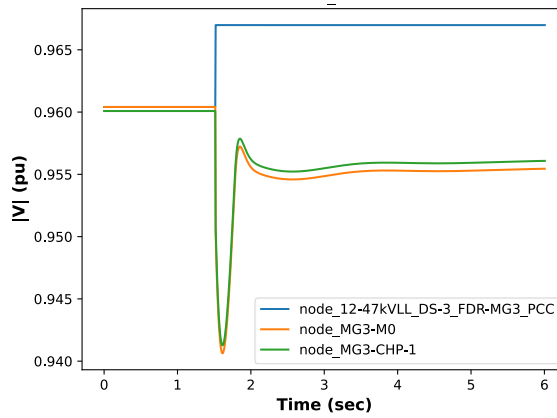


Figure C.11: Voltage magnitude of Phase A of selected nodes (Test-02).

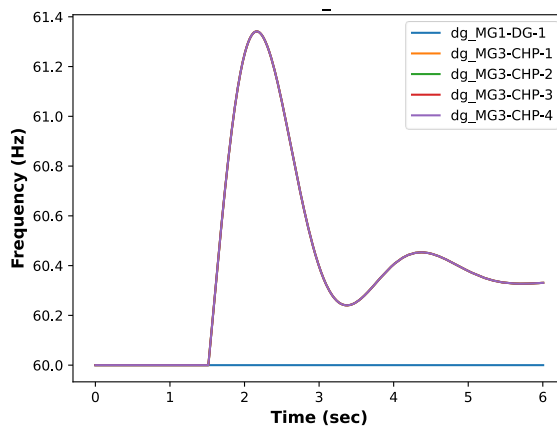


Figure C.12: Frequency of DGs (Test-02).

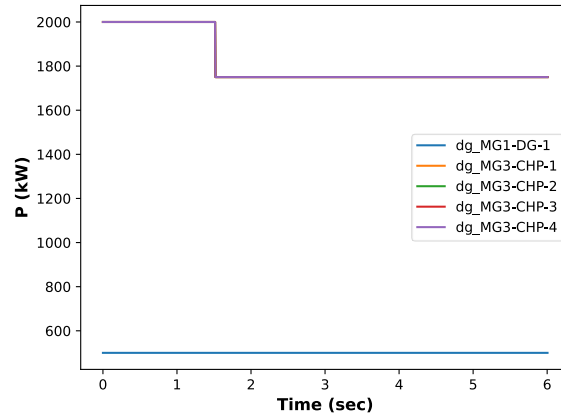


Figure C.13: Active power outputs of DGs (Test-02).

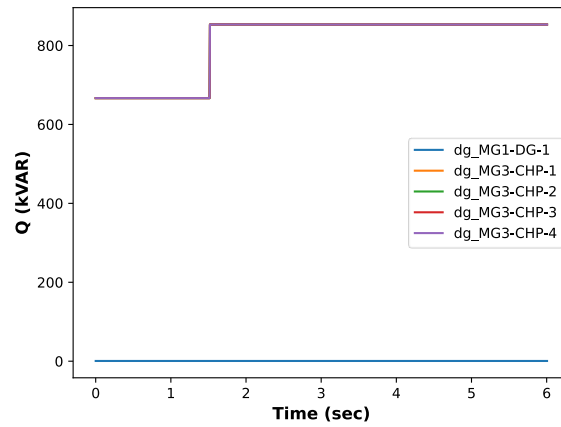


Figure C.14: Reactive power outputs of DGs (Test-02).

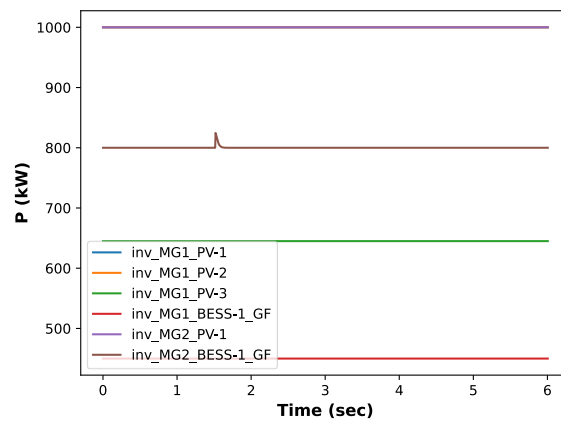


Figure C.15: Active power outputs of inverters (Test-02).

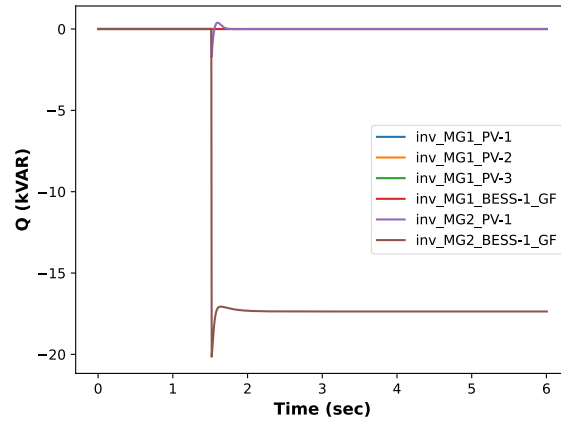


Figure C.16: Reactive power outputs of inverters (Test-02).



<https://gridmod.labworks.org/>